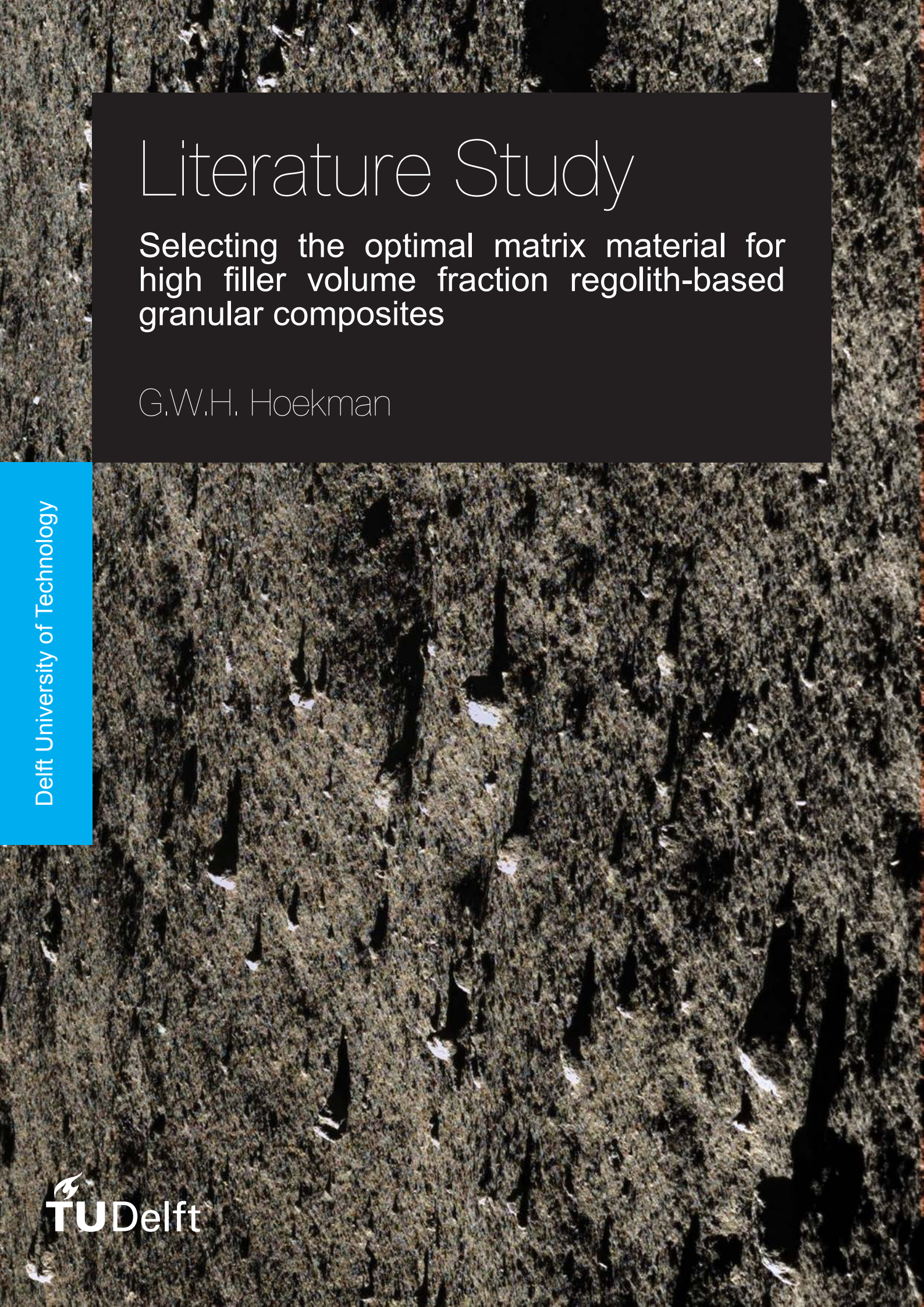

Literature Study

Selecting the optimal matrix material for high filler volume fraction regolith-based granular composites

G.W.H. Hoekman

Delft University of Technology

TU Delft

Abstract

Plans are currently being made for the development of human settlements on the Moon and Mars. The most efficient way of constructing these settlements is by using locally sourced material. Regolith is one of the prime candidates for this due to its availability. However, the challenge becomes stabilizing this granular material. One method is by using a binding matrix. This literature study report investigates the possibility to use regolith in high volume fraction granular composites with the ultimate goal of selecting the optimal binder material (polymer, metal or ceramic) for such composites. This report contains background knowledge about the operating condition of these materials and the properties of regolith, as well as a discussion on the applications and properties of state-of-the-art regolith based materials. It is concluded that choosing an optimal binder is impossible at this stage because of a lack of data required for a proper comparison. However, the material does show promising characteristics and multiple future research fields are identified.

Front cover image retreived from Gizmodo Australia. Last accessed: 30/10/2020.

Contents

List of Tables

List of Figures

Symbols and Abbreviations

BCP Biphasic calcium phosphate

BSA Bovine serum albumin

CMC Ceramic matrix composite

CTE Coefficient of thermal expansion

DMA Dynamic mechanical analysis

ESA European space agency

FoM Figure of merit

FVF Filler volume fraction

FWF Filler weight fraction

GB Glass beads

GCR Galactic cosmic rays

HIP Hot isostatic pressing

I Infrastructure (in table 4.2)

IOH Inorganic-organic hybrid

ISRU In-situ resource utilisation

LaRC-SI Thermoplastic polyimide used in space applications

LPS Liquid phase sintering

LRO Lunar reconnaissance orbiter

M Material (in table 4.2)

MER Mars exploration rover

MMC Metal matrix composite

MT Metric tonne

NASA National aeronautics and space association

NEO Near Earth object

PE Polyethylene

PMA Polymer micro agglomerations

ppm Parts per million

PSD Particle size distribution

RBC Regolith bio composite

SEP Solar energetic particles

SHS Self-propagating high temperature synthesis

SPE Solar particle event

SPS Spark plasma sintering

UHMWPE Ultra high molecular weight polyethylene

UPR Unsaturated polyester resin

VARIM Vacuum assisted resin infusion method

α	Coefficient of thermal expansion	ϵ/K
X	Property, can be substituted for desired transport property	-
ϵ	Strain	-
ν	Poisson's ratio	-
ϕ	Filler volume fraction	-
ϕ_m	Maximum packing factor	-
ρ	Bulk density estimate	kg/m3
ρ	Density	kg/m3
ρ_w	Density of water	kg/m3
σ_{cc}	Composite compressive strength	MPa
σ_{ct}	Tensile strengh of composite	MPa
σ_{cy}	Composite yield strength	MPa

E	Young's modulus	MPa
e	Void ratio	-
E'	Storage modulus	MPa
E_0	Young's modulus of matrix phase	GPa
G	Specific gravity	m3/kg
G_R	Matrix shear modulus	MPa

K	Bulk modulus	GPa
k	Thermal conductivity	W/(mK)
k_E	Einstein coefficient	-
n	Exponent in generalised rule of mixture equation	-
n	Porosity	%
T	Temperature	°C / K
T_g	Glass transition temperature	°C / K
T_m	Melting temperature	°C / K
Z	Atomic number	-

1 Introduction

After the 50th anniversary of the Apollo moon landings, new initiatives have started with the goal of bringing man back to the Moon and, eventually, even further. ESA, NASA and other space agencies have expressed their plans to set foot on the Moon as early as 2024 [1, 2] and on Mars in the early 2040's [2–4]. The main reasons for going to the Moon and Mars are plentiful, but are mostly from a research perspective in order to increase our knowledge and develop the technology necessary for prolonged space exploration and presence by establishing settlements.

Currently there are three main types of settlements defined **[source]**. The first category, Type I, contains habitats that are constructed on Earth and fully usable when landed on the target planet/moon. Habitats in this category contain fully constructed (hard-shell) structures that might be sent using unmanned missions. The Type II structures are structures that are constructed on Earth and assembled on the Moon/Mars. This category contains, for example, inflatable structures that can be fabricated on Earth and deployed in space. The third and final category, Type III, contains structures that are fully manufactured at the destination using local materials. This field of In-situ Resource Utilisation (ISRU) has gained considerable attention in the recent decades.

Regolith, defined as the loose upper layer of material on the surface of planetary bodies, is one of the prime candidates for use in ISRU because of its abundance and easy accessibility. To decrease the energy and infrastructure requirements of settlements it is efficient to use as much un-processed regolith as possible. However, regolith is a loose granular material and therefore requires stabilisation. One method to achieve this is by combining (unprocessed) regolith with a binder (matrix) material, effectively creating a composite material. To make this as efficient as possible, the amount of binder should be minimal. This is because importing material from Earth is very expensive and early in-situ production methods are not likely to produce matrix materials in large quantities. Therefore, high filler volume fraction (FVF) regolith-based granular composites are an interesting material for extra-terrestrial applications.

This report focuses on the feasibility, properties and processing of high FVF regolith-based composites with the goal on selecting the optimal matrix material. First, an understanding of the operating conditions of these composite materials is required. This is discussed in Chapter 2. Next, Chapter 3 gives a description of regolith material for two most important extra-terrestrial bodies (the Moon and Mars) by first looking at the broader concept of In-situ Resource Utilisation (ISRU). This chapter also includes the description of simulant material,

which mimics the properties of actual lunar/Martian regolith. After that, the state-of-the-art research into the use of regolith materials for a variety of applications are discussed in Chapter 4. This is followed by an introduction into granular composites and their properties with different matrix materials in Chapter 5. Finally, a conclusion is made with respect to the optimal matrix material for these kinds of composites and any possible field for further research are identified.

2

Descriptions of the Moon, Mars and the space radiation environment

For materials that are going to operate on extra-terrestrial bodies it is important to know the on-site conditions such that they can be taken into account during the material design. This chapter aims at determining the conditions which materials on the Moon and Mars will have to withstand in order to operate properly. First, the conditions on the Moon are discussed in Section 2.1. Next, the same analysis is performed for Mars in Section 2.2. Thirdly, the important space radiation environment is discussed in Section 2.3. Finally, a summary table is presented for easy referencing in Section 2.4.

2.1. Description of the Moon

This section gives a description of the Moon. First, a general description of the Moon is given, followed by a discussion on the lunar atmosphere, pressure and magnetic field. Next, the Lunar temperature and topology is discussed. Finally, a discussing about water on the Moon is presented.

2.1.1. General Description of the Moon

The Moon is the only natural satellite orbiting the Earth. It is thought that the Moon formed from the debris left over from a large impact between Earth and a different body. This happened not long after the formation of Earth, making the Moon about 4.5 billion years old.

The radius of the Moon is 1738km and it orbits at a distance of 384405 km from the Earth. The Moon is tidal locked with the Earth, meaning that we always observe the same side. Therefore, we can distinguish between a ”near” side and a ”far” side of the Moon. See Figure 2.1 for an image of the Moon.

2.1.2. Lunar Atmosphere, Pressure and Magnetic Field

The Moon does not have an atmosphere. This means that pressures on the surface are very close to vacuum conditions. The pressure on the Lunar surface in the range of $3e^{-12}$ kPa. Additonally, the Moon also lacks a magnetic field. The surface of the Moon is very susceptible to radiation and meteoroid damage because both of these protection methods are missing. The three main radiation sources in space are geomagnetically trapped particles, solar energetic particles (SEP) and galactic cosmic rays (GCRs). More information about these specific types of radiation is given in Section 2.3. Since the Moon has no significant magnetic field of it’s own and it located far enough from Earth to experience minimal impact, the effect of geomagnetically trapped particles on the Moon is negligible [5]. Therefore, the

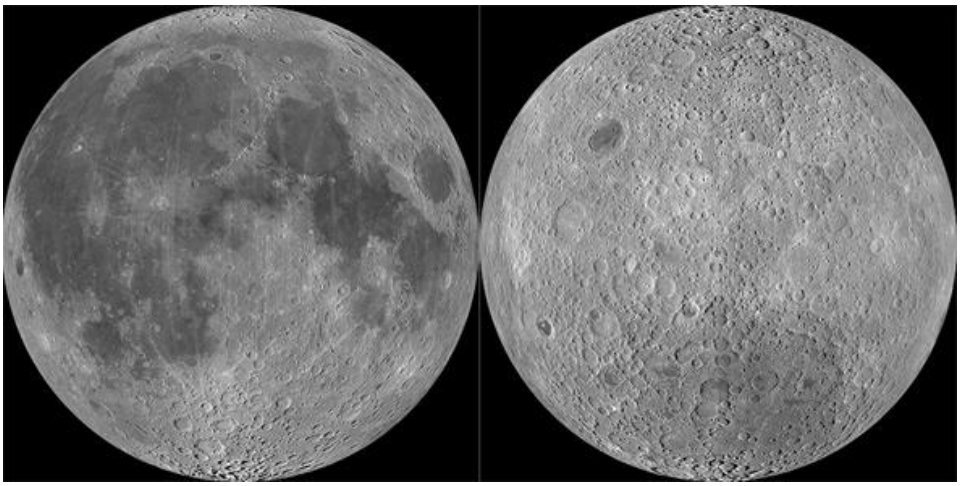

Figure 2.1: *Image of the Moon, showing the near side (left) and the far side (right). (Photo by NASA/GSFC/Arizona State University)*

other two sources create the radiation environment on the Moon. Annually, the moon receives a nominal radiation dose of 25 rem/year. Earth's surface receives 0.360 rem/year, making the dosage on the moon almost 70 times as high. Additionally, single solar events can increase the exposure to 1000 rem over a shot period of time (which is well over the lethal limit of around 600 rem)[5]. Therefore, any structure on the Moon needs to protect astronauts against radiation.

As mentioned, the atmosphere and magnetic field offer little protection from (micro)meteoroids on the surface of the Moon. meteorites can reach a speed of 20-70 km/s and can range from 0.1 μm to several hundred centimeters [5].

2.1.3. Lunar Temperature and Geography

Temperatures on the Moon vary over the duration of a lunar day. At the Moon's equator, the temperature ranges from 126 °C at midday to -173 °C just before the lunar dawn [6]. The reason for this large fluctuation is the absence of a temperature moderating atmosphere or body of water. Temperatures at the poles are even lower, ranging from -113 °C to -258 °C.

The Lunar terrain has several features similar to Earth, like mountains, valleys and craters. However, features on the Lunar surface generally have a different origin than on Earth. For example, on the Moon mountains are not shaped by plate tectonics but by a lack of meteoroid impacts. Ridges formed by mountains or craters might produce areas of permanent darkness at the lunar poles due to the very low inclination of incident solar rays. These areas are generally extremely cold, approaching -258 °C. Another distinct feature of the Moon are lava tubes. These are drained natural caves formed by underground lava rivers. Lava tubes are especially interesting due to their relatively constant temperature (-20 °C), making them interesting for housing lunar bases [6].

2.1.4. Water and Ice on the Moon

No large bodies of water are found on the Moon. Water cannot persist because it quickly dissociates due to solar radiation. Scientists have long suspected that water-ice might persist in permanently shadowed areas at the Moon's poles. Data from the Lunar Reconnaissance Orbiter (LRO) pinpointed areas in craters at the Lunar south pole where hydrogen, and by extension water, is likely to exist.

2.2. Description of Mars

This section aims to give a description of Mars in a similar way that the description of the Moon was given. First, general characteristics of Mars are discussed. Next, features of the martian atmosphere, temperature and pressures are presented. This is followed by an assessment of the Martian topology and magnetic field. Finally, the presence of water and ice on Mars is discussed.

2.2.1. General Characteristics of Mars

Mars, also known as the Red Planet, is the fourth planet from the Sun in our solar system, see Figure 2.2. The reddish appearance is due to the effect of iron oxide on the Martian surface. It orbits at a distance of 227.9 million kilometers from the Sun. Contrary to the orbit of Earth, the orbit of Mars is significantly more eccentric (Eccentricity of Mars is 0.0934 compared to 0.0167 for Earth).

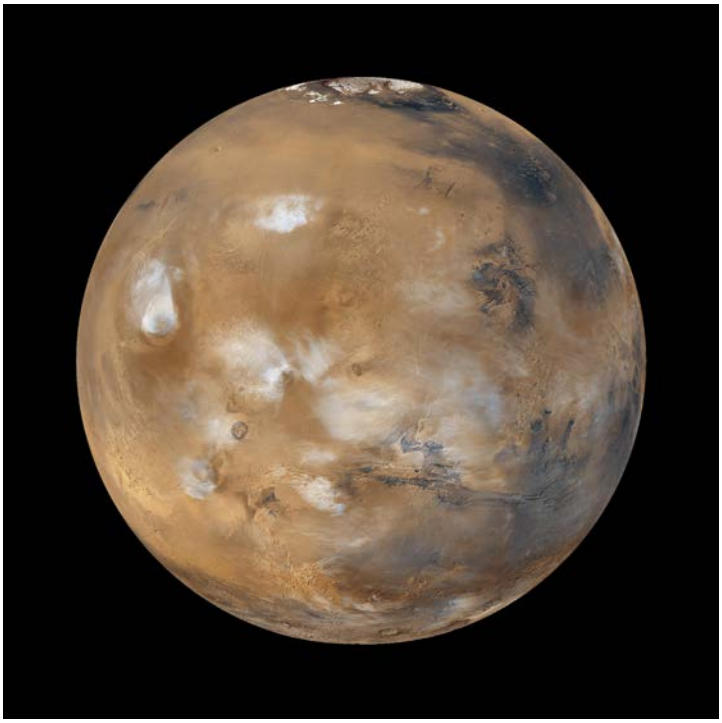

Figure 2.2: *Image of Mars taken by the Mars Global Surveyor in 1999 [7]*

Mars has a rotation rate similar to Earth, which means that the duration of a day is also very similar. However, due to the larger distance to the Sun, a year on Mars takes almost two earth years (365.3 days for Earth compared to 687.0 days for Mars). The rotational axis of Mars is also tilted with respect to the equatorial plane. This means that Mars experiences seasons similar to Earth.

Mars is considerably smaller than Earth, which means, for one, that gravity is lower. Additionally, the lower gravity has has a dramatic effect on the planet's atmosphere. Mars has lost most of it's atmosphere in the past, which is generally attributed to the planet's low gravity. The current atmospheric conditions of Mars are discussed in Subsection 2.2.2. General characteristics of Mars compared to Earth are given in Table 2.2.

2.2.2. Martian Atmosphere, Pressure, Temperature and Magnetic Field

The current Martian atmosphere consists mostly of carbon dioxide. It precipitates to form dry ice on the Martian poles and these polar caps shrink and grow with the Martian seasons. The

composition of the Martian atmosphere is presented in Table 2.1.

Table 2.1: *Composition of the Martian atmosphere in volume percent or parts per million (ppm)[8]*

Gas		Percentage
Carbon dioxide	CO2	95.1
Argon	Ar	2.59
Nitrogen	N2	1.94
Carbon monoxide	CO	0.06
Water Vapour	H20 (v)	210 ppm
Neon	Ne	2.5 ppm

Mars' atmosphere is much thinner than that of Earth. This means that the surface pressure is also much lower. However, it is thought that the Martian atmosphere was much thicker in the past. The current Martian surface pressure at the mean radius ranges between 0.4 and 0.87 mPa depending on the season. The mean pressure is 0.636 mPa [8].

Due to the larger distance to the sun, Mars receives less solar radiation then Earth. This, in combination with the relatively thin atmosphere of Mars means that the planet is generally cooler than the Earth. The average temperature on the Martian surface is -63 °C, with a diurnal temperature variation between -89 and -31 °C.

Contrary to Earth, Mars does not show a structured global magnetic field. This is most likely due to the planet's dynamo seizing to function a long time ago. Instead, Mars displays local areas of magnetization. These have been mapped by the Mars Global Surveyor and show a large variation in magnetic field direction from place to place [9]. Despite the absence of a global magnetic field, aurora's can still be observed on the planet.

2.2.3. Martian Geography

The Martian surface shows mountains, valleys, canyons, volcanoes, craters and much more. The southern half of the planet is much more crated than the north. It is also elevated much higher than the northern hemisphere. This causes a north-south asymmetry commonly referred to as dichotomy [10]. The variation in surface relief of the planet is also high, ranging from -8200 km (floor of Hellas) to 21229 km (top of Olympus Mons).

2.2.4. Water and Ice on Mars

Liquid water cannot exist on Mars due to the low atmospheric pressures. It is thought that liquid water was present in the past when Mars' atmosphere was substantially thicker. Evidence for this is found in the Martian landscape, which shows distinctive sign similar to rivers and delta's found on Earth. Water-ice, however, can exist and is found in the polar regions of the planet. Additionally, water-ice can also be found underground in the permafrost regions (up to 60 degrees latitude). Trace amount of water vapour are present in the Martian atmosphere.

2.3. Description of the space radiation environment

As mentioned in Section 2.1, three main types of space radiation can be identified. These are geomagnetically trapped particles, solar energetic particles (SEPs) and galactic cosmic rays (GCRs).

Geomagnetically trapped particles are energetic particles from the Sun or GCR that are trapped within the geomagnetic field. Particles from space are funneled via the magnetic fields towards the surface,

SEPs originate during solar particle events (SPEs). They are created during two main processes, coronal mass ejections and solar flares respectively. SPEs mainly consists of protons, but can also include the nuclei of elements. Their typical energy is in the range of a few MeV to 100s of MeV [11]. The frequency of solar particle events is correlated to the activity of the sun. Sunspots are used to measure this activity, which follows an 11 year cycle.

Galactic cosmic rays are generally considered to originate outside our solar system and are most likely caused by supernova explosions [12]. They can be divided into two groups: primary and secondary rays. Primary GCR rays mainly consists of high-energy protons (85%), alpha particles (14%) and heavy nuclei (1%). The typical energy range of this type of radiation is 10 MeV to 10 GeV [11]. Secondary GCR rays are caused by the decay of primary GCR's when they interact with an atmosphere or structure. These secondary rays includes gamma rays, neutrons, pions, positrons and muons [12]. A major downside of secondary rays is the presence of penetrative particles and rays, requiring additional shielding material.

2.4. Summary tables of the Moon and Mars

Table 2.2: *General characteristics of the Moon and Mars compared to Earth*

Characteristic		**Moon [13]**	**Mars [8]**	**Earth [14]**
Mean distance from sun	km	378,000	2.279 e^8	1.496 e^8
Eccentricity		0.0549	0.0934	0.0167
Day	hours	655.7208	24.6229	23.9345
Year	days	655.7208	686.980	365.256
Mass	e^{24} kg	0.07346	0.64171	5.9724
Radius	km	1737.4	3389,5	6371.0
Surface gravity	m/s2	1.62	3.71	9.798
Surface pressure	kPa	3 e^{-12}	0.4 - 0.87	101,400
Surface temperature (average)	°C (K)	-	-63 (210)	15 (288)
Surface temperature (diurnal range)	°C (K)	-178 to 117 (95 to 390)	-89 to -31 (184 to 242)	10 to 20 (283 to 293)

3

In-situ Resource Utilisation and Regolith

3.1. In-situ Resource Utilisation: definition and importance

In-situ Resource Utilisation (ISRU) is the process of converting local resources at a space destination for the production of useful infrastructure and commodities [15]. It stemmed from the realisation that humanity will need to be able to gather, process and use materials at the sites of settlements on different planetary bodies [16]. This is especially important if humanity ventures further into the depths of space. Therefore, developments of these methods is vital for the future success of space exploration and settlement efforts.

As mentioned, ISRU uses local materials found on other planetary bodies. It is known that the initial bodies targeted for human settlement (e.g. the Moon and Mars) have a surface covered in a loose granular soil called regolith. Regolith is formed by (micro)meteorite impacts and weathering effects. Because of the abundance of this material, it is a prime candidate for use as a base material for IRSU methods. This means that a proper understanding of regolith material is required. The next two sections aim at providing an overview of the properties of this important material.

3.2. Lunar regolith material and simulants

It is important to understand the properties of regolith material because of the large role it is going to play in ISRU. Because initial efforts are focused on the Moon, it is important to understand the Lunar regolith material first. The properties of this material are discussed in Subsection 3.2.1. Next, the properties of different materials that simulate lunar regolith are discussed in Subsection 3.2.2 followed by a comparison between the actual and simulant materials in Subsection 3.2.3.

3.2.1. Lunar regolith material

Most of the knowledge gained about the composition of the Moon's regolith comes from multiple remote-sensing missions and sample return missions that have taken place over the past decades. The lunar regolith contains iron, aluminum, silicon, titanium, oxygen and traces of hydrogen, helium3 and nitrogen in various minerals [17].

The composition of these minerals changes depending on their origin. There are two different types of geology that are commonly distinguished when discussing regolith and its composition. The first is regolith stemming from the lunar highlands. They are thought to be the

original crust of the moon [18]. Lunar highlands are rich in calcium (Ca), aluminium (Al), silicon (Si) and oxygen (O), but relatively poor in magnesium (Mg) and iron (Fe).

The second location is the lunar maria, basaltic plains on the Moon formed by volcanic eruptions. The mineral composition of these fields differ between lava flows. Relatively speaking, the lunar maria are richer in Mg, Fe and titanium (Ti) and relatively poorer in Ca and Al. Figure 3.1 shows an example of chemical compositions of these two areas based on three Apollo landing missions.

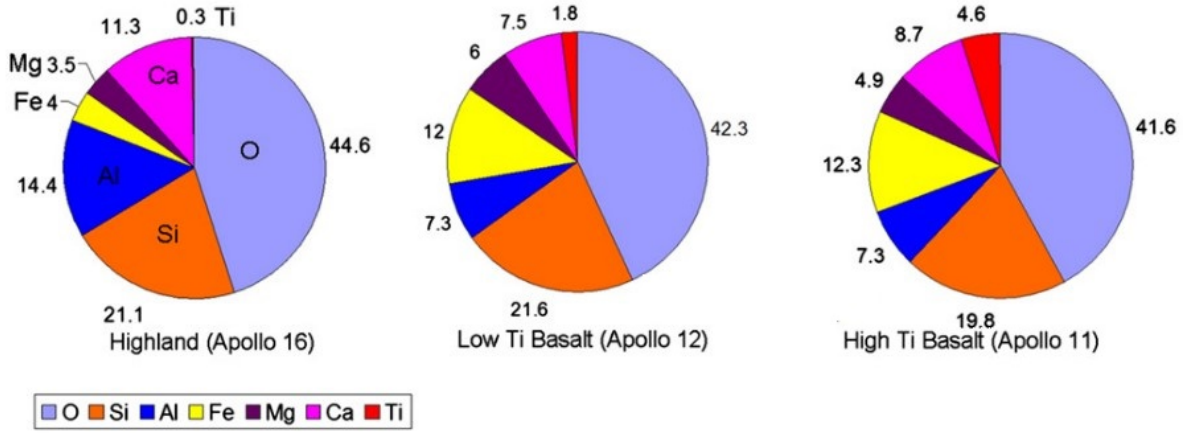

Figure 3.1: *Chemical compositions of: (a) lunar highland minerals (Apollo 16); (b) low-Ti basalts (Apollo 12); and (c) high-Ti basalts (Apollo 11). Based on data collated by Stoeser et al. (2010), adapted from [19]*

Another common and special component of lunar regolith are agglutinates. These structures, sometimes referred to as glass-welded aggregates in early literature, are formed after micrometeorite impact on the lunar regolith and therefore have no terrestrial equivalent. This is possible because the lack of atmosphere on the Moon does not slow incoming projectiles. During impact, a small amount of regolith melts and subsequently cools rapidly in the vacuum environment of form glass. Agglutinates consist of this glass mixed with other regolith material. They are complex in morphology and have a large amount of vesicles. Agglutinates are very common in the lunar regolith, making up about 25-30 vol% on average, but this percentage ranges to as high as 65% [20].

The regolith varies in thickness, from several meters in the mare regions to possible 10 or more meters thick in highland regions [18]. The upper part of this layer, about a few centimeters in thickness has a powdery consistency, while deeper parts are more consolidated. The relative thickness becomes 90% at a depth of 30cm [21]. This abundance makes regolith material very interesting for various applications, see Chapter 4.

Because regolith is a granular material, it's granulometric (i.e. particle size and shape) composition determines its physical and mechanical properties to a large extent [22]. Therefore, it is important to know these parameters. Several investigations into the particle size, shape and distribution have been conducted on Lunar regolith samples returned by the USA's Apollo missions and the Russian Luna missions.

The particle size distribution shows variation when the maturity of the regolith is considered. In general, when the maturity grows, the mean particle size decreases. Additionally, the amount of agglutinates and sorting of the particles increases, see Figure 3.3 [23].

Evaluation of the particle size resulted in an average particle size of 70 μm and a mean

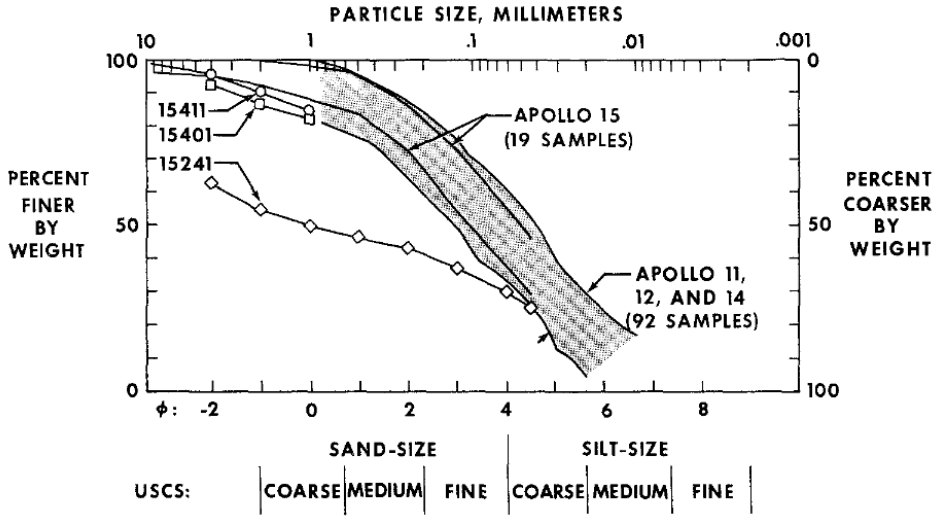

Figure 3.2: *Particle size distribution of Lunar regolith samples from several Apollo missions [24]. The bands show that most samples fall within the same size distribution.*

particle size of 40 to 130 µm [24]. The particle size distribution of the lunar samples showed an approximately linear distribution on a lognormal scale. The size of the particles ranges from around 1 to 0.01 millimeters, see Figure 3.2. Samples from different Apollo landing sites show similar distributions, indicating minimal variation of the distribution on the Lunar surface [24].

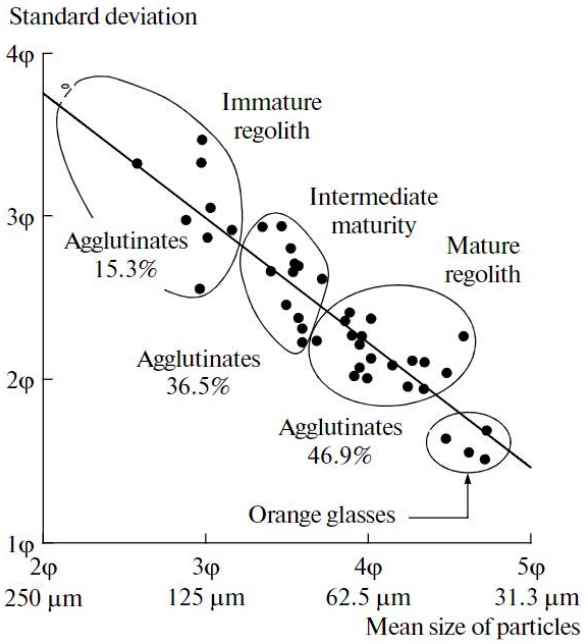

Figure 3.3: *Change in mean particle size with regolith maturity [23], originally from [25]*

Next to the particle size, the particle shape is also important. One shape parameter that can be defined is the aspect ratio, defined as the ratio of the minor axis to the major axis of a particle. These axes are determined from a fitted ellipse to the particle shape using a least-squares method. Liu et al. analysed the shape of lunar dust particles and concluded that most particles are slightly elongated subangluar to angular grains [26].

As mentioned, the granulometric composition determines the properties of in-situ regolith. One parameter that is of special interest is the bulk density of the material. This parameter influences, among others, the stability, thermal conductivity and the depth of penetration of ionizing radiation. Next to the bulk density, the particle density is also often used. The difference between these two is that the bulk density includes voids and the particle density represents the density of a fully dense material. Estimates for the bulk density are given in Table 3.1 [27].

Table 3.1: *Estimates of the average bulk density for different depth ranges, from [27]*

Depth range (cm)	Average Bulk Density (g/cm^3)
0 - 15	1.50 ± 0.05
0 - 30	1.58 ± 0.05
30 - 60	1.74 ± 0.05
0 - 60	1.66 ± 0.05

The average bulk density of the Lunar regolith can be used to calculate a best estimate for the average porosity using Equation 3.1. Porosity is defined as the void volume divided by the total volume. The results are given in Table 3.2 for several depth ranges.

$$n = 1 - \frac{\rho}{G \cdot \rho_w} = 1 - \frac{\rho}{3.1} \tag{3.1}$$

where n is the porosity, G is the specific gravity, ρ_w is the density of water and ρ is the estimate for the bulk density. The value 3.1 comes from the recommended value for the specific gravity of lunar soil and the density of water is taken to be 1 [21]. Using the porosity the void ratio can be calculated. This is a different geotechnical engineering parameter equal to the ratio of void space volume between particles to volume of solid particles.

Table 3.2: *Lunar soil in-situ porosity estimates, from [21]*

Depth range (cm)	Average Porosity, n (%)	Average Void Ratio, e
0 - 15	52 ± 2	1.07 ± 0.07
0 - 30	49 ± 2	0.96 ± 0.07
30 - 60	44 ± 2	0.78 ± 0.07
0 - 60	46 ± 2	0.87 ± 0.07

Generally, material properties like the Young's and bulk modulus of granular materials are unavailable unless they are further processed in a compact state. No straight forward method exists for loose granular materials and therefore these properties are not reported in literature. This is because loose soils only show elastic effects under insignificant stresses, making it hard to define a Young's modulus [23].

Other material properties, like the Poisson's ratio (ν), have been determined. The Poisson's ratio relates the lateral deformation to the longitudinal deformation. It depends on the mineralogical composition and porosity of the soil. Using data from the Luna missions, the Poisson's ratio for lunar soil was calculated to be between 0.2 and 0.31 [23].

3.2.2. Lunar Regolith Simulant

Because actual regolith material is very scarce, efforts have been made to create equivalents of Lunar regolith using terrestrial soils and minerals. These so called "simulants" try

to approximate different attributes of regolith material. These attributes include the chemical composition; particle shape, size and distribution; and other components (like agglutinates) of the regolith material.

Most terrestrial simulants of Lunar regolith have volcanic or basaltic origins and are processed and supplemented to resemble the granulometric properties of regolith material. Currently there are dozens of different simulants in use, all with their advantages and disadvantages. To help evaluate and compare simulants to actual regolith material, hypothetical regolith samples or other simulants, Figures of Merit (FoMs) have been defined for specific parameters or sets of parameters. In these algorithms, a reference sample serves as a benchmark for comparing the second sample [28–30].

The chemical composition of several frequently used simulants of lunar regolith can be found in Table 3.3.

Table 3.3: *Chemical composition of several Lunar regolith simulants. Values in compiled from several sources [6, 19, 31–33].*

Simulant Source	FJS-1 [31]	JSC-1 [31]	JSC-1A [31]	JSC-1AF [6]	MLS-1 [32]	NU-LHT-1M [31]	NU-LHT-2M [19]	OB-1 [33]
Oxide								
SiO2	49.1	47.71	46.67	47.1	43.86	47.6	46.7	48.4
Al2O3	16.2	15.02	15.79	17.1	13.68	24.4	24.4	31.6
CaO	9.1	10.42	9.9	10.3	10.13	13.1	13.6	15.4
FeO	8.3	7.35	8.17	7.57	13.4	4.3	–	–
Fe2O3	4.8	3.44	12.5	3.41	2.6	–	4.16	1.33
MgO	3.8	0.18	9.39	6.9	6.68	8.5	7.9	0.35
Na2O	2.8	2.7	2.83	3.3	2.12	1.4	1.26	2.47
TiO2	1.9	1.59	1.71	1.87	6.32	–	0.41	0.08
K2O	1	0.82	0.78	0.86	0.28	–	0.08	0.08
P2O5	0.44	0.66	0.71	0.76	0.2	–	0.15	0.01
MnO	0.19	–	0.19	0.18	0.2	–	0.07	0.01
Cr2O3	–	0.04	–		–	–	–	–
Total	97.63	89.93	108.64	99.35	99.47	99.3	98.73	99.73

Because simulants are supposed to accurately represent actual Lunar regolith, they can (after proper processing) be used to estimate material properties. For example, using different Lunar regolith simulants and processing methods an estimate of the Young's modulus can be given. Arslan, Batiste, and Sture and Dewoolkar et al. [34, 35] used a triaxial compression test system to estimate, among others, the Young's modulus. This was done by confining simulants of different density values under different confining stresses. The value of the Young's modulus was found to increase with increasing density and confining stress. It ranged between 11-36 MPa [34] and 19 - 65 MPa [35] respectively. Using this triaxial test, Dewoolkar et al. also calculated the Poisson's ratio of GRC-3 simulant. It ranged between 0.27 and 0.42.

3.2.3. Comparison between actual and simulated Lunar regolith

A comparison between actual and simulated lunar regolith can determine whether the stimulant is actually a good representation of the material. As mentioned before, figures of merit

(FoMs) exist to compare the material for some parameters. Where possible, these FoMs will be used to support the comparisons below. Other comparisons will be based on literature.

Most simulants are specifically formulated to represent a specific lunar reference material. Therefore, the chemical compositions of the simulants are generally close to that of actual regolith, see Table 3.4 for an example of a close chemical composition.

Table 3.4: *Comparison of JSC–1 and MLS–1 with targeted Apollo composition (values in oxide weight percent). Adapted from [36]*

Oxide	JSC-1	”Apollo 14 Average soil”	MLS-1	”Apollo 11 Soil 10002”
SiO2	47.71	48.1	43.9	42.2
Al2O3	15.02	17.4	13.7	13.6
CaO	10.42	10.7	10.1	11.9
FeO	7.35	10.4	13.4	15.3
Fe2O3	3.44	–	2.6	–
MgO	9.01	9.4	6.7	7.8
Na2O	2.7	0.7	2.1	0.47
TiO2	1.59	1.7	6.3	7.8
K2O	0.82	0.55	0.2	0.16
P2O5	0.66	0.51	–	0.05
MnO	0.18	0.14	0.2	0.2
Cr2O3	0.04	0.23	–	0.3
LOI	0.71	–	–	–

However, next to looking at just the chemical composition, the simulant should also represent the proper particles. Especially in the early lunar simulants (JSC, MSL) there were no agglutinates present. Later simulants (for example the NU-LHT series) have tried to solve this by incorporating manufactured or pseudo-agglutinates.

Simulating the proper particles also includes the particle shape, size and distribution. For the latter a figure of merit has been determined. Marshall et al. compared the particle size distribution (PSD) of some commonly used regolith simulants to a sample material, the results of the FoM calculation are shown in Table 3.5. A higher number means a closer match to the sample. From the table, it becomes clear that most of the simulants have a very low score. This means that the current simulants do not have a good PSD indicating room for improvement. Note that these numbers only correspond to the PSD FoM and therefore the simulants might be very suitable according to another.
The particle shape can be compared by looking at the angularity of the simulants. This is shown in Table 3.6. According to Liu et al., most lunar regolith particles are angular to subangular. Comparing this to the values in the table it becomes clear that the bulk of the particle shapes of these simulants does not fall within this classification. Therefore, the angularity of simulants can be improved as well.
It is difficult to make a comparison between the mechanical properties of lunar regolith and simulant as this information is unknown for the actual regolith material. However, a comparison can be made about the calculated Poisson’s ratios mentioned in earlier sections. These values, 0.2-0.31 for actual regolith and 0.27-0.42 for simulant, seem to comply with one another. This indicates that the simulant accurately reflects this parameter. However, more investigation into the other mechanical properties is needed in order to give a proper comparison.

Table 3.5: *Particle side distribution FoM size results for all simulants against 64001/64002 lunar reference material, adapted from [28]*

	”64001/2 Bulk Average”	”64001/2 <1-mm Average”	”64001/2 Average to 9 μm”
OB-1 (section image analysis)	0.23	0.54	–
NU-LHT-1M (section image analysis)	0.23	0.58	–
NU-LHT-2M (section image analysis)	0.17	0.48	–
JSC-1 (section image analysis)	0.22	0.53	–
JSC-1A (section image analysis)	0.25	0.56	–
JSC-1AF (section image analysis)	0.06	0.23	0.6
MLS-1 (section image analysis)	0.2	0.29	–
FJS-1 (section image analysis)	0.26	0.45	–
OB-1 (dry sieve)	0.59	–	–
NU-LHT-1M (dry sieve)	0.26	0.75	–
JSC-1A (dry sieve)	0.35	0.74	–
NU-LHT-1M (laser diffractometry)	0.26	0.64	–
NU-LHT-2M (laser diffractometry)	0.29	0.82	–
JSC-1A (laser diffractometry)	0.28	0.74	–

Table 3.6: *Lunar simulant shape parameters, derived from QEMSCAN analysis. Adapted from [37]*

Particle Shape Classification	FJS-1	JSC-1	JSC1A	JSC-1AF	MLS-1	NU-LHT-1M	NU-LHT-2M	OB-1
Very angular	2	2.9	4.7	1.1	0.4	2.4	1.5	1.7
Angular	4.2	5.1	7	3.1	3	4.2	1.8	2.3
Subangular	20.9	17	16.3	13	11.5	15.3	7.3	10.4
Subrounded	49.2	42.9	40	39.2	37.5	43.3	36.2	40.7
Rounded	23.6	31.9	31.6	43.4	30.8	34.4	52.8	44.5
Well rounded	0.1	0.1	0.3	0.3	16.9	0.2	0.6	0.3
Total	100	100	100	100	100	100	100	100

In conclusion, a lot of parameters exist that can be used to compare regolith simulants to the actual lunar samples. Depending on the chosen parameter, a simulant can be either good or bad, but a bad figure score does not necessary eliminate the simulant for use in other applications. More effort is needed in order to create simulants that have a proper particle size distribution, angularity and composition.

3.3. Martian Regolith Material and Simulants

Mars is the next destination targeted for extra-terrestrial exploration after the Moon. Because the composition of Mars is different than the Moon, other considerations have to be made with respect to ISRU methods. Therefore, an understanding of Martian regolith is also important. In Subsection 3.3.1 the current understanding of Martian regolith is presented in terms of the same properties used for Lunar regolith. Similar to the previous section, Subsection 3.3.2 discusses the Martian simulants which are compared to the actual material in Subsection 3.3.3.

3.3.1. Martian Regolith Material

Unfortunately, to date, no sample return mission to Mars has taken place. The first planned sample return mission involves the Mars 2020 (”Perseverance”) rover currently on its way to the red planed. This rover will collect and store samples which will be transported back to Earth by a collaborative effort between NASA and ESA [38]. The returned samples will be able to drastically improve our understanding of the Martian regolith. Therefore, knowledge about the Martian regolith is mostly obtained from remote sensing missions, lander missions and several rovers. Especially the latter category provided insight into the material. An image of the martian soil, taken by the Curiosity rover, can be seen in Figure 3.4.

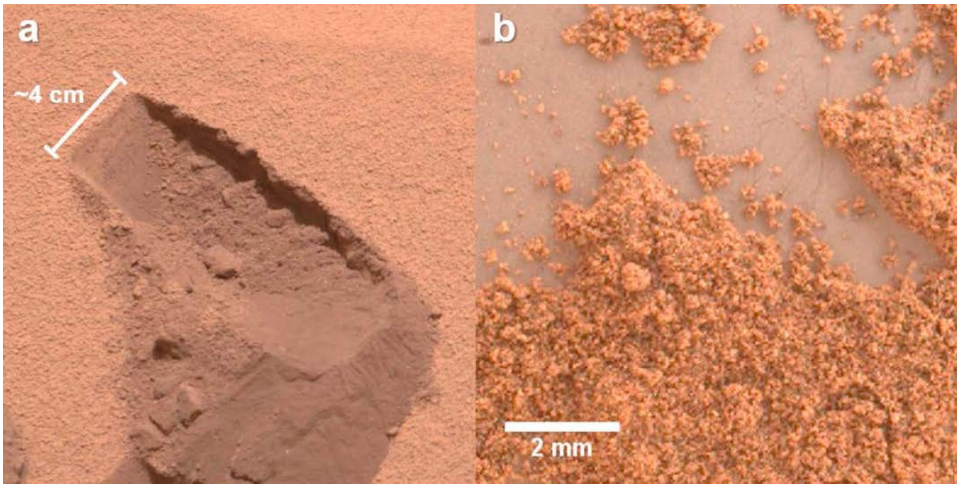

Figure 3.4: *Martian soil as photographed by the Curiosity rover. a) photograph of the Rocknest trench. b) Close-up image of Rocknest <150 μm sample [39]*

The Martian regolith mainly consists of basaltic soils with minerals similar to the Moon’s regolith. The average bulk composition of these soils can be seen in Table 3.7. The different measurements were obtained from the Mars Exploration Rover (MER) Curiosity (Gale Crater), the MER Opportunity (Meridiani Planum) and the MER Spirit (Gusev Crater).

Martian regolith is known to predominantly consist of small grains [41]. Nevertheless, a large particle size variation exists. For example, data from the Viking landing sites processed by Shorthill et al. showed a PSD between 10 and 2000 μm for material at or near the surface. Weitz et al. identified a bimodal particle size distribution at Merdiani Planum with one population mode given by particles <125 μm and the other by particles between 1 and 4.5 mm in size [43]. A similar bimodal distribution was observed in the Gale Crater with a mode at 100-250 μm and and the second at 500-2200 μm [39]. The same study showed that the particle shapes for all grains are subangular to rounded with a high degree of circularity, which indicates an extensive history of abrasion [39].

The thermal properties of martian regolith material depend on the bulk density and the porosity of the material. To give an estimate of the thermal properties of regolith, thermophysical properties obtained from orbital data can be used. This data, together with relationships established in the laboratory, were used by Morgan et al. to estimate the thermal conductivity of Martian regolith. Their calculations showed a value between 0.017 and 0.048 W/(mK), with a median value of 0.032 W/(mK) [44]. This corresponds to to 150-170 μm unconsolidated grains [45].

Table 3.7: *Average bulk composition of basaltic soils in the Gale Crater, Meridiani Planum and Gusev Crater. Adapted from [40]*

Oxide	Gale Crater average	Meridiani Planum average	Gusev Crater average
SiO2	43.16	46.14	46.32
Al2O3	9.16	9.39	10.14
CaO	7.08	6.95	6.35
FeO_T	19.33	18.17	16.04
MgO	8.6	7.42	8.61
Na2O	2.72	2.23	3.01
TiO2	1.05	1.03	0.87
K2O	0.5	0.49	0.44
P2O5	0.92	0.85	0.82
MnO	0.42	0.37	0.32
Cr2O3	0.46	0.4	0.35
Cl	0.77	0.66	0.72
SO3	5.83	5.91	6.01
Total	100	100.01	100

Bulk densities for Martian regolith have also been determined by the different Viking Landers and MERs. Measured bulk density values vary between 1150 kg/m3 for drift material to 1636 kg/m3 for crusty material [46]. The low bulk densities of the drift materials infers a large amount of porosity (Equation 3.1). Estimates for the porosity of Martian regolith are few, but Viking Lander suggests a porosity between 31 and 58 % for grain densities of 2600 kg/m3 and bulk densities between 1100 and 570 kg/m3 [47].

3.3.2. Martian Regolith Simulants

Similar to Lunar regolith simulants, Martian regolith simulants are also obtained from basaltic sources. One of the first Martian simulants to be developed was JSC-Mars-1, see Figure 3.5. The chemical composition of this simulant, together with that of other frequently used Martian simulants, can be seen in Table 3.8.
The grain size and shape of Martian regolith simulants are determined by the processing methods of the raw material. The characteristics of multiple simulants have been investigated for these two parameters. All of the current Martian simulant samples exhibit very angular to sub-angular shapes with a low circularities [46, 50, 52]. The particle size distribution for several simulants, including JSC-Mars-1, can be seen in Figure 3.6. It is observed that the particle size varies between $1 - 1000\mu$m.

Several researchers have tried to investigate the thermal properties of Martian regolith simulant under Martian conditions. Because the thermal conductivity depends on the pressure, several measurements at different pressures were performed. The measurements for the thermal conductivity of JSC-Mars-1 simulant in low pressure conditions are shown in Figure 3.7. The JSC-Mars-1 samples were first dried before being tested. For the pressures on Mars, the thermal conductivity was found to range approximately between 0.055 and 0.18 W/(mK).

Figure 3.5: *Image of a small pile of JSC-Mars-1 simulant [48]*

Table 3.8: *Chemical composition of several Martian regolith simulants. Values in percent of total, data sources noted in table.*

Simulant Source	JMSS-1 [49]	JSC-Mars-1 [31]	MMS [50]	TJ-1 [32]	MGS-1 [51]	OUEB-1 [52]
Oxide						
SiO2	49.28	39.25	49.4	47.7	50.8	50.44
Al2O3	13.64	21	17.1	16.2	8.9	7.10
CaO	7.56	5.5	10.45	8.21	3.7	9.52
FeO_T	16	13.5	10.87	10.75	13.3	19.32
MgO	6.35	3	6.08	5.04	16.7	10.71
Na2O	2.92	2.25	3.28	4.92	3.4	1.33
TiO2	1.78	3.5	1.09	2	0.3	0.28
K2O	1.02	0.55	0.48	2.29	0.3	0.71
P2O5	0.3	0.8	0.17	0.58	0.4	0.52
MnO	0.14	0.25	0.17	0.15	0.1	0.19
Cr2O3	–	–	0.05	ND	0.1	0.179
SO3						0.448
Total	98.99	89.6	99.14	97.84	98	100.73

The bulk density of Martian regolith simulants is reported to range between 835 kg/m3 for JSC Mars-1 [55] and 1950 kg/m3 for OUHR-1 [52]. Ramkissoon et al. also determined the porosity of their new Martian regolith simulants. They obtained values ranging between 47.7 and 51.7% for bulk densities of 1950 and 1620 kg/m3 respectively [52].

The mechanical properties of several simulants have been investigated [46, 52, 55, 56]. Delage et al. investigated three different simulants (MSS-D, Mojave simulant and Eifelsand) and provided a value for the Poisson's ratio based on measured seismic velocities. These seismic velocities were measured in a triaxial compression test using different confining pressures. A value of 0.22 was determined. In addition, Delage et al. calculated the Young's modulus using

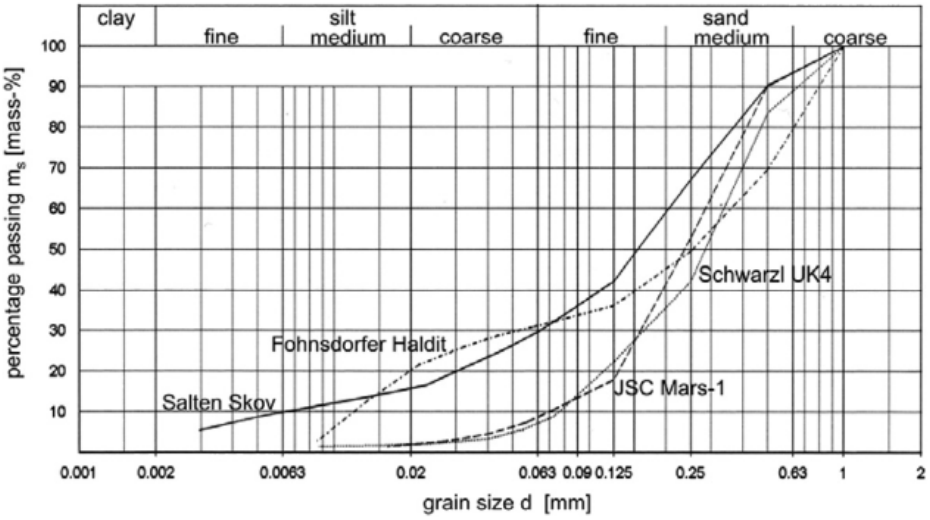

Figure 3.6: *Particle size distribution of JSC-Mars-1 and other Martian regolith simulants [53]*

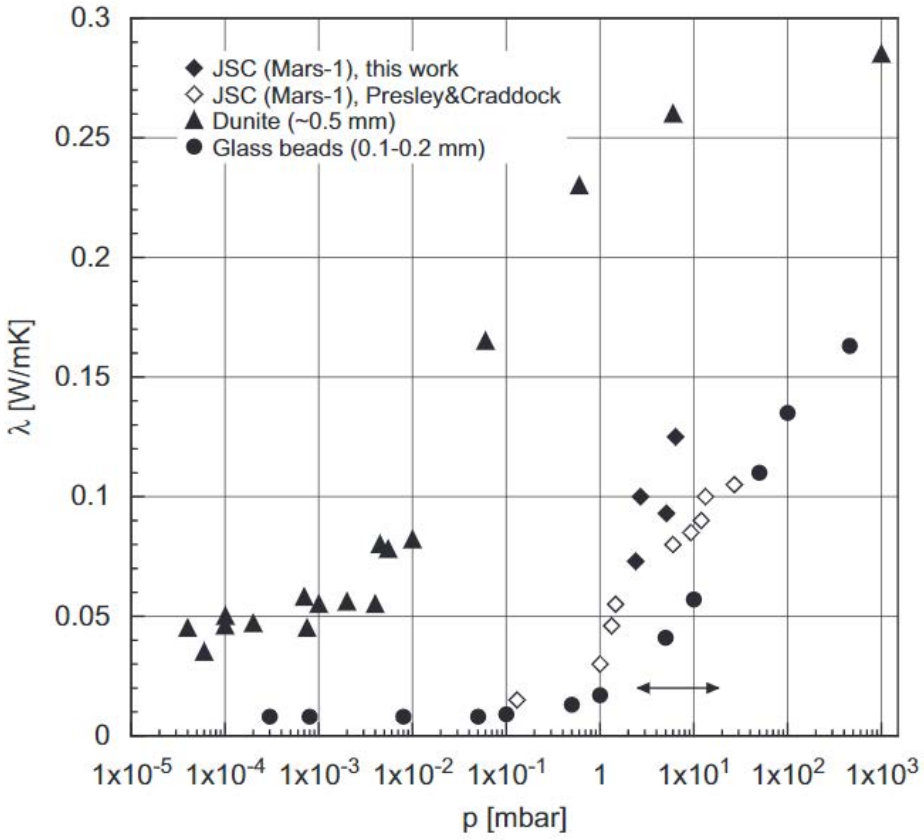

Figure 3.7: *Thermal conductivity of JSC-Mars-1 simulant under different pressures. Open diamonds: Seiferlin et al.[53] , closed diamonds: Presley and Craddock[54]. The arrows indicate the pressure range on Mars, retrieved from [53].*

these seismic velocities and the regolith density. A range of 43.5 - 51.2 MPa for the Young's modulus was calculated for densities ranging between 1300 and 1533 kg/m3 [56].

3.3.3. Comparison between actual and simulated Martian regolith

A proper comparison between actual and simulated Martian regolith is very difficult due to the lack of actual samples. Nevertheless, some properties of Martian regolith have been investigated in-situ and can be compared. The first of these properties is the chemical composition. Comparing Table 3.8 and Table 3.7 it is clear that the regolith simulants approach the compositions of actual regolith material.

The particle size distribution from Figure 3.6 falls within the boundaries specified for Martian regolith (10-2000 μm). However, the PSD does not show any of the bimodal behaviour observed in-situ. Therefore, in order to give a better approximation the simulant needs to be sieved in order to reach this bimodal distribution.

The particle shape differs between Martian regolith simulant and actual material. The actual regolith is subangular to rounded, whereas most simulants are angular to subangular. This is a result of the processing methods used (mostly crushing). Therefore, to create a better simulant representation, the material needs to be processed to create a smoother particle.

Another noteworthy difference is the amount of water in the simulant. The early simulant JSC-Mars-1 contains a considerable amount of water, whereas the actual Martian regolith is very dry [55]. Other simulants, like MMS, have less hydroscopic tendencies, e.g. lower water absorption over time and volatile content (which is thought to be predominantly water) [50]. It is known that water absorption can change the physical properties of a material [50], indicating that a less hydroscopic simulant is preferable.

The bulk densities of the regolith simulants show a larger spread than the bulk densities observed on Mars, but in general comply to the specific types of simulant (soil, dust, etc). Care needs to be taken in the regolith selection that the bulk density does not fall out of the range.

Because the Poisson's ratio and the Young's modulus have not been determined in-situ, we can only compare these values to other similar materials. These can be of terrestrial or Lunar origin. When comparing the Poisson's ratio to that found for lunar regolith (0.2-0.31) to that found by Delage et al. (0.2) it is clear that the value falls within this range. Therefore, the estimate for the Poisson's ratio is assumed accurate. A similar comparison can be made for the Young's modulus. The estimates for Martian regolith fall within those for Lunar regolith simulants.

The porosity of actual regolith is estimated to be between 31 and 50%, which corresponds to the values found for several simulants by Ramkissoon et al. Therefore, these estimates are deemed accurate.

The thermal conductivity shows a large variation between derived values for actual regolith and those observed for simulants. This is most likely due to the differences in density, which has a high effect on the thermal conductivity. The values for simulants are approximately two times that of the estimates for actual regolith. This means that this parameter is still highly variable and care must be taken in selecting the proper value.

In conclusion, the particle shape and size distribution are the most promising areas for improvement of the Martian regolith simulants. The particle shape needs to be made rounder and the PSD should show a bimodal distribution. Other mechanical parameters agree with those found for Lunar regolith and simulants, providing feasible estimates.

3.4. Derived resources from in-situ materials

Next to using regolith material as-is, it can also be processed into several other useful materials. This section aims to give an overview of the possible materials and compounds that can be obtained from existing Lunar and Martian resources using specific processing methods as well as discussing their application. First, the production of water and oxygen is covered followed by a discussion on ISRU metal production. Finally, polymer production on the Moon and Mars is discussed.

3.4.1. Hydrogen, Oxygen and Water

Hydrogen, oxygen and water are expected to be among the first compounds to be produced in-situ. This is because they can be used to sustain a human population (hydrogen as fuel in fuel cells, oxygen for breathing and water for consumption) as well as produce different useful materials. Key in this application is the production of oxygen for use as rocket fuel [15]. Especially on Mars this is very attractive, since the carbon dioxide rich atmosphere can be used to produce methane fuel, meaning no additional fuel needs to be imported from Earth.

On the Moon, hydrogen might be produced from hypothesised polar ice deposits or implanted solar wind particles in the upper layers of the regolith. On Mars, hydrogen might be obtained by the electrolysis of water from water-ice deposits as well as from hydrolysed minerals.

Oxygen can be produced using several different methods. For a comprehensive overview, readers are referred to the discussion by Schrunk et al. ([6], Appendix E). Schrunk et al. identify several different processing groups for oxygen production. These are: gas/solid systems, gas/liquid processes, bulk electrolysis processes, pyrolysis processes, slurry/solution processes and caustic dissolution and electrolysis. Next to oxygen, some of these methods also produce metals that can be used for different applications.

3.4.2. Metal Production

Metals can be obtained as byproducts of the water and oxygen production on the Moon and Mars. Therefore, they become readily available for use in other applications, like the creation of structural materials. Nano-particle iron, which if found in Lunar regolith, can be easily separated out using magnetic separation. The other metals can be obtained using refining processes. Alloys can be made from all the major elements and minor elements, although carbon (critical for manufacturing steel) is not common enough on the Moon and therefore needs to be imported [17]. On Mars, on the other hand, the relatively CO2 rich atmosphere provides a way to create carbon, possibly as a byproduct of oxygen production [15].

One of the difficulties in producing metal is the refining process. This because the metal is only found in difficult to refine compounds, like primary oxides. Generally, there are several steps to be taken in the refining process: concentration, metal separation, purification and alloying. After this, additional steps like heat-treatment and forming methods are often required to create alloys with the desired properties. Due to the many steps involved, an extensive industrial infrastructure needs to be established in order to support this [17].

That being said, metals find their applications in a variety of fields and therefore a simplified metal production technology is desired in the early stages of colony development. In order to make this as efficient as possible, the energy requirement for production needs to be as low as possible. This makes steel the primary candidate, as it can be refined with much less energy compared to other metals like aluminium (for which the energy requirement is about six times as high [57]) [17].

Generally, the Moon is rich in iron, silicon, aluminium, titanium and magnesium. All of these metals are common engineering materials. These five metals are also found on Mars and are generally considered to be of high value. Therefore they are also interesting choices

as matrix materials for the described research.

3.4.3. Polymer Production

Next to the production of metals, polymers can also be produced using ISRU methods. This is mainly focused on Mars, where the carbon dioxide rich atmosphere and the availability of water (although in limited quantities) facilitates polymer production. The simplest polymer that can be synthesised in-situ is polyethylene (PE). This is done by first synthesising ethylene from methane by using oxygen. Subsequently, ethylene is polymerized to form polyethylene.

3.5. Summary of Regolith Properties

Table 3.9 gives a summary of the regolith properties that are discussed above for easy future reference. Properties of both actual and simulant material are presented.

Table 3.9: *Summary of regolith properties. Values for both actual and simulant material are presented.*

Property	Lunar Actual	Simulant	Martian Actual	Simulant
Bulk density [kg/m3]	1500 - 1660	-	1150 (drift) - 1636 (crusty)	835 - 1950
Grain density [kg/m3]	-	-	2600	
Average particle size	40 - 130 μm	-	-	
Mean particle size	70 μm	-	-	
Particle size distribution (PSD)	0.1 - 1 mm	0.1 - 1 mm	10 - 2000 μm	
PSD shape	Approx linear on log scale	Approx linear on log scale	Bimodal. Merdiani Planum - Mode I: <125 μm, Mode II: 1-4.5 mm Gale Crater - Mode I: 100 - 250 μm, Mode II: 500-2200 μm"	Approx linear on log scale
Particle shape	Slightly elongated subangular to angluar	Subrounded to rounded	Angular to rounded, high degree of circularity	Angular to subangular
Average porosity [%]	44-52 $\pm$ 2		31 - 58	47.7 - 51.7
Average void ratio	0.78 - 1.07 $\pm$ 0.07		-	-
Young's modulus, E [GPa]	-	11-36 Mpa - 19 - 65 Mpa	-	43.5 - 51.2 Mpa
σ_c [MPa]	-	-	-	-
Flexural modulus [GPa]	-	-	-	-
Fracture toughness [MPa$\sqrt{m}$]	-	-	-	-
Bulk modulus [GPa]	-	-	-	-
Poisson's ratio, ν	0.2 - 0.31	0.27 - 0.42	-	0.2
T_m [°C]	1320 - 1350	TBD (not reported before, action point)	TBD (not reported before, action point)	TBD (not reported before, action point)
k [W/(mK)]	-	-	0.017 - 0.048 (0.032 median)	0.055 - 0.18
CTE [ϵ/K]	-	-	-	-
Cost [EUR/kg]	TBD	TBD	TBD	TBD

4

Regolith applications and considerations

There has been a large interest in the application of regolith material over the past decades. This has resulted in a host of different studies focusing on the applications of regolith material. This chapter covers the application of different regolith for different purposes in Section 4.1. However, several considerations have to be made before regolith material is used. These consideration are discussed in Section 4.2. Finally, Section 4.3 gives a summary of some important regolith efforts to use regolith as a filler and the resulting properties of the composite materials.

4.1. Application of Regolith material

Due to the abundance of regolith material on extra-terrestrial bodies it has long been an interesting resource to use in various different applications. Four main applications can be identified. These are structural, radiation shielding, thermal and impact protection. Structural and radiation shielding applications have been the most investigated among these. Each of the subsequent subsections deals with one of these applications.

4.1.1. Structural application of regolith

Regolith can be processed in order to create materials fit for structural application. These construction materials need to have high properties. This includes high strength, ductility, durability, stiffness, tear, puncture and abrasion resistance [17]. They also must have a high stability and low thermal expansion. Several researchers have attempted to create such a (composite) material from regolith by using different processing methods.

By melting regolith, a cast basalt material can be made. Melting lunar regolith requires high temperatures in the range of 1320 to 1350 °C [58]. The resulting homogeneous solid material has glassy features and can be used to create materials suitable for construction. It can be manufactured into bricks and other structural members using molding methods [31]. A downside of this processing method is the high energy requirement. The energy requirement for this processing methods is as high as 360 kWh/MT [17]. Cast lunar regolith can also be processed into Lunar glass, see Table 4.1 for some mechanical properties of lunar glass. Molten basalt can also be processed (drawn) to produce fibers with an estimated tensile strength of 2-2.9 GPa and Young's modulus of 80 GPa [59]. Naser compiled a list of properties for cast and sintered basalt from a variety of literature sources. In this review it is shown that cast basalt has a compressive strength ranging between 162 - 550 MPa and 162-490 MPa for lunar and Martian cast basalts respectively [31]. Using the approximated ratio of compressive strength to tensile strength by Happel of 15:1 [57], the estimated tensile strength range is 10.8

- 36.7 MPa and 10.8 - 32.7 MPa respectively. Both of these are higher than commonly used concrete [31] and Portland cement [60].

Table 4.1: *Properties of cast and drawn lunar materials, adapted from [31]*

Property		Lunar glass	Lunar cast regolith
Compressive strength	[MPa]	–	538
Tensile strength	[MPa]	0.7 - 3000	34.5
Young's modulus	[GPa]	450	100
Flexural modulus	[MPa]	125-630	-
Density	[kg/m^3]	2700	900-3000

A different process that involves heating the material is sintering. In this case the regolith is heated to a temperature below the melting point, making it more interesting from an energy point of view. For lunar regolith, sintering is done at around 1000-1200 °C [31, 61]. During sintering particles of a powdered material fuse together creating one solid piece. However, pores are created during the sintering process and porosity is known to affect material strength [62]. Indyk and Benaroya investigated the effect of porosity on samples sintered from lunar regolith. They tested samples of two different porosities, 1.44% and 11.78% respectively. The samples were created from JSC-1A lunar simulant sieved into two grades, the first with particles <212 μm and the second with particles larger than 212 μm. The finer powder became the low porosity sample set and the coarser the larger. Sintering of the pre-pressed samples took place at 1120 °C for 15 minutes. An image of the sintered samples can be seen in Figure 4.1. The study found that decreasing porosity increases the material properties. The tests showed an average compressive strength of 218.8 MPa and 84.6 MPa for 1.44% and 11.78% porous samples respectively [62]. Unfortunately, no data for sintered Martian regolith simulant was found in literature.

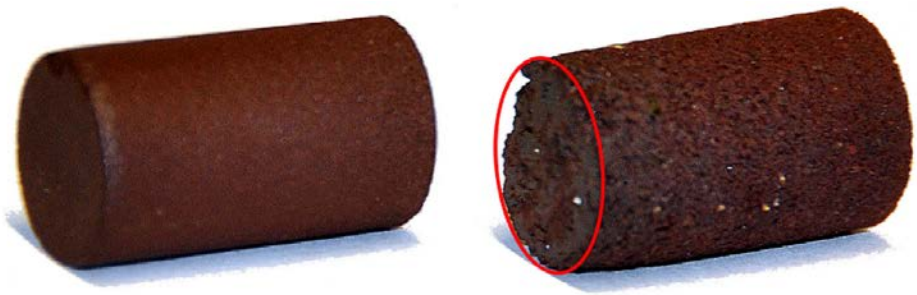

Figure 4.1: *Sintered lunar regolith samples of different porosities of 1.44 % (left) and 11.78 % (right) respectively. Adapted from [62]*

Similar to melt processing of regolith, sintering requires a large amount of energy. Spedding, Nuttall, and Lim calculated that the energy requirement for thermally sintered regolith is 381 kWh/MT [61]. Another downside of sintered regolith, next to the formation of pores, is that it generally shows a high degree of variability. The material is highly heterogeneous and properties are difficult to characterize. Based on current knowledge, a sophisticated structural design using this material is appears not feasible. Nevertheless, it is a good candidate for non-structural applications like radiation shielding and launch/landing debris barriers [17].

Faierson et al. showed that a ceramic material can be made from lunar regolith using a self-

propagating high temperature synthesis (SHS) method. In this method a geothermite reaction occurs which reaches temperatures high enough to melt the lunar regolith. In a subsequent study, Faierson et al. used a mixture of 67 wt% JSC-1AF and 33 wt% aluminium powder to create physical assets usable for construction. After cool down, the compressive strength was found to vary between 10 and 18 MPa [64]. Corrias et al. performed similar experiments, this time with added ilmenite (FeTiO3) and aluminum to several different lunar and martian regolith simulants. Their regolith weight fraction ranged between 10 and 45.2 % with the rest made up by aluminium (15.99 - 34.79 wt %) and ilmenite. They reported a maximum reaction temperature in the range of 1500-2000 K, high enough to melt the regolith. The materials displayed compressive strengths of 27.2 MPa and 25.8 MPa for 20 wt% and 30 wt% lunar regolith samples respectively. Delgado and Shafirovich investigated the use of magnesium as a substitute for aluminium. Their experiments were performed in a vacuum chamber and involved several different weight fractions of magnesium, ranging between 7 and 26 wt%. Steady propagation of the combustion front for non preheated samples was observed at a magnesium fraction of 13 wt%. Preheating the samples to 100 °C decreased this limit to 10 wt%. They also investigate the effect of SHS sample compression just after the reaction. This resulted in an increase in density of 60-66 %. A maximum compressive stress of 10.2 MPa was found for a mixture of 26 wt% magnesium and 74 % regolith simulant compacted at 19.6 kN. Processing temperatures reached between 1288 °C and 1375 °C during the experiments [66]. Importantly, they also noted that the process should be performed under pressure in an inert gas environment to prevent vaporization of magnesium on the Moon [66]. These issues are less critical on Mars

Creating concrete like materials with regolith as a filler is another method to create materials suitable for structural applications. This is a trivial step to make, since concrete production and properties are well understood for the material on Earth. Several different types of concrete can be produced. Firstly, 'ordinary' concrete using Portland cement and water can be made. However, this requires large amounts of water and is difficult to do on the Moon. This is because curing water-based concrete requires a pressurised environment. Casting and curing is just one of the challenges. Manufacturing cement is also a challenge, as it is a complex and energy intensive operation. Cement requires 2200 kWh/MT [17]. It also requires a large infrastructure to be established, and so will only occur late in the establishment of a colony [17]. Heemskerk, Van Westrenen, and Foing investigated different concretes made from lunar and martian regolith and ordinary Portland cement. He reported that the minimum compression strength and flexural strengh of lunar concrete were 24.41 MPa and 7.30 MPa. For Martian concrete these values are 24.36 MPa and 4.76 MPa respectively. A downside of this investigation was that no experiments were performed under actual environmental conditions.

Next to traditional cement, different binder materials can be used that might provide a feasible alternative to regular concrete. These alternatives include sulphur based concrete [68–71], polymer concrete [72–75], geopolymer concrete [76] and magnesium based concrete [77].

Lunar concrete based on regolith with a sulphuric matrix is claimed to be very useful for habitat construction [68]. The main reasons for this is the abundance of material and high strength and durability. Glass fibers can also be drawn from regolith and incorporated in to the concrete in order to create tensile loading capabilities [68]. A downside of sulphur concretes for lunar applications is that the binder is not compatible with the large temperature range on the lunar surface [74]. Schwandt et al. also investigated the use of sulphur concrete but this time for use on Mars. Several different simulant and sulphur mixtures were produced. The mixutures were heated to a temperature above 120 °C to melt the sulphur and were thoroughly mixed. Next, the mixture was poured into aluminium moulds and left to cool to room temperature. Mechanical tests were performed after 24h. The optimal mixture was found to consist of 50 %

sulphur and 50 % simulant. The compressive stress exceeded 50 MPa for this mixture ratio. Flexural strength was found to be 7.24 MPa. Recycling by means of recasting was found possible and produced similar strength results.

Lee et al. demonstrated in a feasibility study that lunar concrete landing pads can be made using lunar regolith material and a polymer binder. To increase the strength, they incorporated glass fibers in their second prototype tile. An image of the second prototype can be seen in Figure 4.2. This tile was tested in compression, resulting in a compressive strength of 2.7 MPa. It was shown that this is sufficient for landing the Japanese SELENE-B lander [78]. Different studies from the same researcher focused on creating polymer concrete from lunar regolith material and a polyethylene (PE) binder. Two approached were used, the top-down [79] and bottom-up heating [80]. Both investigations used a mixture of 90 wt% lunar regolith simulant to 10 wt% polymer binder and experiments were preformed in vacuum. In the case of the top-down heating approach, the material was heated to 230 °C and attained a maximum compressive strength of 12.9 MPa after 5h [79]. The bottom-up approach lowered the processing temperature to 200 °C and a maximum compressive strength of 5.7 MPa was reached. However, even though the compressive strength was considerably lower, it was still deemed applicable for lunar construction. Additionally, the bottom-up approach solidified two times faster than the top-down approach [80]

Figure 4.2: *Scaled up landing pad tile made from lunar regolith simulant, glass fibers and a polymer binder [78]*

.

Sen, Carranza, and Pillay also investigated creating polymer concrete from regolith simulant and polyethylene. In their experiments they used two different production methods. The first was a liquid infiltration technique. This produced specimens for compression, radiation and impact testing. Regolith simulant was mixed with certain weight percentages polyethylene and heated to 140 °C to completely met the polymer. Next, pressure up to 240 MPa was used to infiltrate the void spaces with polymer. They uses mixtures of 0, 20 and 40 wt% PE. The second was an extrusion-compression process which resulted in specimens for flexural testing. 60 wt% regolith was mixed with 40 wt% polymer and mixed in a rotational drum mixer. Afterwards it was extruded and, while heated, compressed. This method was considered to be an improvement over the liquid infiltration method by the authors. The maximum compressive stress and flexural strength were found to be 40.1 MPa and 45 MPa respectively [72]. Sen, Carranza, and Pillay also subjected their 40 wt% binder composite to a number of temperature cycles and evaluated the effect of these cycles on the mechanical properties. They cycled their material between ambient and liquid nitrogen temperatures. The results of these tests for the Young's modulus and compressive strength can be seen in Figure 4.3. From the

figure it becomes clear that the properties hardly changed during thermal cycling, indicating a good thermal stability.

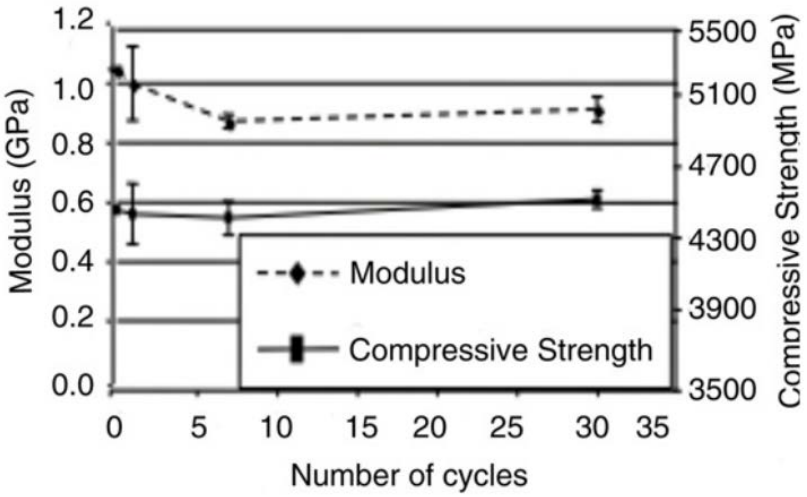

Figure 4.3: *The effect of thermal cycling on the Young's modulus and compressive strength. Temperature varied between ambient and liquid nitrogen [72]*

Scott and Oze demonstrated the feasibility of Magnesium-based cement for the production of concrete on Mars. Although in this study no actual regolith simulants were used, materials with similar properties were locally sourced and provided a sufficient approximation to the actual material according to the authors. The study showed that olivine, a regionally abundant material on Mars, can be potentially used to create Mg-based cement as well as atomic Hydrogen (H2) that can be used as fuel. Since this process uses a serpentinization reaction, the energy requirement is relatively low. Use of this method is primarily constrained to the availability of water [77].

Additive manufacturing methods are also used to create structures from regolith. Several different methods for additive manufacturing using regolith exist. These include the use of sintering to consolidate the layers [81], using sulphur/polymers as a binder [82, 83] or a specialized binding liquid [84]. The last method, known as the D-shape process, was introduced by Cesaretti et al. They showed that this method worked in vacuum conditions [84] and requires little binder mass (around 10 % [61]). The mechanical properties of D-shape processed speciments were also determined. The maximum compressive stress, Young's modulus and flexural strength were found to be 20.35 MPa, 2.35 GPa and 7.10 MPa respectively [84]. Also, minimal heating is needed in the process which results in a low processing energy requirement. Spedding, Nuttall, and Lim assumed a value of 10 kW required power for this process [61].

Roedel, Lepech, and Loftus created a regolith biocomposite (RBC) by mixing a protein binder with regolith simulant. Lunar JSC-1A regolith was used mixed with a Bovine Serum Albumin (BSA) protein solution in a vacuum assisted resin infusino method (VARIM). Protein weight percentages varied between 6.6 and 7.6 wt%. Compression tests were performed on specimens cut from the vacuum infused block. The Young's modulus caried between 850 and 1300 MPa for 6.6 and 7.6 wt% samples respectively. The ultimate compressive stress varied between 6.28 and 12.5 MPa for 6.6 and 7.5 wt% samples respectively. The authors noted that the energy and up-mass requirements of RBC are similar to other proposed methods [75]

Chen et al. [73] developed a method to create an inorganic-organic hybrid (IOH) materials suitable for structural application. These materials are made from a small amount of binder material mixed with a large amount of (in this case lunar) regolith. The material can also be pressed to high pressures to increase the properties. Binder fractions can be as low as 2-5 wt% [74]. During pressing, the binder forms bridges connecting the filler grains creating a series of polymer micro-agglomerations (PMA's), see Figure 4.4.

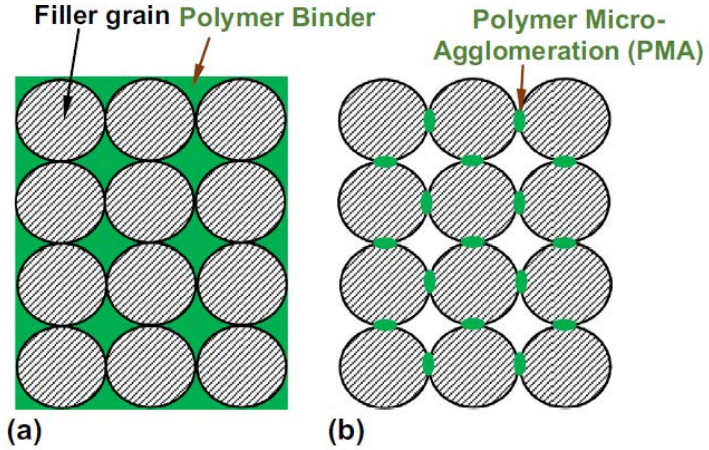

Figure 4.4: *Schematics of (a) close-packed filler grains, with the interstitial space being filled by 8.6 wt% binder; and (b) polymer micro-agglomerations (PMA) that bridge the filler grains together in an IOH [74]*

Pressures during this process can range between 30 and 700 MPa [85]. During pressing, binder droplets are squeezed between filler grains. Subsequently, PMA's are formed by large capillary forces driving binder material around direct contact points. A schematic representation of this process is shown in Figure 4.5.

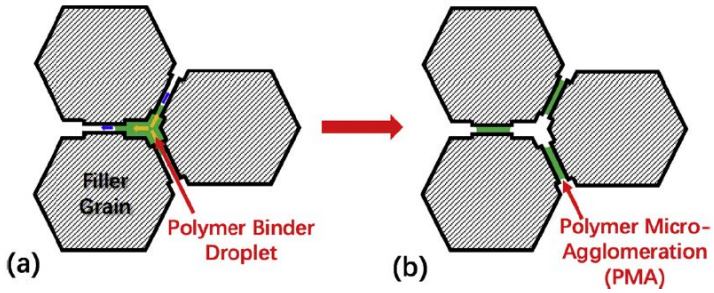

Figure 4.5: *Schematics formation of PMA's. (a) a binder droplet is squeezed in between filler grains; (b) large capillary force drives the binder into the narrow space around direct contact points, forming PMA's [74]*

Different polymer binders can be used in this process. These include PE [73], unsaturated polyester resin (UPR) [85] and epoxy [74]. No pressure was applied in mixtures using a PE binder. Different binder weight fractions, ranging between 2.2 and 30.3 wt% were hand mixed with a spatula and subsequently heated to 300 °C for 10 minutes. Flexural strength was measured using three-point bending tests. This resulted in values between 0.8 and 11.5 MPa depending on PE content. A threshold value of 10-15 wt% PE was identified above which flexural strength varies little with binder content [73]. The samples made with UPR and epoxy

resin followed similar production methods. First, the binder was mixed with the simulant material and stirred using a spatula. Afer this, the mixture was transferred to a steel mould and subsequently pressed, broken up and repressed several times. The compression duration at max pressure ranged from one minute to one/several hour(s) An optimal pressure of 200-350 MPa was determined [74]. Most binder content reduction was seen after one minute [85]. After pressing the samples were cured in a 100 °C box furnace for one hour. The flexural strength was finally measured similar to the PE samples. For both binders the flexural strength ranged between 30 - 40 MPa, significanlty higher than the values for PE. However, the epoxy mixture required less binder, 2-5 wt% vs 6.5-8.7 wt% respectively [74, 85].

4.1.2. Regolith for use in radiation shielding

In Section 2.3 the different types of space radiation and their effect and importance has been discussed. In this subsection different methods to use regolith for radiation shielding are presented. Specific attention is paid to the processing methods and radiation shielding effectiveness.

Radiation protection is mainly focused on protecting organic lifeforms, material and structures from the two main sources of harmful radiation in space: Galactic Cosmic Rays (GCR's) and Solar Particle Events (SPE's). Commonly two different strategies are distinguished to provide radiation protection. These are active and passive radiation protection. Active shielding relies on the generation of a electric/magnetic field to deflect space radiation. This is unlikely to be used in the early stages of space exploration due to the complexity mass and energy requirement involved. Therefore the second strategy, passive radiation protection, is most often used. In this strategy, a material is placed in between the radiation source and the elements to protect. It is based on attenuation of radiation by absorption in the material or decay of incident particles. Fragmentation of incident particles decreases their energy and harmful effect. However, during these interactions secondary radiation might be created. Next to projectile fragmentation, target fragmentation can also occur. This degrades the radiation shielding material thereby lowering the shielding effectiveness. Therefore, when designing radiation shielding materials, projectile fragmentation is preferred over target fragmentation [11]. For habitats on other bodies, local regolith can be used to provide passive radiation protection in several different ways.

One method to use regolith for radiation shielding uses unprocessed regolith. This readily available material is relatively easy to obtain and can be deposited on top of a structure in a significantly thick layer in order to provide enough protection. It is estimated that this layer will be around 2.5m thick [37]. A downside of using unprocessed regolith is the relatively large amount of secondaries that are generated. Figure 4.6 shows that some of these secondaries only diminish slowly with depth, requiring additional protection strategies. However, it can be shown that lunar regolith is more effective in shielding than, for example, aluminium Figure 4.7.

On Mars, martian regolith can be used for radiation protection too. However, because of Mars' atmosphere and the possibility of Martian regolith to contain light elements, this layer can be thinner than on the Moon. A proposed layer thickness that takes into account both the impact and radiation protection is 1m, while a 2m thickness would reduce exposure to almost negligible levels [86].

A different method is, again, by combining regolith with a binder material to form a composite. This conclusion can also be drawn by looking at Figure 4.7, where it is implied that the shielding efficiency of regolith improves when you combine it with a better shielding material. Polymers are a common choice for binder material as they are lightweight, easy to process and are

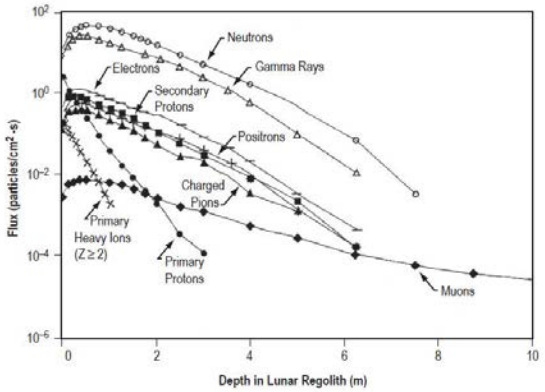

Figure 4.6: *Particle flux vs depth in lunar regolith [12]*

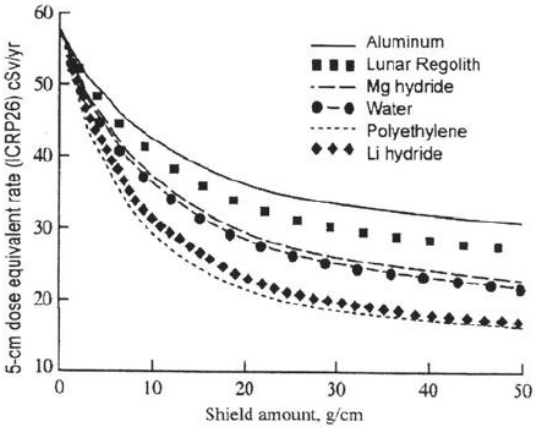

Figure 4.7: *Dose equivalent rate vs shield amount for several different materials. [12]*

rich in hydrogen. Low atomic number, or Z, materials such as hydrogen have been shown to provide effective shielding against GCR's and SPE's [11]. Therefore, several researchers have attempted to create composites with polymer binders for radiation protection [72, 87, 88].

Kim et al. investigated he theoretical radiation attenuation of Martian regolith and regolith composites made with an epoxy binder. The models were generated by solving the Boltzman equation using a HZETRN system [89] and evaluated the theoretical absorbed dose and dose equivalent values. The results of these model evaluations can be seen in Figure 4.8 and Figure 4.9 for the absorbed dose and dose equivalent respectively. From the figures it is clear that both the absorbed dose and the dose equivalent values decrease for increasing binder fraction. They concluded that adding epoxy enhances shielding abilities. This was attributed to the hydrogenous constituents of epoxy [88].

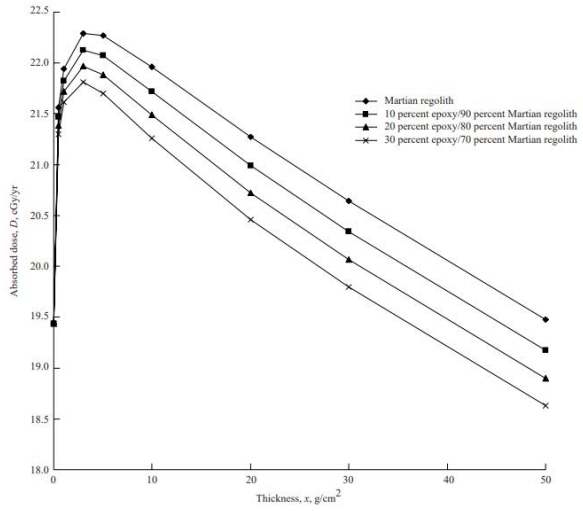

Figure 4.8: *Absorbed dose per year for Martian simulant and several different composites of different binder weight fractions and thicknesses [88]*

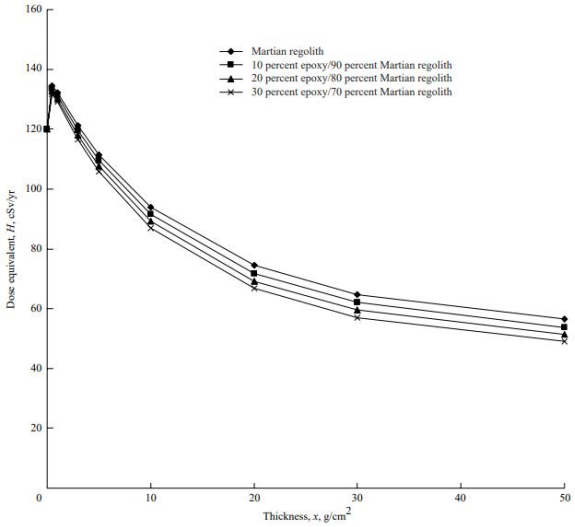

Figure 4.9: *Dose equivalent per year for Martian simulant and several different composites of different binder weight fractions and thicknesses [88]*

In a later study by the same author a different polymer composite was investigated. This

time the composite was made from Martian regolith simulant and LaRC-SI polyimide binder. They investigated both the mechanical as well as the radiation protection properties. Two different samples of 20 and 40 wt% polymer were used during the study. The samples were fabricated at 320 °C using a compression moulding process (2.66 MPa of pressure applied). 15x15 cm cross section samples were created. Experiments under proton beam testing showed that the samples with 40 wt% binder were more effective at shielding than the 20 wt% samples. During mechanical testing, samples that were exposed to the proton beam exhibited higher Young's moduli than the unexposed samples. One explanation for this is the formation of crosslinks in the irradiated sample, increasing strength. Neutron exposiure decreased the Young's modulus by about 10 %. The ultimate compressive strength of 20 wt% polymer binder samples was higher than those of 40 wt% samples, 195 MPa vs 230 MPa for baseline (non-irradiated) samples respectively [87].

As mentioned above, the polymer composite by Sen, Carranza, and Pillay can also be used for radiation protection. They evaluated the radiation shielding effectiveness using a radiation transport code. This code solves the one-dimensional Boltzmann equation, similar to Kim et al. The results of this calculation can be seen in Figure 4.10. From the figure it becomes clear that the largest amount of PE (40 wt%) results in the best dose-equivalence values. Using this mixture, a wall thickness of approximately 20 cm was determined by the model. Samples containing 20 wt% PE were fabricated of 3.81x3.81x2.54 cm^3 for radiation testing. During testing, a 0.5 GeV/u ^{56}Fe beam was used as an approximate representation of the GCR environment. These samples were compared to pure simulant values and the fragmentation characteristics were investigated. The result can be seen in Figure 4.11. It is clear that the composite sample has a greater capability of projectile fragmentation [72].

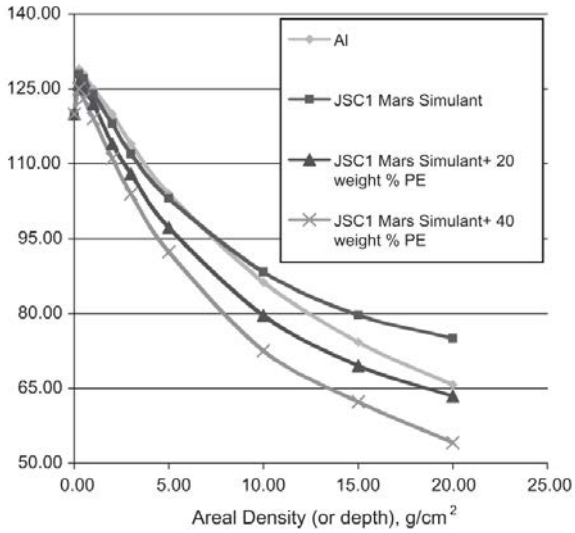

Figure 4.10: *Dose equivalent as a function of material thickness for several materials. The 1986–1987 solar-minimum GCR environment was used for the calculations. Similar results were obtained for the solar-maximum environment [72]*

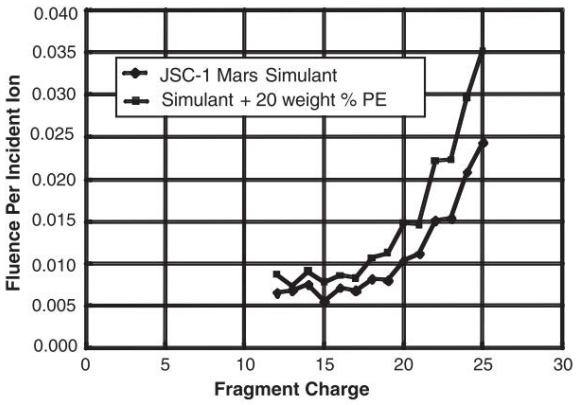

Figure 4.11: *Fragment charge vs fluence per incident ion, indication that composite samples have a higher capability of fragmenting the incoming radiation [72]*

4.1.3. Thermal protection/isolation using regolith

A loose lunar regolith layer can also be used as thermal insulation because of the low thermal conductivity of lunar regolith [37]. A regolith layer in the range of centimeters to meters would

be enough to protect against the large thermal fluctuations experienced on the Moon [5]. For logistic reasons, the required layer thickness needs to be minimised, while still also providing adequate protection from radiation and meteoroids. On Mars the average temperature is higher and the temperature difference is lower, which indicates that the thermal situation on Mars is less harsh than on the Moon. The thermal shock behaviour and thermal stability of materials in important in these type of rapidly changing temperature conditions.

4.1.4. Impact protection using regolith

Unprocessed lunar regolith can also be use for impact protection. Again, a layer of material of a specific thickness needs to be deposited atop a structure/habitat. Using the Fish-Summer penetration equation and selecting an estimate (7cm) for the maximum size meteor such a blanket will protect against, a minimal layer thickness of 45.9cm is calculated [5]. As mention in the section above, on Mars the required regolith layer thickness would be lower that that on the Moon, with values in the range of 1-2m [86].

Sen, Carranza, and Pillay demonstrated that the strain to failure is an important parameter for evaluating the impact resistance of polymer regolith composites. Addition of polyethylene significantly increased the strain to failure and thereby the impact protection of their samples [72].

4.2. Considerations for using regolith material

The previous section shows that a lot of different materials can be made using/incorporating regolith. These materials are created using specific production processes and amounts of regolith. Focus in the previous section was placed on the mechanical, thermal and other useful properties of the final composite material, but little consideration was made for additional factors that influence the choice for the most optimal material. This section aims at discussing some of those considerations. Specifically, the energy required for production, the mass considerations and the sustainable/renewable production methods are discussed. Finally, a quantitative trade-off between several production methods is presented based on the data from the previous sections.

4.2.1. Energy consideration for the use of regolith

In the previous sections many different production methods for regolith based (composite) materials. The amount of energy required for these production methods differ substantially and warrant a discussion about the available energy for production on the Moon/Mars.

Currently, no infrastructure of any kind is present on any extra-terrestrial body. This means that a large supply of power is also not available. Production processes that require a lot of energy, like the sintering process, therefore pose additional challenges compared to less energy intensive processes like compression moulding. Additionally, processes that require maintaining specific ambient parameters like pressure and temperature are also very energy intensive. This is especially important for concrete production using ordinary Portland cement, as the optimal material properties are only achieved under certain production conditions (e.g. specific temperature and pressure).

4.2.2. Mass consideration for the use of regolith

Most of the mentioned regolith applications above use regolith in a composite material. These composites are generally made of (minimally processed) regolith and some kind of binder material. This means that the binder material needs to be available as well in order to create the composite. These additional materials can be obtained from a variety of sources, but three

main ones can be identified. The first is to import the material from Earth, the second from nearby bodies (near Earth objects - NEO's and planets other than Earth) and the third one is sourcing the material locally.

The last two sources probably require a material to be processed in order to obtain a compound usable for the composite. One advantage of importing material from Earth, in this case, is that all materials can be fully produced on Earth and are therefore immediately usable on site. The main downside, however, is that importing material from Earth is very inefficient and expensive. This is because Earth's large energy well makes it difficult to send large quantities of materials to different bodies and the current cost of launches is high. Therefore, importing material from Earth to use in composites is only viable if the composite material requires a minimal amount of material from Earth. This means that the composite should mainly be made of locally sourced material (e.g. regolith) with minimal binder required.

A different mass consideration is related to the required infrastructure for processing. This is not necessarily related to the processing energy. A low energy requirement process, such as compression moulding, still requires the transportation of (large amounts) of potentially heavy equipment. Therefore, a production process might be attractive in terms of energy, but not in terms of the required infrastructure required. Therefore, the most optimal solution for the production of resources on extra-terrestrial bodies is found by a trade-off between required energy and required infrastructure.

4.2.3. Renewable production

Any material that is not readily available on an extra-terrestrial body needs to be considered as valuable since easy replacement is not possible. This means that most imported and all locally produced materials have to be considered as such. The latter is true because any locally produced material required precious energy and time in order to produce usable (e.g. large) quantities. Optimal use of these valuable compounds can only be made if the produced materials are renewable. This means that they can be recycled or at least down-cycled. Renewable production methods using recyclable materials need to be developed in order to be able to do this. Therefore, choosing a renewable production method is an additional consideration when choosing materials and processing methods for the production of regolith derived materials.

4.2.4. Trade-off per processing method

As testified by the previous two sections, choosing the most optimal method to process regolith requires a trade-off between several different factors. One method to perform this trade-off is via the use of a quantitative trade-off table. This table can be seen in Table 4.2 for several different processing methods.

From the table it becomes clear that all different processing methods have their strength and weaknesses. Choosing a specific processing method therefore depends on the specific assumptions and boundary conditions we want to place on the subsequent research. However, since the scope of the research is focused on filled composite with the lowest amount of binder, one aspect still needs to be evaluated before making a final decision. This aspect is porosity. Porosity has an effect on most characteristics of a material and therefore these effects in low volume fraction regolith composites on the mechanical, thermal and radiation protection aspects needs to be known.

Additionally, when compiling the table it became clear that a good distinction between the different required masses and energies is not commonly considered. An example for this is the required up-mass in terms of infrastructure for polymer concrete production. In literature, it is not specified what type of infrastructure is required, how much it weighs and what kind of energy requirements are needed for operation. This point of energy and mass considerations

needs to be investigated further.

4.3. Regolith application summary table

To summarize the information presented in the previous sections and to provide a reference database, an applications summary table has been made. This table can be found in Appendix A. In the table, the processing method, simulants/binders used, filler volume fractions and some mechanical properties are presented. Additionally, some small notes are supplied for reference.

Table 4.2: *Quantitative trade-off table for regolith processing methods*

Processing method	Required up-mass - M	Required up-mass - I	Processing energy	Processing temperature	Processing time	Mechanical properties	Early applicability
Melting	None	high	moderate	high	short	high	no
Sintering	None	high	moderate	high	short	high	no
3D printing	low	variable	low	low	moderate	moderate	maybe
Self-propagating	high	low	low	very high	short	low	maybe
Regular concrete	high	high	high	low	long	moderate	no
Sulphur concrete	high	low	low	moderate	moderate	moderate	maybe
Polymer concrete	high	low	low	moderate	moderate	low - moderate	maybe
Protein binding	moderate	low	low	low	moderate	low	maybe
IOH	low	moderate	low	moderate	short	moderate	maybe

5

Introduction and properties of granular composites

As shown, there are different applications for regolith (structural, protection, etc). To do this, a variety of different methods and materials are used, ranging from pure, untreated regolith to sintered regolith, from binder-less applications to applications with binder. One relatively less explored material classes are the granular composites that can be made using regolith material. This class falls in the category of materials that use regolith with a binder. It might be suited for the mentioned applications if their properties are sufficient enough. Granular composites can be made with a variety of different binders (or matrix materials), ranging from polymers to metals and ceramic. To assess whether this material might suitable, first the general characteristics of this material class need to be investigated.

This chapter covers the general properties of granular composites for composites with a polymer, metal and ceramic matrix respectively in order to understand their characteristics. Where possible, specific attention has been paid to composites with a high filler volume fraction (FVF).

5.1. Introduction to granular composites

A composite material can be defined as a combination of two or more materials with significantly different physical or chemical properties. Combining these materials results in a composite material that has better properties than the individual components. Generally, two main phases can be identified in a composite material, a matrix phase and a reinforcement phase. Usually, the matrix phase is continuous and the reinforcement phase is embedded within this matrix. This reinforcement phase, also called embedded or dispersed phase, is of a discontinuous form.

Composite materials can be classified based on their matrix material. Generally, three classifications are used: polymer matrix composites, metal matrix composites and ceramic matrix composites. These materials can be further classified based on the morphology of the reinforcing phase. Here, we distinguish between fibre composites, particulate composites, flake composites and filler composites as shown in Figure 5.1.

In our case, granular composites are investigated because of our use of granular regolith material. Specifically, granular composites with extremely high filler volume fractions (larger

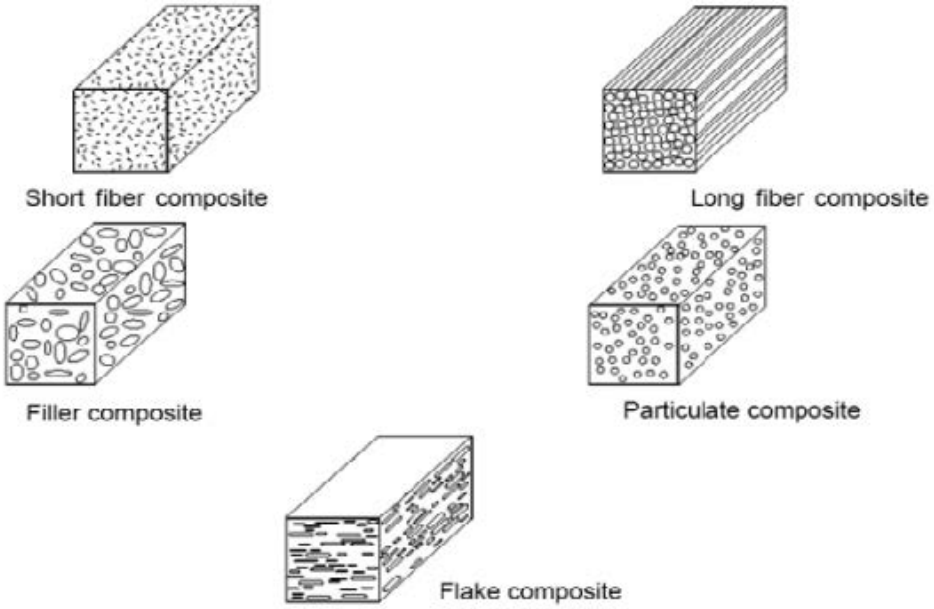

Figure 5.1: *Different types of composite materials [90]*

than 70%) will be considered. These materials are widely used because of their compromise between strength and toughness [91]. In granular composite materials, the granulate, also called particulate, is dispersed in a matrix material. This matrix material is yet to be chosen from polymers, metals or ceramics.

The mechanical, thermal and electrical properties of the composite are determined by the following parameters: 1) the properties of the matrix phase; 2) the properties of the particulate phase; 3) the interfacial properties between the matrix and the particulate and 4) the dispersion of the particulate phase in the matrix phase.

The properties of the matrix phase depend on the matrix material and continuity within the composite. For example, a continuous conductive matrix can form conductive paths within a composite, whereas a discontinuous matrix might hinder conduction.

The properties of the particulate phase depend on its volume fraction; particle shape, size and distribution; and the orientation and dispersion within the composite. These properties can be adjusted both from starting material conditions and processing techniques. For example, mechanical sieving changes the particle size distribution of the particulate phase. The dispersion of the particulate phase is especially important for creating a homogeneous material. It is known that smaller particles are harder to disperse, thereby making it harder to create a homogeneous material. This is because small particles are more likely to form agglomerates, e.g. gatherings of smaller particles in larger size units [92].

The interfacial properties depend on the interface area and morphology, which are determined by the particulate phase, and the wetting characteristics of the matrix phase. Particles with a high specific surface area (aggregates and minerals with high porosity) provide the largest interfacial area, mineral particles the lowest. Highly porous particles can also provide a way of mechanical bonding between matrix and particle. This is due to matrix locking within sufficiently large pores [92]. Changing either the matrix or the particulate phase has an effect on the interface properties. For example, by changing the matrix material, the wetting properties are altered. And, by changing the size of regolith particles, the interface area can be influenced.

The above shows that designing particulate composites requires careful consideration due to the many variables involved. This also results in a large range of properties that are possible with these material, making them very attractive.

5.2. Properties of Granular Composites

In this section the general properties of granular composites are discussed. Unless explicitly stated, most of the properties are matrix unrelated. Specific attributes related to the matrix material are discussed in sections 5.3 through 5.5. In order to predict the properties of a particulate composite from the known properties of its constituents and their respective volume fractions, different theories were developed. These models will be used to get an understanding of the mechanical (Subsection 5.2.1) and thermal (Subsection 5.2.2) properties of granular composites.

5.2.1. Mechanical properties of Granular Composites

The mechanical properties of a material determine the behaviour of that material under the action of external forces. They are commonly used to determine whether a material is suitable for a specific application. Additionally, different materials can be compared to each other by comparing their mechanical properties.

The mechanical properties of a granular composite material depend on the four main parameters discussed above. For the mechanical properties of composites in general, the particle-particle and particle-matrix interactions are more important than the matrix material. Therefore, the subsequent discussion focuses on general mechanical characteristics independent of matrix material. Models to predict the mechanical properties are discussed below. First, some general first estimation methods are discussed, followed by some specific empirical expressions for and information about the Young's modulus, the tensile and yield strength, impact resistance, compressive strength and the fracture behaviour.

General first estimation methods

First estimates of the properties of a granular composite can be obtained by two different averaging methods which are based on different loading conditions. These are equal strain and equal stress loading. These load cases cases can be explained using a continuous fibre composite. Isostrain occurs when the composite is uniaxially loaded along the fiber direction (phases in parallel), isostress occurs when the composite is loaded perpendicular to the fiber direction (phases in series).

For the isostrain case, the total deformation of the composite is equal over both phases. By summing the total force, after some manipulation, the following equation is found:

$$\mathrm{X}_c = \mathrm{X}_f \cdot \phi + \mathrm{X}_m \cdot (1 - \phi) \tag{5.1}$$

where:

X is the specific property;
ϕ is the filler volume fraction (FVF).
and subscripts c, f and m indicate the composite, filler and matrix respectively.

This equation is also known as the rule of mixtures. Many material properties, like the Young's modulus, can be substituted for X. Since we are considering regolith to be the filler in our present study, we will be using the regolith filler volume fraction throughout the following discussion.

For the isotress loadcase (series load case), the expression changes. This time the elongation of each phase has to be calculated separately. After some manipulation, the expression in Equation 5.2. Readers are referred to Shackelford[93] for a full derivation of the past two equations.

$$\mathrm{X}_c = \frac{\mathrm{X}_f \mathrm{X}_m}{\phi \mathrm{X}_m + (1-\phi)\mathrm{X}_f} \tag{5.2}$$

Similar to Equation 5.1, different properties can be substituted for X. The equal strain condition results in a theoretical upper bound whereas the equal stress condition represents a theoretical lower bound of a combined (averaged) property. This can be seen in Figure 5.2 where the Young's modulus of an epoxy-E-glass composite is given for several different filler fractions of glass fibre.

Equation 5.1 and Equation 5.2 can be written in the general form:

$$\mathrm{X}_c^n = \mathrm{X}_f^n \cdot \phi + \mathrm{X}_m^n \cdot (1-\phi) \tag{5.3}$$

In this equation the exponent n is limited to values between -1 and 1. For the first approximation for a higher-modulus aggregate in a lower-modulus matrix can be represented by the case where $n \approx 0$ [93]. Graphs for several different values of n for the same epoxy-E-glass composite can be seen in Figure 5.3.

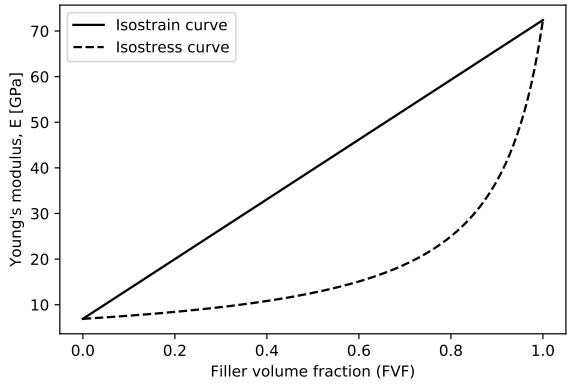

Figure 5.2: *Composite Young's modulus estimate based on the glass fibre filler volume fraction. The limits are given by the modulus of pure epoxy and pure glass fibre. Note how the rule of mixtures presents an upper bound and the series solution a lower bound. Adapted from [93].*

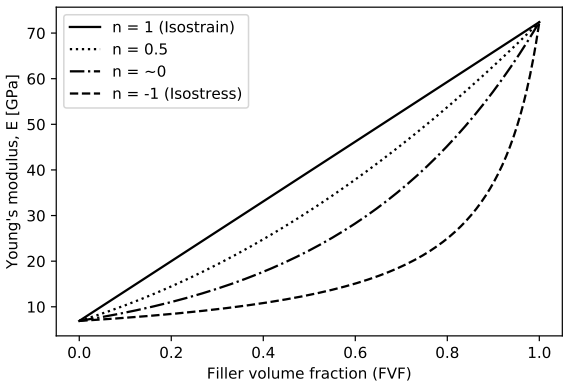

Figure 5.3: *Composite Young's modulus estimate based on the glass fibre filler volume fraction from Equation 5.3 for different values of n The limits are given by the modulus of pure epoxy and pure glass fibre. Adapted from [93].*

Young's Modulus

The Young's modulus is a mechanical property that measures the stiffness of a material. It is frequently used to characterize and compare different materials. Several empirical models, in addition to the models discussed above, exist that give a prediction of the Young's modulus at low filler volume fractions. A first estimate is given by the Einstein viscosity equation modified by Guth and Gold, Equation 5.4 [92, 94].

$$\mathrm{E} = \mathrm{E}_0 \left(1 + 2.5\phi + 14.1\phi^2\right) \tag{5.4}$$

where:

E is the Young's modulus of the composite;
E_0 is the Young's modulus of the matrix phase;
and ϕ is the filler volume fraction (FVF).

Einstein's equation assumes that the viscosity of a filled system is a linear function of a small volume fraction. Another assumption in this equation is that the viscosity of the filler is much higher than the viscosity of the medium [94]. The analogy can be made for the Young's modulus, requiring that the Young's modulus of the filler is much higher than the matrix. Because of the assumptions, this equation is only valid for small filler volume fractions up to around 10% [95].

The Young's modulus of particle-filled composites is often described by the Kerner equation. The derivation of this method is based on the calculation of several mechanical properties (bulk and shear modulus) for a macroscopically isotropic and homogeneous composite. This equation can also be used to determine the bulk and shear moduli of filed composites. When the filler particle is much more rigid than the matrix and good adhesion between the matrix and particles is assumed, the Kerner equation can be simplified to the form [96]:

$$E = E_0 \left[1 + \left(\frac{\phi}{1-\phi} \right) \left\{ \frac{15(1-\nu)}{8-10\nu} \right\} \right] \tag{5.5}$$

where:

E, E_0 and ϕ are the same as in Equation 5.4;
and ν is the Poisson's ratio of the matrix.

Similar to the previous model, this equation is only valid for low FVF. For filler fractions approaching unity, it can be seen that the equation tends to an infinite stiffness which is physically impossible. Another downside of these methods is that they start to deviate for high filler fractions. A different empirical method is the given by the Halpin-Tsai equations. These are an approximation of the Kerner equation [97] and are given by:

$$E = E_0 \left\{ \frac{1 + \xi\nu\phi}{1 - \nu\phi} \right\} \tag{5.6}$$

where

$$\nu = \frac{R-1}{R+\xi} \tag{5.7}$$

and

$$\xi = \frac{7-5\nu}{8-10\nu} \tag{5.8}$$

for spherical fillers. ξ is a measure of the reinforcement geometry, R is the ratio of filler modulus to matrix modulus [98]. These equations can also be used to provide boundaries to the properties of a composite [97].

Tensile and Yield Strength

The tensile strength describes the maximum stress a material can withstand without breaking when it is being pulled. Similar to the Young's modulus, it is commonly used to characterize and compare materials. The yield strength of a material describes the stress at which a material starts to deform plastically. The tensile and yield strengths of a particulate composite depends on the filler concentration, particle shape, size and distribution and the particle-matrix interaction. Smaller particles, especially nano-sized ones, typically contribute to an increase in tensile strength [91, 92]. The aspect ratio of a particle, determined by the particle shape and size, has been found to be an important parameter as well. If it falls within a certain range, the tensile strength of the composite is increased. Good adhesion between the particle and matrix has been shown to improve the tensile strength of a composite material. This means that choosing the proper composite system is important for reaching the optimal properties.

Empirical models have been developed that describe the tensile properties of filler materials. Since the tensile and yield strength of a material depend on similar parameters, a parallel between the equations can be drawn. Therefore, unless explicitly stated, the methods discussed below can be used to estimate both the yield and tensile strength. For the discussion, the tensile strength will be used. A general equation for the tensile strength can be seen in Equation 5.9 [92].

$$\sigma_{\mathrm{ct}} = \sigma_{\mathrm{m}} \left(1 - \mathrm{a}\phi_{\mathrm{f}}^{\mathrm{b}} + \mathrm{c}\phi_{\mathrm{f}}^{\mathrm{d}}\right) \tag{5.9}$$

where:

σ_{ct} is the tensile strength of the composite;
σ_m the tensile strength of the matrix;
and ϕ_f volume fraction of filler

In this equation, a, b, c and d are constants. The constant "a" usually relates to stress concentrations, "b" is given the arbitrary value of 0.67 and "c" and "d" include the effects of particle size. Decreasing particle size increases the value of these constants. A decrease in particle size, according to the formula, leads to an increase in tensile strength. In composites with poor filler adhesion, values for "a" range between 1.21 (spherical particles) to 1.23 (non-spherical particles) [92]. Many modifications of this general equation are used to fit experimental data.

One frequently used modification is an adaptation of the Einstein equation by Nicolais and Narkis. In this equation, the second term of Equation 5.9 is omitted and the constants "a" and "b" are assigned the values 1.21 and 2/3 respectively. This equation can be seen in Equation 5.10 [99]:

$$\sigma_{ct} = \sigma_m(1 - 1.21\phi_f^{\frac{2}{3}}) \tag{5.10}$$

A downside of the above mentioned equations is that neither considers the particle-filler interaction. One equation that does include this effect is given by Pukanszky and VÖRÖS[100]:

$$\sigma_{\mathrm{cy}} = \sigma_{\mathrm{m}} \frac{1 - \phi}{1 + 2.5\phi} \exp(\mathrm{B}\phi) \tag{5.11}$$

where:

σ_{cy} yield stress of composite;
σ_{m} yield stress of matrix;
ϕ volume fraction of filler;

and ”B” is the parameter encompassing the effect of interface interaction, including interlayer thickness, interface strength and filler specific surface area.

Impact Resistance

Fillers are known to improve the impact strength of filled materials. Different factors contribute to this. The first is the particle size, which increases the impact strength for certain ranges, see Figure 5.4. Next, the aspect ratio (particle shape) of the particle filler is most important. Additionally, the particle rigidity has an effect, with hard particles generally increasing impact resistance and soft particles decreasing the property. The last factor is crystallinity, which can be improved by fillers creating nucleation points.

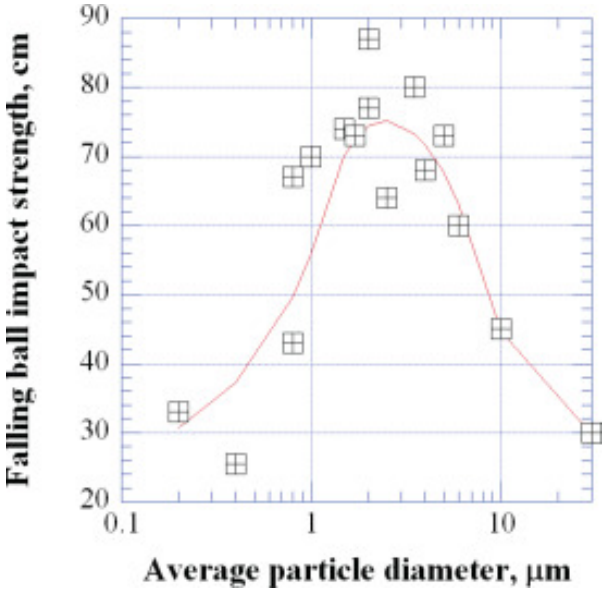

Figure 5.4: *Impact strength vs average particle diameter, from [92]*

Lower filler concentrations lead to higher impact performance. This is because interparticle distances are increased while agglomerate formation is decreased, leading to better performance.Where proper matrix adhesion is preferred in mechanical properties like tensile strength and Young’s modulus, the maximum impact strength is often found for non-perfect adhesion. This is because the matrix is more constrained in the case of perfect adhesion, resulting is a stiffer and more brittle material and thereby reducing impact strength. This means that a specific trade-off between the desired properties needs to be made.

Compressive Strength

The compressive strength of a material can be related to other mechanical properties via [92]:

$$\sigma_{cc} = KG_R = K\left[\frac{E}{2(1-\nu)}\right] \tag{5.12}$$

where σ_{cc} is the compressive strength, K is a constant, G_R is the matrix shear modulus, E_τ is the Young’s modulus and ν is the Poisson’s ratio. From the equation it becomes clear that the compressive strength depends on the stiffness, and therefore the parameters affecting the Young’s modulus also affect the compressive strength.

Fracture Resistance

Fracture of particle composites can occur in several different fracture modes depending on the amount of filler material. These range from ductile failure to brittle failure, with quasi-brittle failure in between. For high filler volume fractions with hard filler particles, it is likely that ductile failure will not occur. Therefore, in the following discussion, focus is placed on quasi-brittle and brittle fracture. Of these two, the latter is the most likely as filler concentration will likely be above 50 %.

For the quasi-brittle fracture of type C, see Figure 5.5a, failure stars by the formation and growth of voids along the particle inclusions. Next, these voids coalesce laterally and fracture initiates, see Figure 5.5b. For fractures of type D, fracture initiates at one side and propagates at an angle. As the crack grows, the fracture path will change direction and become almost perpendicular to the loading direction, see Figure 5.5c. In fracture mode E, brittle fracture, there is no indication of particle debonding. Instead, particles fractures together with the matrix.

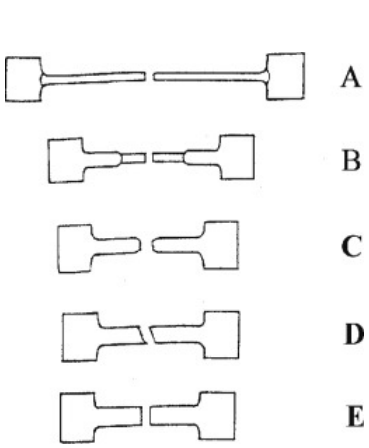

(a) *Five tensile failure modes. A) ductile failure mode, B) neck propagation mode, C) quasi-brittle neck formation, D) macro-shear-banding failure and E) brittle failure*

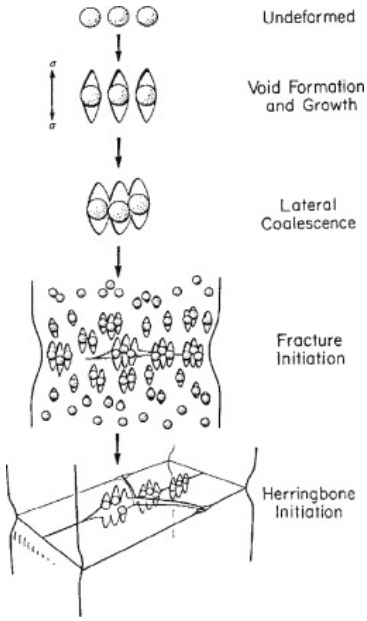

(b) *Schematic representation of mode C failure*

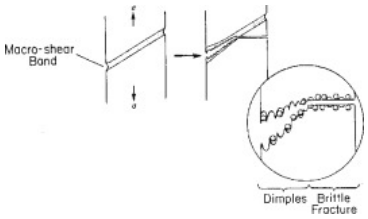

(c) *Schematic representation of mode D failure*

Figure 5.5: *Fracture modes in tensile failure with schematic representations for quasi-brittle failure [92]*

From the above discussion, it becomes clear that the adhesion between particle and matrix is very important in the fracture resistance [101], but an optimum can be defined. To much adhesion and the matrix loses some of its ability to deform, thereby becoming more brittle, lowering the fracture resistance. To little adhesion and the effective load carrying cross section is drastically reduced, lowering the fracture resistance as well. Some models for lower filler volume fractions (in the range of 0 - 50 %) exist. One of these is the modified Einstein equation, Equation 5.13 [92], in which no adhesion between the filler and matrix is assumed.

$$\sigma_c = \sigma_m \left(1 - 1.21\phi^{2/3}\right) \tag{5.13}$$

where:

σ_c is the fracture strength;
σ_m the fracture strength of the matrix;
and ϕ is the filler volume fraction.

In this equation, the fracture strength decreases with increasing filler volume fraction. However, fracture stress might also increase. For random-packed monodisperse spheres of filler volume fraction in the range of 0 to .56, the constant in Equation 5.13 changes from -1.21 to 1.06. This indicates a slight increase with increasing filler volume.

5.2.2. Thermal Properties of Granular Composites

The thermal characteristics of a material are used to determine the material response to heating or cooling. The thermal properties of granular composites depend on three main factors: 1) the type of filler material used; 2) the thermal properties of the matrix material and 3) the interactions within the material. Generally, polymer and ceramic matrices are considered to be insulators whereas metallic matrices are conductors. Similarly, most non-metallic fillers are thermal insulators and metallic fillers are conductors. Because regolith material mainly consists of ceramic compounds, it can mostly be considered an insulating filler. Although many thermal properties can be defined for a material, here the focus will be placed on the thermal conductivity and coefficient of thermal expansion.

Thermal Conductivity

The thermal conductivity of a material is a measure of the material's ability to conduct heat. For a composite material, it depends on the matrix material, the particle material and the amount of filler in the composite. Generally, fillers used for reinforcement purposes have much lower CTE than metals and plastics [92]. Heat is conducted within a material via two processes. The first is via phonon transmission, also known as lattice vibration. Phonon or latice waves transmit energy in their direction of motion from a high temperature region to a low temperature one. The second process is via free electron movement. Here, electrons gain kintetic energy in a high temperature region, move to a low temperature region and lose dissipate the extra energy via atom collisions. For most non-metallic materials heat transfer predominantly occurs via phonon transmission.

The easiest way to facilitate phonon transmission is by the presence of connected conducting paths. In granular composites the presence of these continuous paths depend on the filler volume fraction. When the filler volume fraction of the material increase above a certain level, continuous paths start to form due to particle-particle interaction. This level is known as the percolation limit and stems from percolation theory.

In the filled granular composites currently under consideration, it is highly likely that the percolation limit of the material is surpassed due to the high filler volume fraction. Therefore, connected particle-particle paths are very likely to exist. Similarly, for extremely high filler volume fractions it is equally likely that a connected matrix phase no longer exists. This has to be taken into account when selecting the proper model for this property. However, initially models were developed for low FVF composites with spherical fillers. Although these models are not directly suitable for our applications, they serve as a basis for the development of more applicable models. Therefore, these basic models will be discussed first, working towards more complex and suitable models.

Several different empirical methods exist for estimating the thermal conductivity of low FVF

materials. In most of these methods, the filler material is assumed to be isotropic, homogeneous and randomly distributed within the matrix material. For spherical particles with no interactions, the heat conductivity of the composite is calculated using the Maxwell-Eucken equation for a two phase system [102, 103]:

$$\frac{k_c}{k_m} = \frac{2k_m + k_f + 2\Phi\left(k_f - k_m\right)}{2k_m + k_f - \Phi\left(k_f - k_m\right)} \tag{5.14}$$

where:

Φ is the filler volume fraction and k_c, k_f and k_m are the conductivities of the composite, filler and matrix respectively. For different particle shapes that are close to circular, a variation of the Halpin-Tsai equation (Equation 5.6) can be used [104]:

$$\frac{\mathrm{k}_c}{k_m} = \frac{1 + AB\Phi}{1 - B\Phi} \tag{5.15}$$

where:

$$A = k_E - 1 \tag{5.16}$$

and:

$$B = \frac{k_f/k_m - 1}{k_f/k_m + A} \tag{5.17}$$

In these equations, "A" is a function of the geometry of the filler particles depending on the Einstein coefficient "k_E". An advantage of the second method over the first is that it takes the particle shape into account. However, both of these equations assume that there are no particle-particle interactions, which is virtually impossible at higher volume fractions. Building on his model for predicting the elastic modulus, Nielson [105] proposed a model that also included the effect of maximum filler content, see Equation 5.18. Adding the parameter "ψ" does this by including the maximum packing factor for the dispersed phase (ϕ_m), which also helps to account of agglomeration [104]. Note how similar this equation looks to the Halpin-Tsai equation. However, this model again only applies to low filler volume fraction composites.

$$\frac{k_c}{k_p} = \frac{1 + AB\phi}{1 - B\psi\phi} \tag{5.18}$$

where:

$$\psi \doteq 1 + \left[\left(1 - \phi_m\right)/\phi_m^2\right]\phi \tag{5.19}$$

However, neither of these above mentioned methods take the particle-particle interactions into account. In the case that the particles are conductive, interacting particles form conduction paths that allow easy heat conduction. To account for particle-particle interactions, the Bruggeman model can be used [104, 106]. This model applies to interacting spherical particles. The Bruggeman model can be derived from the Maxwell equation [104] and the final thermal conductivity is obtained as a solution of the nonlinear equation:

$$\frac{k_f - k_c}{k_f - k_m}\left(\frac{k_m}{k_c}\right)^{\frac{1}{3}} = 1 - \phi \tag{5.20}$$

Drozdov and Christiansen[104] showed that the continuation of the Halpin-Tsai equation for large filler volume fractions using the integration embedding method resulted in an equation

very similar to the Bruggeman model, see Equation 5.21. This model is also suited for large volume fractions of particles taking the particle size in effect.

$$\frac{k_f - k_c}{k_f - k_m}\left(\frac{k_m}{k_c}\right)^{\frac{1}{A}} = 1 - \phi \tag{5.21}$$

Thermal Expansion Coefficient

Most materials expand when heated and contract when cooled. Thermal expansion occurs because of the asymmetric shape of the potential energy well. The change in length of a material with a change of temperature can be expressed with the following formula [107]:

$$\frac{l_f - l_0}{l_0} = \alpha_l (T_f - T_0) \tag{5.22}$$

where:

l_f is the final length of the material;
l_0 is the original length;
α_l is the linear coefficient of thermal expansion (CTE);
and $(T_f - T_0)$ represents the temperature change.

The coefficient of thermal expansion, α, is a material property that indicates the amount a material expands upon heating. For composite materials that consists of two or more different materials, these coefficients might be very different. This mismatch in CTE results in the build-up of residual stresses upon heating or cooling. These residual stresses might surpass the yield strength of the components, might induce debonding/delamination and can cause cracking [107].

The first estimate for the CTE of a two-phase composite material can be calculated using the rule of mixtures:

$$\alpha_c = \alpha_f \phi_f + \alpha_m \phi_m \tag{5.23}$$

where:

α_c, α_f and α_m are the CTEs for the composite, filler and matrix respectively;
and ϕ_f and ϕ_m the filler and matrix volume fractions respectively.

However, several other factors contribute to the CTE causing deviations from the rule of mixtures. The occurrence of plasticity and the internal structure of the composite are examples of these factors [108]. As an improvement on the rule of mixtures The Kerner equation [109] can be used. It takes into account the stiffness of the constituent materials as well as the volume fractions. The Kerner model assumes discontinuous spherical filler particles uniformly coated with matrix material. The equation reduces to the rule of mixtures for composites for which the bulk modulus of the components is equal. An expression for the Kerner model is given by [95, 108–110]:

$$\alpha_\mathrm{c} = \alpha_\mathrm{m}\phi_\mathrm{m} + \alpha_\mathrm{f}\phi_\mathrm{f} + \phi_\mathrm{m}\phi_\mathrm{f}(\alpha_\mathrm{f} - \alpha_\mathrm{m})\frac{K_\mathrm{f} - K_\mathrm{m}}{\phi_\mathrm{m}K_\mathrm{m} + \phi_\mathrm{f}K_\mathrm{f} + 3K_\mathrm{m}K_\mathrm{f}/4G_\mathrm{m}} \tag{5.24}$$

where:

K_f and K_m are the bulk moduli of the filler and matrix respectively;
and G_m is the shear modulus of the matrix material.

A simpler model that still takes into account the bulk modulus of the material is the Turner model [111]. This model assumes that strain is homogeneous throughout the composite and that the only stresses in the phases are uniform hydrostatic stresses unable to disrupt the composite [108]. The Turner model can be expressed in terms of volume fraction as [108]:

$$\alpha_{\mathrm{c}} = \frac{\alpha_{\mathrm{f}}\phi_{\mathrm{f}}K_{\mathrm{f}} + \alpha_{\mathrm{m}}\phi_{\mathrm{m}}K_{\mathrm{m}}}{\phi_{\mathrm{f}}K_{\mathrm{f}} + \phi_{\mathrm{m}}K_{\mathrm{m}}} \tag{5.25}$$

When a composite is made of components that have nearly equal values of Poisson's ratio, the bulk moduli are nearly proportional to corresponding Young's moduli. This means that the bulk modulus in Equation 5.25 can be replaced with the Young's modulus.

Moreover, the Turner model is used to describe composites with a percolating reinforcement [112]. This means the models is also expect to work well with high volume fraction granular composites in which the percolation limit has been exceeded.

Upper and lower bounds for the coefficient of thermal expansion can be used to give a ballpark range for this material property. Schapery [113] proposed a method based on energy principles. In his method, the upper and lower bound for the CTE are given by Equation 5.26 and Equation 5.27 respectively [108, 113].

$$\alpha_c^{(+)} = \alpha_f + \left(\alpha_m - \alpha_f\right)\frac{\frac{1}{K_c^{(-)}} - \frac{1}{K_f}}{\frac{1}{K_m} - \frac{1}{K_f}} \tag{5.26}$$

$$\alpha_{\mathrm{c}}^{(-)} = \alpha_{\mathrm{f}} + (\alpha_{\mathrm{m}} - \alpha_{\mathrm{f}})\frac{\frac{1}{K_{\mathrm{c}}^{(+)}} - \frac{1}{K_{\mathrm{f}}}}{\frac{1}{K_{\mathrm{m}}} - \frac{1}{K_{\mathrm{f}}}} \tag{5.27}$$

In these equations, the upper and lower bound for the bulk modulus ($K_c^{(+)}$ and $K_c^{(-)}$ respectively) need to be calculated. It is in the bulk modulus calculation that the only effect of filler volume fraction is found. Expressions for the upper and lower bound for the bulk modulus are given by Schapery as:

$$\hat{K}^{(-)} = K_m + \frac{\phi_f}{\frac{1}{K_f - K_1} + \frac{\phi_m}{K_m + \frac{4}{3}G_1}} \tag{5.28}$$

$$\hat{K}^{(+)} = K_f + \frac{\phi_f}{\frac{1}{K_m - K_f} + \frac{\phi_m}{K_f + \frac{4}{3}G_f}} \tag{5.29}$$

He concluded that these expressions are equal to those proposed by Hashin and Shtrikman[114].

Now that the general mechanical and thermal properties of granular materials has been discussed, it is time to go deeper into the analysis by considering matrix specific effects and their effect on the granular composite. This will be done for granular composites with a polymer matrix (Section 5.3), metal matrix (Section 5.4) and ceramic matrix (Section 5.5). Again, attention will be paid to the mechanical and thermal properties of these composites and the effect of the matrix thereon.

5.3. Granular composites with a polymer matrix

Composites with a polymer matrix have received a lot of attention over the past decades. This is because the combination of lightweight polymers with several different type of fillers (particles, fibres, etc) offer the possibility to create highly tailored materials with properties combining both the positive aspects of the polymer matrix and the filler material. Pure polymers have relatively low mechanical properties, making them unattractive on their own, but using fillers of different types can greatly increase these properties. This section aims at giving an overview of the properties of a specific type of filled composites, namely those with a granular/particulate filler.

Typical particulate fillers for polymer matrix granular composites are glass beads (GBs) and minerals. Especially the former has been used commonly as a filler because of the improved stiffness, hardness, compressive and impact strengths, dimensional stability, abrasion resistance and reduced thermal conductivity, dielectric permeability, shrinkage and costs [115].

5.3.1. Mechanical properties of polymer matrix granular composites

The mechanical properties of granular composites with a polymer matrix depend largely on the properties of the components, the polymer and filler material. In order to create composites that exhibit superior performance compared to the bare polymer material, hard filler materials are usually added [116]. Additionally, the polymer-matrix interaction plays a large role in the mechanical properties of the composite. In order to approximate the tensile behaviour of a filled composite, the rule of mixtures can be used [117].

An additional parameter of influence in the mechanical behaviour of polymer-matrix based composites is the crystallization behaviour of the matrix polymer. In some (semi-)crystalline polymer composites, the matrix might crystallize at the filler surface changing the mechanical properties. This indicates that the polymer orientation might affect the mechanical properties [92].

Several empirical methods exist in order to describe the effect of filler fraction on the modulus of the composite. One common method for polymer matrix composites is the Kerner equation (Equation 5.5). This is applicable for a systems where the filler is much more rigid than the matrix [96].

Several researchers have investigated the effect of intermediate filler fractions (0 - 50 volume percent) on the mechanical properties of filled polymers for a variety of different systems [101, 117, 118]. The results of these investigations vary and are sometimes contradictory. For example, some researchers found an increase in tensile strength [117] and some found a decrease [118] for increasing filler volume fractions, see Figure 5.6.

A crucial factor influencing the strength of the composite is the is the bonding at the interface [117]. This effect is investigated by Hsieh et al. in their study with GB modified polymers. Here, they test three different samples: one control, one with a positive effect on interface bonding (Silane treatment) and one with a negative effect (Frekote treatment). The results show that the Silane treated system generally shows better performance than the control or Frekote treated systems. Interestingly, no apparent effect of interface bonding was visible in the fracture toughness response of the composite, suggesting that this increase might be attributed to other effects. Graphs showing the effect of surface treatments on the Young's modulus and fracture toughness can be found in Figure 5.7 and Figure 5.8.

An additional element to take into account when using polymers is their temperature dependent mechanical properties. Generally, polymers lose mechanical strength at increased temperature mainly due to a loss of stiffness (Young's modulus). This effect has been known for a long time. An example of the decrease in stiffness can be found in Figure 5.9 for ultra-high molecular weight polyethylene (UHMWPE). At lower temperatures polymers tend to become more brittle. This decrease in mechanical properties with an increase in temperature is known

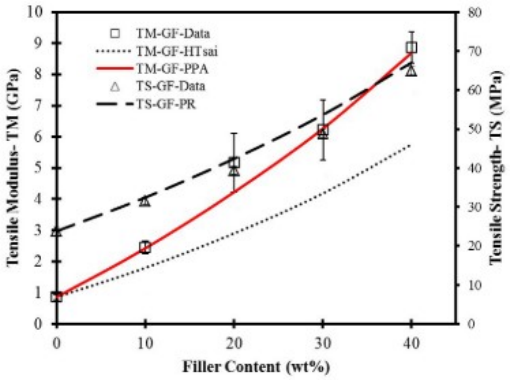

(a) *Increasing filler fraction leads to increasing tensile strength [117]*

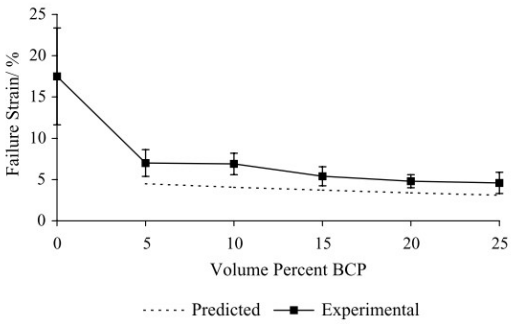

(b) *Increasing filler fraction leads to decreasing tensile strength [118]*

Figure 5.6: *Differences in tensile strength response, showing both increase and decrease.*

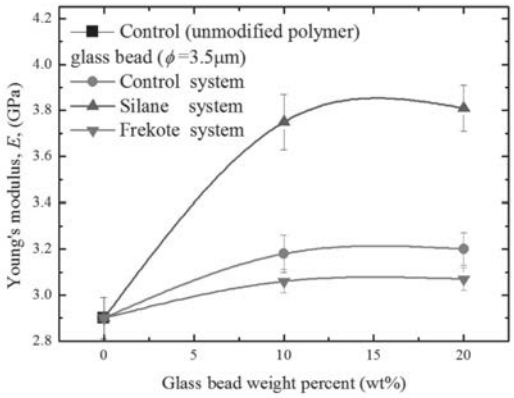

Figure 5.7: *Young's modulus of GB modified polymers with different surface treatments [101]*

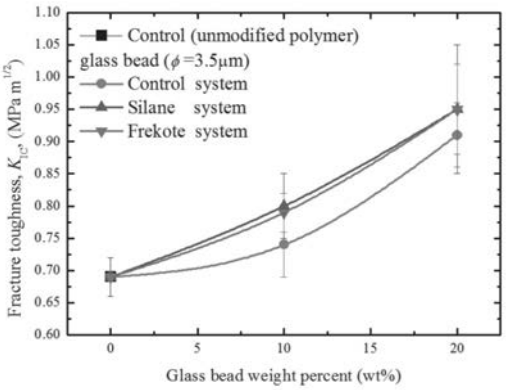

Figure 5.8: *Failure strain vs BCP content, showing the trend towards the predicted values [118]*

as glass transition in semi-crystalline polymers. Amorphous polymers gradually lose mechanical strength with increasing temperature, they do not experience a glass transition. The maximum service temperature for polymers is generally taken 10 degrees Celcius lower than the glass transition temperature. Table A.2 gives an overview of the properties of commonly used engineering polymers. It also notes their glass transition and melting temperatures. Comparing these to the temperature range on the Moon is is found that the maximum temperature is above the service temperature for polyurethane and epoxy. Ultra-high molecular weight PE (UHMWPE) and Polycarbonate barely meet the requirement. This indicates that the temperature variation on the Moon is an important consideration for designing the materials. Additionally, the Moon's very low temperatures might cause these polymers to become more brittle, thereby making them more susceptible to damage by (micro)meteorite impact.

The different models in Section 5.2 can be compared to data points gathered by the authors discussed in Chapter 4. This might provide insight in which methods are applicable to our research goal of estimating the properties of highly filled regolith composite materials. An important factor in plots similar to Figure 5.2 is the end values, e.g. the value for pure well consolidated regolith material. However, because regolith is a loose granular material, these

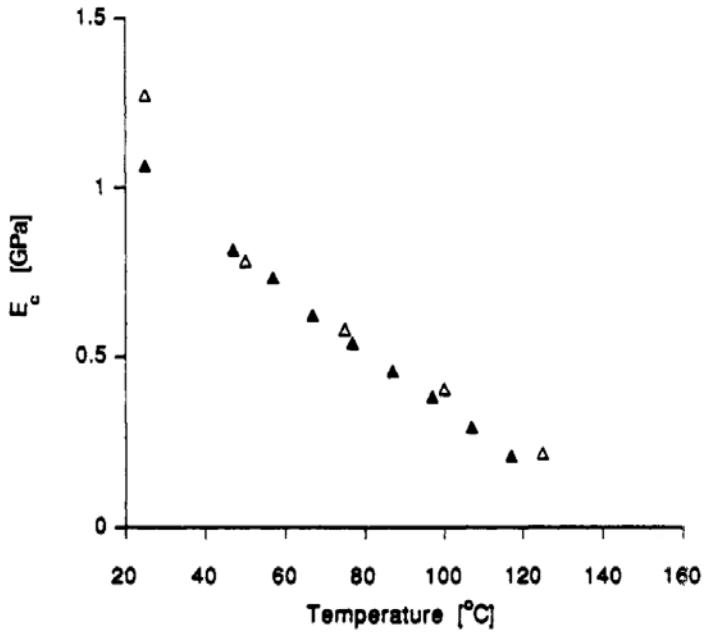

Figure 5.9: *Change of Young's modulus (open symbols) of UHMWPE for different temperatures [119]. The subscript "c" denotes the coil segments.*

well consolidated values for pure regolith values are hard to find. To the authors knowledge, none exist in literature. Therefore, as a first approximation, the values reported for sintered regolith simulant by Indyk and Benaroya [62] are used.

One downside with this approximation is that any phases/minerals in the regolith might have changed during the sintering process. This remains to be investigated. Another assumption in these plots is that the equations given by Equation 5.1 and Equation 5.2 are also applicable for the different weight fractions. This assumption is only valid when the densities of both materials is similar, which is not the case for polymers. However, most entries in literature did not mention the density required for converting these values and therefore it is assumed that both equations are also applicable for the weight fraction of a composite. Additionally, only the shape of the curve might change because of the difference between weight and volume fractions, as the limiting cases for fractions of 0 and 1 still converge to pure polymer and regolith respectively.

Different plots can be created for different matrix materials and different properties. Again, the material properties of several commonly used polymers can be found in Table A.2. Figure 5.10 and Figure 5.11 give the theoretical Young's modulus for regolith based composites with different binders, PE and LaRC-SI respectively, according to several of the models discussed before. Relevant binder type markers from literature are shown in red.

From the figures it is clear that the data points reported in literature have a large spread. Additionally, note that the Halpin-Tsai equations show an asymptotic for a specific FWFs. This again shows that this models is only applicable for low filler fractions. Therefore, it is concluded that this model is not suitable for our purposed. Comparing the matrix specific data points with their respective models, it is clear that the general approximation methods via the isostrain and isostress criteria seem to estimate the properties the best. However, since only few data points are available in a narrow spread of FWFs, it is hard to draw final conclusions.

Similar graphs can be produced for different properties. The graps for the compressive strength and flexural strength (modulus of rupture) can be found in Figure 5.12 and Figure 5.13

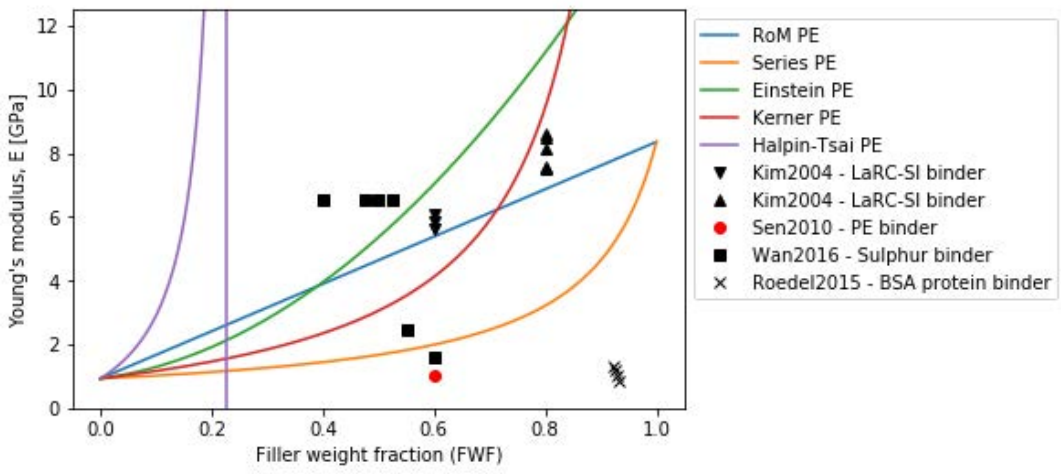

Figure 5.10: *Theoretical Young's modulus (E) vs FWF for PE-regolith composites according to different models and literature data. Kim2004 [87], Sen2010 [72], Wan2016 [71], Roedel2015 [75]*

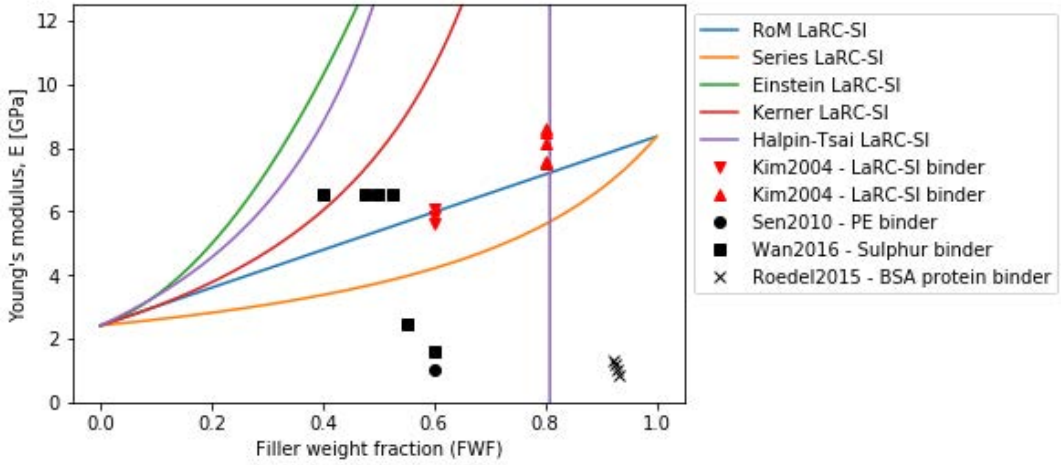

Figure 5.11: *Theoretical Young's modulus (E) vs FWF for LaRC-SI-regolith composites according to different models together with literature data. Kim2004 [87], Sen2010 [72], Wan2016 [71], Roedel2015 [75]*

respectively. For the flexural strength of sintered regolith, a value by Ruess, Schaenzlin, and Benaroya was used. Again, no clear approximation method seems to estimate the values well.

5.3.2. Thermal properties of polymer matrix granular composites

One of the methods to test thermal properties of a material is by using dynamic mechanical analysis (DMA). Several factors influence the dynamic behaviour of filled polymers, which include the nature of the polymer matrix, filler size, shape and distribution and interface properties, specifically related to surface modifiers [121]. The large amount of parameters shows that predicting the material behaviour is a complex task.

One way to give an estimate of the thermal behaviour is to use the storage modulus (E') of a composite. It is mostly associated with the elastic response of the material can be used for a stiffness indication. The temperature at which a sudden drop in modulus occurs can be used as

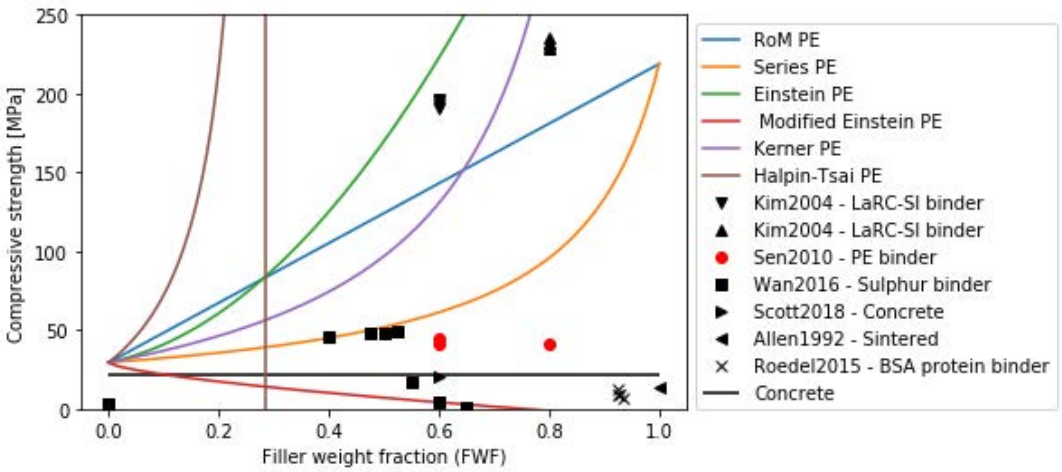

Figure 5.12: *Theoretical compressive strength vs FWF for PE-regolith composites according to different models and literature data. Relevant binder type markers from literature shown in red. Kim2004 [87], Sen2010 [72], Wan2016 [71], Scott2018 [77], Allen1992 [120], Roedel2015 [75], Concrete [84]*

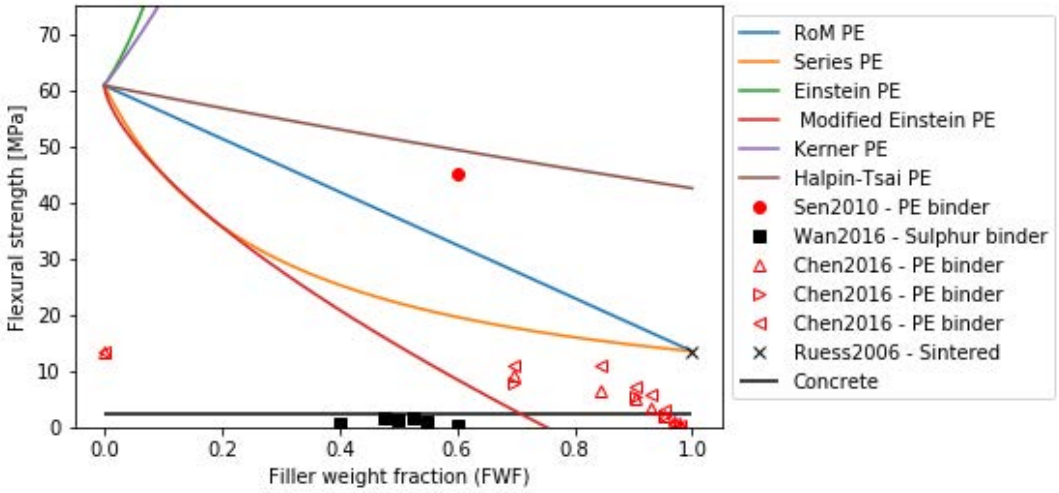

Figure 5.13: *Theoretical flexural strength vs FWF for PE-regolith composites according to different models and literature data. Relevant binder type markers from literature shown in red. Kim2004 [87], Sen2010 [72], Wan2016 [71], Chen2016 [73], Ruess2006 [17], Concrete [84]*

an estimate for the glass transition temperature (Tg) of the composite. Above this temperature, generally a loss of mechanical properties is observed. With increasing filler volume fraction, it is observed that the storage modulus generally increases [117]. This increase can be attributed to mechanical limitations imposed on the matrix by the filler material [117], increasing stiffness and delaying glass transition. Upon heating, it is generally observed that the storage modulus decreases due to matrix softening and the initiation of the relaxation process [122]. Bleach et al. found that an increase in volume fraction BCP resulted in a linear increase of the glass transition temperature for low filler fractions (up to 25%), see Figure 5.14.

Increasing the stiffness of the material also has an effect on the coefficient of thermal expansion (CTE) of the material. The pure polymer usually exhibits a larger thermal expansion

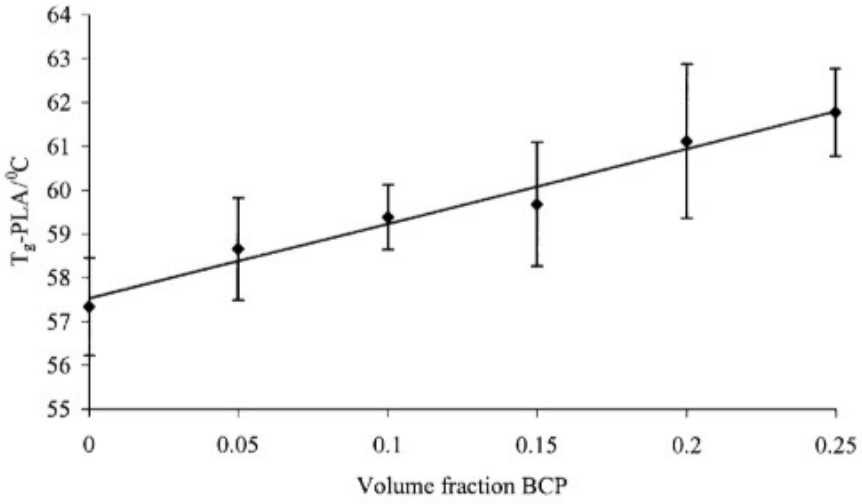

Figure 5.14: *Glass transition temperature (Tg) vs BCP content, showing linear increase with increased filler fraction [118]*

than the filled composite. This is, again, due to the filler material. In this case, it is less easy for the matrix to expand with increasing temperature due the the filler material restricting this motion [117].

The literature sources used above in the mechanical strength subsection did not specify the thermal properties of the obtained regolith composites. Therefore, similar plots to Figures 5.10 - 5.13 are impossible to create. These thermal properties of polymer matrix granular composites remains an area to be researched.

5.3.3. Impact and fracture properties of polymer matrix granular composites

The impact resistance of a filled polymer matrix depends on the nature of the polymer as well as the filler volume fraction. Soft thermoplastic polymers are ductile and have a high toughness, indicating that they have higher impact resistance because they can absorb and dissipate the impact energy more easily. Hard thermoset polymers, like epoxy, are inherently brittle due to their high degree of cross-linking. Combining these polymer systems with particulate fillers changes the characteristics of the composite.

In the case of a composite containing a thermoplastic polymer and hard filler material, the filler materials will improve the mechanical properties and the polymer component retains part of the original impact resistance. When the FVF increases to very high numbers, the impact resistance goes down again as the filler material dominates the impact characteristics and a continuous matrix interaction for energy dissipation might no longer be present.

In the case of hard polymer systems, like thermoset epoxy, the high degree of cross-linking is responsible for the materials low impact strength, fracture toughness and small elongation at break [123]. In this case, inclusion of solid particles might increase the impact resistance of the composite by decreasing the cross-linking density with minimal loss of mechanical performance.

5.3.4. Processing and Fabrication of polymer matrix granular composites

The processing method and ease depend on the chosen composite system. Systems that use a thermoset polymer, like epoxy, have a low viscosity and can processed and left to cure over time. Thermoplastic systems require heating above the glass transition temperature before

processing and are usually more viscous, limiting the manufacturing possibilities.

Filler volume fraction also impacts the processing of the composite. For FVF of 50% or larger, strong particle-particle interactions can result in poor possibility, particularly if they are of the network type [121]. Additionally, large FVF causes the composite to be more viscous, making it very difficult to process them via mixing or blending [124]. However, large FVF are required in order to achieve good combinations of strength, hardness and stiffness [125].

Current research focuses on different manufacturing methods in order to increase the maximum particle fraction and achieve even better properties of the final approached. A lot of these efforts are related to bio-inspired processes in order to mimic highly filled composites found in nature (e.g. nacre with a calcium carbonate volume fraction of 95% and about 5% polymer [126]). However, one thing to note is that the applications of these novel methods are not meant for large structural applications. That being said, novel manufacturing approaches are compaction of encapsulated (nano)particles [125], spouted bed spray granulation [127] and layer-by-layer methods [128].

5.4. Granular composites with a metal matrix

Similar to polymer matrix composites, metal matrix composites have also seen a lot of research interest over the past decades. This is mainly due to their higher (specific) strength and high (specific) modulus [129, 130]. Metal matrix composites are made of a metal matrix and a reinforcement. This reinforcement can be continuous, discontinuous or a combination of the two (hybrid). For an in depth review of the later category the reader is referred to the discussing by Zhou et al.[131]. When the reinforcement is carefully controlled, metal matrix composites can also exhibit other favourable mechanical and thermal properties. These include high electrical conductivity, high thermal conductivity, high dimensional stability and high wear resistance [132]. This section aims to give an overview of the general properties of metal matrix composites with a granular/particulate reinforcement. Where possible, specific attention is paid to mineral ceramic reinforcements, as these most closely represent regolith material. Unfortunately, to the authors knowledge, few data is available for the mechanical properties of metal matrix composites made from regolith. Therefore, this is a possible area of interest for future research. The closes thing to metal matrix composites manufactured with regolith is material made by self-propagating high temperature synthesis (SHS, Subsection 4.1.1).

5.4.1. Mechanical properties of metal matrix granular composites

Several parameters can be identified that have an effect on the mechanical properties of metal matrix composites. These parameters are the homogeneous dispersion of reinforcement, good interfacial bonding and structural integrity of the reinforcement [131]. Additionally, the mechanical properties of both the reinforcement and the matrix are important as well. Table A.1 in Appendix A gives an overview of commonly used metal matrix materials. These include aluminium, titanium and magnesium [131]. Additionally, iron is included as this metal is also commonly available on the Moon and Mars (Subsection 3.4.2).

The mechanical properties of metal matrix composites depend on the processing method used to create them. The two main processing methods for creating metal matrix composites is powder metallurgy and liquid metallurgy processes. A more detailed discussion about this process is given below.

Different researchers investigated the mechanical properties of metal matrix composite and the effect of different filler volume fractions [133–135]. Huang et al. investigated the effect of different particulate reinforcement fractions on the mechanical properties of an titanium matrix MMC made using a powder metallurgy process, hot-press sintering. The results of their research is shown in Figure 5.15. They found that the compressive and yield strengths

both increased with increased particle fraction.

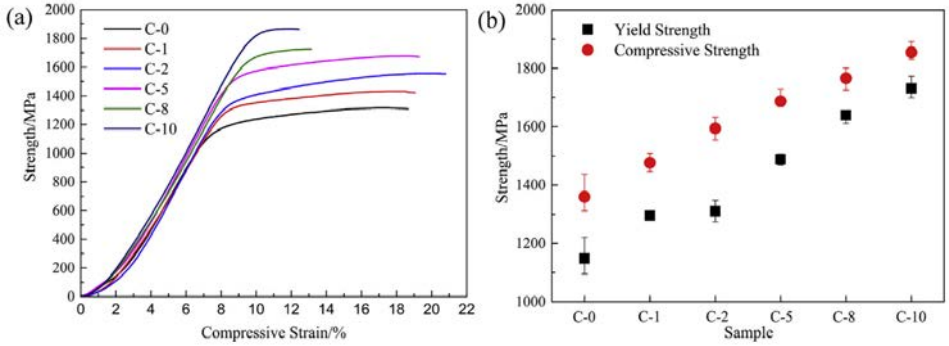

Figure 5.15: *Compressive stress-strain curves (a) and strength values (b) for different metal matrix composites. The number in the sample indicator indicate wt% reinforcement [133].*

In a similar investigation, Shalaby et al. investigated the effect of particle reinforcements on an aluminium based MMC. They used a different processing technique, namely squeeze casting (see Subsection 5.4.4). They showed that squeeze casting produced lower porosity values than regular casting (Figure 5.17). Generally, an increase in both yield strength and ultimate tensile stress was observed, accompanied by a decrease in fracture strain (see Figure 5.16). Again, only low filler weight fractions were investigated.

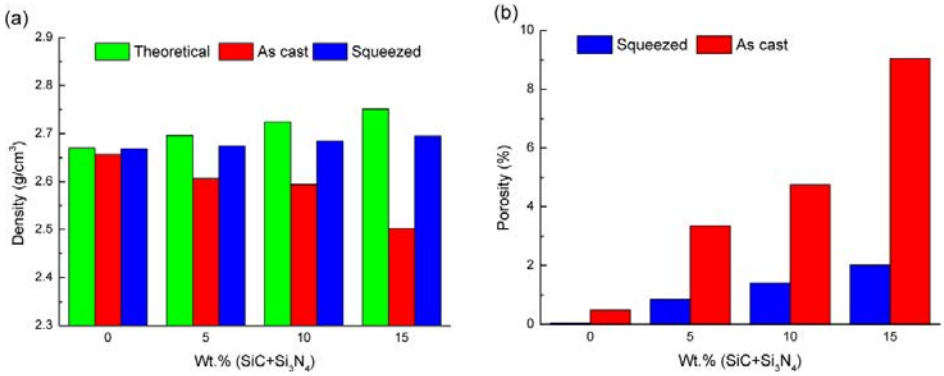

Figure 5.16: *Density (a) and porosity (b) of squeezed and cast metal matrix composites with different reinforcement fractions [134]*

A downside of both of these investigations is the low reinforcement fraction that was investigated, which makes the result less applicable to our current investigation. However, a different metal material class exists that closer resembles our high filler fraction interests. These material class is known as *cermets*.

Cermets are an interesting class of MMC's as they exhibit high hardness and wear resistance, making them especially suitable for cutting and drilling applications. Additionally, they can also be used to create metal forming tools [136]. Cermets can be created using a variety of fillers and matrix materials. For high filler fractions, commonly used matrix metals are Cobalt and Nickel. Kübarsepp and Juhani summarized the current state of knowledge on Wolfram (W) free cermets bonded with Fe-alloys [136].

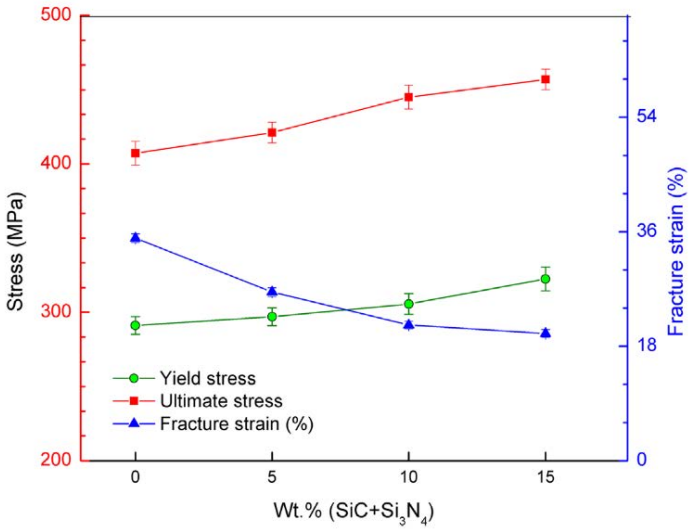

Figure 5.17: *Mechanical properties of MMC's of different reinforcement weight fractions [134]*

As mentioned before, the closest material to MMC's that uses regolith is obtained via the self-propagating high temperature synthesis process [64–66]. These sources all reported the compressive strengths of the final material. Therefore, a graph of the theoretical compressive stress similar to the one in the polymer matrix section can be constructed. This graph can be seen in Figure 5.18.

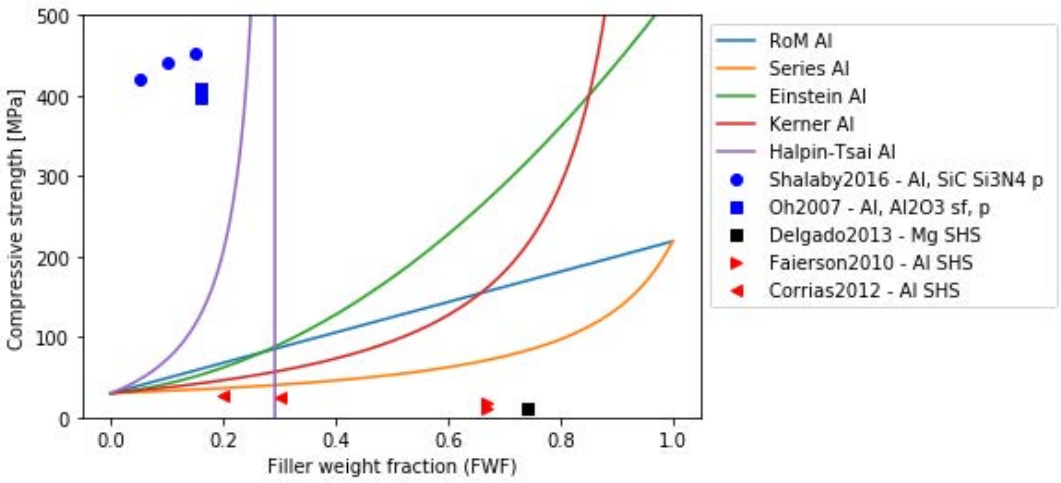

Figure 5.18: *Theoretical compressive strength vs FWF for Al based regolith composites according to different models and literature data. Relevant binder type markers from literature shown in red, blue markers indicate reference values for MMCs with ceramic particulate reinforcement. Shalaby2016 [134], Oh2007 [137], Delgado2013 [66], Faierson2010 [64], Corrias2012 [65].*

Again a large scatter is present in the data points. For low regolith fractions it appears that the model obtained via the isostress assumption is the best fit. For higher filler fractions, which is the current region of interest, no one model appears to predict the values well.Data points obtained for the SHS production method using regolith are significantly lower than those obtained via the squeeze casting method. Therefore, the properties of squeeze cast regolith

MMCs and liquid infiltration methods are possible future areas of research.

5.4.2. Thermal properties of metal matrix granular composites

Metals are known for their good thermal conductivity and relatively high coefficient of thermal expansion. Ceramics like regolith, on the other hand, are known for the opposite. This is evident by comparing the values from Table A.1 and Table 3.9. Combining these materials in a metal matrix composite therefore has a major effect on the thermal properties of the resulting material. Several researchers investigated the thermal properties of metal matrix composites [138–140]. A general observation are that 1) the processing methods influence the thermal conductivity, 2) the CTE is lowered and 3) the thermal conductivity is lowered. The lower CTE is generally attributed to interfacial effects and phases formed in the composite, with an effect similar to that observed in polymers (e.g. expansion is hindered by the reinforcement). Especially for highly filled MMC's the thermal conductivity can be drastically decreased. This is because no continuous conduction matrix path might exist, making heat conduction more difficult as it has to go though the less conductive reinforcement.

5.4.3. Impact and Fracture properties of metal matrix granular composites

Metals exhibit superior impact and fracture properties than ceramics due to their higher ductility. Including ceramic particles in a metal matrix reduce the ductility of the composite and hence the impact and fracture properties. This reduced ductility results in a smaller strain to failure (Figure 5.17. This loss of ductility may be attributed to intermetallic compounds forming in the composite, resulting in stress concentrations [134]. After an initial decrease in fracture toughness when the reinforcement is introduced, it is observed that the fracture toughness increases with increasing reinforcement for hybrid reinforcements [137].

5.4.4. Processing and Fabrication of metal matrix granular composites

Metal matrix composites can be manufactured using two main processing branches: in-situ and ex-situ processing techniques. In-situ techniques form the reinforcement during the processing, whereas ex-situ does not [131]. For the purpose of our discussion, only the ex-situ techniques will be discussed as our intended reinforcement (regolith) is already available.

As mentioned, a widely used processing method of MMC's is powder metallurgy. This technique generally consists of three steps: 1) dispersion, 2) compaction and 3) sintering. After sintering additional processing can occur to consolidate the material as well as further disperse the reinforcement. These techniques include hot extrusion, hot forging and hot rolling [131]. Generally the first and the third step are considered the most important. Proper dispersion is needed to obtain a homogeneous material. Here, smaller matrix grains can aid to improve dispersion. Sintering effects the mechanical properties as by influencing the porosity of the material. Lower porosity indicate well consolidated samples with good properties. Sintering also effects interfactial bonding. Dense products with good interfacial bonding require sintering at high temperatures for long periods of time [131].

The second method is via liquid metallurgy, e.g. casting. This is a simple process in which a reinforcement is mixed within a molten matrix. Downside of this process is that it is hard to achieve uniform dispersion of the reinforcement and the increased energy requirement as melting requires more energy than sintering. However, a major advantage of this processing technique is that it is easier to fabricate larger size products [131]. An upcoming variety of casting is squeeze casting, in which the cast is compressed and left to solidify under pressure. One advantage of this technique is that it can eliminate casting defects [131].

Liquid infiltration is the third widely used production technique for MMC's. In this method a porous preform is made which is subsequently infused with liquid metal matrix. High filler fraction composites can also be obtained using this method. This method is more energy intensive

than powder metallurgy because it requires higher temperatures. However, it is suitable for high reinforcement fractions, which makes it interesting for the scope of this research [131, 141].

Cermets are generally produced using sintering methods (Liquid Phase Sintering, LPS, Spark Plasma Sintering, SPS, Hot Isostatic Pressing, HIP, etc.) or melt-infiltration methods. Both of these methods require the matrix material to be heated up to close to or above the melting temperature of the matrix, which is an energy intensive process. Using these methods, materials can be produced with very high relative density values (in the range of 95-99%) and high mechanical performance. Subsequent processing of the sintered material using heat treatments can impact the mechanical characteristics.

5.5. Granular composites with a ceramic matrix

Ceramic matrix composites (CMCs) have a continuous ceramic matrix phase and a distinct reinforcement phase. This reinforcement can be continuous or discontinuous. The main types of reinforcement are continuous fibres, short fibres and particles. CMCs are known for their good mechanical properties and damage tolerant behaviour compared to ordinary ceramics. CMCs are also used for their high abrasion resistance, wear resistance and retaining good properties in a large temperature range. The mechanical properties are influenced by the properties of the composite components, the reinforcement volume fraction, size shape and orientation. The amount of interface between reinforcement and matrix also has a profound effect on the properties of the composite. Tailoring the reinforcement can result in additional properties like high dimensional stability. This makes them an interesting material for space applications where this is required [130]. The ceramic matrix is usually a technical ceramic manufactured using complex processes. High purity raw materials are required to create good matrix properties. The properties of several common technical ceramics and reinforcements can be found in Table A.3 in Appendix A.

To the author's knowledge, currently no ceramic matrix composites have been created using regolith and a pure ceramic matrix material. That being said, there are some ways that regolith can be used to create such materials. As introduced above, most ceramic matrix composites are made with a pure ceramic material and some kind of reinforcement. In Subsection 4.1.1 it was shown that fibres can be drawn from molten regolith. These fibers can potentially be used in a CMC. On Mars, with sufficient processing infrastructure and available energy, the technical ceramics can theoretically be fabricated. In the process, carbon for carbides is obtained from CO2 in the atmosphere. On the Moon this is more difficult because of the low amount of carbon available.

5.5.1. Mechanical properties of ceramic matrix granular composites

The mechanical properties of CMCs is different than ordinary ceramics. The reinforcement phase generally result in anisotropic properties. Additionally, CMCs have higher thermal shock resistance and improved toughness.

5.5.2. Thermal properties of ceramic matrix granular composites

Ordinary ceramics have a low coefficient of thermal expansion and high thermal stability. These properties are retained in CMCs.

5.5.3. Impact and fracture properties of ceramic matrix granular composites

Ceramic matrix composite with a continuous fibre reinforcement generally exhibit better fracture and impact properties than ordinary ceramic. This is due to a variety of toughening mechanism also observed in polymer composites. These toughening mechanisms include crack

deflection, fibre-pull out and fibre-bridging. This means that the interface between the fibre and matrix is generally designed to be weaker as fibre pull-out must occur before further matrix cracking. This is contrary to other materials, where the interface is designed to be strong.

5.5.4. Processing and Fabrication of ceramic matrix granular composites

Most of the processing methods for conventional ceramics can be applied to ceramic matrix composites. These processes include sintering, hot isostatic pressing (HIP), self-propagating high temperature synthesis (SHS) methods as well as other material specific processes. Some of these processes are the same as those used for metal matrix composites e.g. liquid infiltration. During sintering, a mismatch between CTE in matrix and reinforcement can create tensile stresses that inhibit densification. Therefore the volume fraction of reinforcement is generally kept below 40 wt% and sintering takes place over long periods of time [130].

A different processing method for CMCs is via a vapour infiltration process. In this process a reinforcement preform is infused with a vapourized matrix phase and a carrier gas. The matrix builds up around the reinforcement. However, this production method can lead to the inclusion of pores [130].

5.6. Comparison between the different matrix materials

It is clear that a large spread of properties exist when looking at the data points in the figures containing the model predictions. In the case of polymers, the specific polymer used as a binder material has a large effect on properties of the resulting composite. A comparison between the different matrix materials is hard to make as few data point are available for a variety of properties. However, a comparison can be made in terms of the compressive strength. The data points for polymer based regolith composites and those obtained for SHS manufactured composites are shown in Figure 5.19. In this figure the points are coloured according to their matrix material. Polymer bound materials are shown with open markers, SHS fabricated materials with closed markers. An indicative compressive strength for concrete is also included.

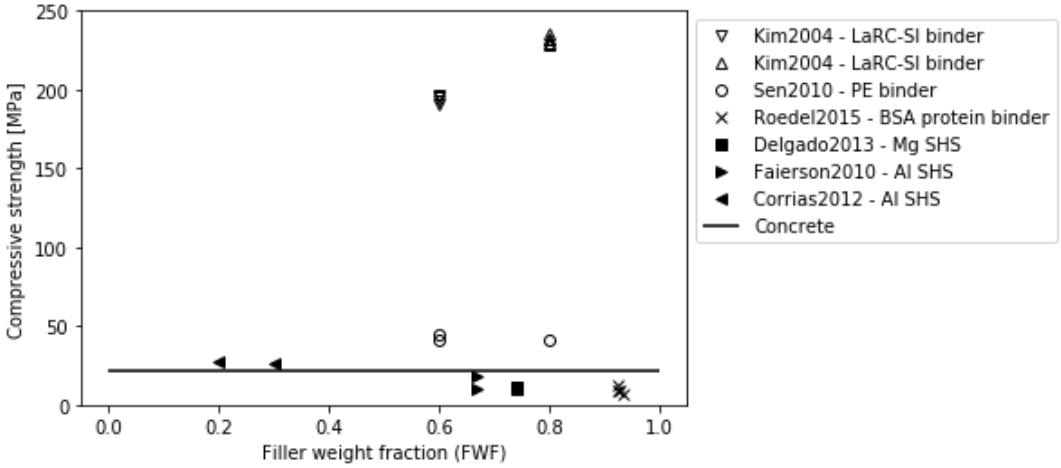

Figure 5.19: *Theoretical compressive strength vs FWF for polymer based (open markers) and SHS fabricated materials (closed markers). A compressive value of concrete is shown for comparison. Kim2004 [87], Sen2010 [72], Roedel2015 [75], Delgado2013 [66], Faierson2010 [64], Corrias2020 [65], Concrete [142]*

It is clear that the polymer composites outperform the SHS manufactured materials w.r.t. this property. However, a different MMC production method (like liquid infiltration) might pro-

duce completely different results. This should be investigated first before any final conclusions are drawn.

6

Conclusion

This literature study report investigated the possibility to use regolith in high volume fraction granular composites with the ultimate goal of selecting the optimal matrix material for such composites. The goal of such a composite is to create a material with the advantages of both its constituents. It is shown that regolith is an important resource for future space exploration within the in-situ resource utilisation method. To achieve this ultimate goal, multiple state-of-the-art regolith composite materials have been investigated for their mechanical, thermal, impact and fracture properties as well as the involved up-mass and energy requirements. The properties of granular composites are also compared to other materials made from regolith, both with and without added binder, to see how they compare. Sintered regolith, cast regolith, additive manufactured material and inorganic-organic hybrid (IOH) materials are used for this comparison. Furthermore, the operating conditions and challenges that these materials face have been investigated.

Past research into granular regolith composites mainly focused on low filler volume fractions. Different models were discussed in order to provide estimates for high filler fraction composites. This was done based on the three possible matrix materials, e.g. polymers, metal and ceramic. From the report it is clear that the polymer binder based regolith composites are far more developed than the metal or ceramic matrix counterparts. Unfortunately, the analysis showed that none of the different models investigated in this report seemed to predict the properties of high volume fraction composites to a good extent. A possible reason for this is the lack of a proper reference point for the properties of pure regolith. This should be investigated in the future. The lack of data for metal and ceramic matrix composites makes it impossible to give a conclusion at all on a suitable model, let alone compare different matrix materials. This makes it practically impossible to select an optimal matrix material at this stage. More research into metal matrix and ceramic matrix composites using regolith is required before a final conclusion can be drawn.

As mentioned above, the lack of data made it impossible to give a well-founded conclusion for the optimal matrix material. It became clear that research into several areas is required to provide a better understanding of regolith-based materials. These areas are the properties of sintered Martian regolith, the radiation and thermoshock characteristics of sintered regolith in general, the potential of IOH composites and the use of metal matrix composites using regolith.

Although an optimal matrix material cannot be selected at this stage, binder based regolith composites still remain a large area of interest for future research due to the promising potential of this material class. More research into higher filler fraction composites made from different matrix materials is needed to investigate the merits of this material class.

Bibliography

[1] Erin Mahoney. *Sending American Astronauts to Moon in 2024: NASA Accepts Challenge*. Last accessed on 30-10-2020. 2020. URL: https://www.nasa.gov/feature/sending-american-astronauts-to-moon-in-2024-nasa-accepts-challenge/.

[2] Mohannad Z. Naser and Alaa I. Chehab. *Materials and design concepts for space-resilient structures*. Apr. 2018. DOI: 10.1016/j.paerosci.2018.03.004.

[3] Alan Taylor. *China's Manned Space Program*. Last accessed on 30-10-2020. 2013. URL: https://www.theatlantic.com/photo/2013/07/chinas-manned-space-program/100549/.

[4] Jesse Astorga. *Permanent Mission to Mars*. Last accessed on 30-10-2020. URL: https://www.nasa.gov/sites/default/files/atoms/files/permanent_mission_to_mars_by_jesse_astorga.pdf.

[5] Nancy J Lindsey. *Lunar Station Protection: Lunar Regolith Shielding*. Tech. rep.

[6] David G Schrunk et al. *The Moon: Resources, Future Development, and Settlement (Second Edition)*. Praxis Publishing Ltd, 2007. ISBN: 978-0-387-36055-3. DOI: 10.1007/978-0-387-73982-3.

[7] *Space Images | Mars Daily Global Image from April 1999*. URL: https://www.jpl.nasa.gov/spaceimages/details.php?id=PIA02653.

[8] NASA. *Mars Fact Sheet*. Last accessed on 14-10-2020. URL: https://nssdc.gsfc.nasa.gov/planetary/factsheet/marsfact.html.

[9] *NASA - New Map Provides More Evidence Mars Once Like Earth*. URL: https://www.nasa.gov/centers/goddard/news/topstory/2005/mgs_plates.html.

[10] Michael H Carr. *The Surface of Mars*. Cambridge, UNITED KINGDOM: Cambridge University Press, 2007. ISBN: 9780511268168. URL: http://ebookcentral.proquest.com/lib/delft/detail.action?docID=288500.

[11] Shruti Nambiar and John T W Yeow. "Polymer-Composite Materials for Radiation Protection". In: (2012). DOI: 10.1021/am300783d. URL: www.acsami.org.

[12] Alessandra Menicucci. "Radiation environment and affects for planetary sciences". PowerPoint, part of the AE4876-II course of the TU Delft. Mar. 2020.

[13] NASA. *Moon Fact Sheet*. Last accessed on 14-10-2020. URL: https://nssdc.gsfc.nasa.gov/planetary/factsheet/moonfact.html.

[14] NASA. *Earth Fact Sheet*. Last accessed on 14-10-2020. URL: https://nssdc.gsfc.nasa.gov/planetary/factsheet/earthfact.html.

[15] Stanley O. Starr and Anthony C. Muscatello. *Mars in situ resource utilization: a review*. Mar. 2020. DOI: 10.1016/j.pss.2019.104824.

[16] Haym Benaroya, Philip Metzger, and Anthony Muscatello. *Special issue on in situ resource utilization*. Jan. 2013. DOI: 10.1061/(ASCE)AS.1943-5525.0000282.

[17] F. Ruess, J. Schaenzlin, and H. Benaroya. “Structural design of a lunar habitat”. In: *Journal of Aerospace Engineering* 19.3 (July 2006), pp. 133–157. ISSN: 08931321. DOI: 10.1061/(ASCE)0893-1321(2006)19:3(133). URL: http://ascelibrary.org/doi/10.1061/%28ASCE%290893-1321%282006%2919%3A3%28133%29.

[18] Ian A. Crawford. “Lunar resources: A review”. In: *Progress in Physical Geography* 39.2 (Apr. 2015), pp. 137–167. ISSN: 03091333. DOI: 10.1177/0309133314567585.

[19] Carsten Schwandt et al. “The production of oxygen and metal from lunar regolith”. In: *Planetary and Space Science*. Vol. 74. 1. Pergamon, Dec. 2012, pp. 49–56. DOI: 10.1016/j.pss.2012.06.011.

[20] Bradley L. Jolliff et al. *New Views of the Moon*. Vol. 60. Reviews in mineralogy and geochemistry. Mineralogical Society of America, 2006.

[21] W. David III Carrier, Gary R. Olhoeft, and Wendell Mendell. “Lunar Sourcebook - a user’s guide to the Moon”. In: Cambridge University Press, 1991. Chap. Physical Properties of the Lunar Surface.

[22] V. Gromov. “Physical and mechanical properties of lunar and planetary soils”. In: *Earth, Moon and Planets* 80.1-3 (1998), pp. 51–72. ISSN: 01679295. DOI: 10.1023/a:1006353510204. URL: https://link.springer.com/article/10.1023/A:1006353510204.

[23] E. N. Slyuta. *Physical and mechanical properties of the lunar soil (a review)*. Sept. 2014. DOI: 10.1134/S0038094614050050. URL: https://link.springer.com/article/10.1134/S0038094614050050.

[24] W. David Carrier. “Lunar soil grain size distribution”. In: *The Moon* 6.3-4 (Sept. 1973), pp. 250–263. ISSN: 00270903. DOI: 10.1007/BF00562206. URL: https://link.springer.com/article/10.1007/BF00562206.

[25] D. S. McKay et al. “Grain size and the evolution of lunar soils.” In: *Lunar Science Conference*. Vol. 1. Houston, Texas: Pergamon Press, Inc., New York, Mar. 1974, pp. 887–906. URL: https://ui.adsabs.harvard.edu/abs/1974LPSC....5..887M/abstract.

[26] Y Liu et al. “Shape Analyses of Lunar Dust Particles for Astronaut Toxicological Studies”. In: 38 (2007), p. 1383.

[27] J. K. Mitchell et al. *Apollo soil mechanics experiment S-200*. Tech. rep. Final report, NASA Contract NAS 9–11266. University of California, Berkley, 1974. URL: https://ntrs.nasa.gov/citations/19740019219.

[28] George C Marshall et al. *Lunar Regolith Simulant User’s Guide*. Tech. rep. 2010. URL: http://www.sti.nasa.gov.

[29] Christian M. Schrader et al. “Lunar regolith characterization for simulant design and evaluation using figure of merit algorithms”. In: *47th AIAA Aerospace Sciences Meeting including the New Horizons Forum and Aerospace Exposition*. American Institute of Aeronautics and Astronautics Inc., 2009. ISBN: 9781563479694. DOI: 10.2514/6.2009-755.

[30] Christian M. Schrader et al. “Constraining Particle Variation in Lunar Regolith for Simulant Design”. In: *AIAA SPACE 2008 Conference and Exposition*. NTRS - NASA Technical Reports Server, Sept. 2008. URL: https://ntrs.nasa.gov/citations/20090023133.

[31] M. Z. Naser. *Extraterrestrial construction materials*. Aug. 2019. DOI: 10.1016/j.pmatsci.2019.100577.

[32] Mingjing Jiang, Liqing Li, and Yugang Sun. “Properties of TJ-1 Lunar Soil Simulant”. In: *Journal of Aerospace Engineering* 25.3 (July 2012), pp. 463–469. ISSN: 0893-1321. DOI: 10.1061/(asce)as.1943-5525.0000129. URL: https://ascelibrary-org.tudelft.idm.oclc.org/doi/abs/10.1061/%28ASCE%29AS.1943-5525.0000129.

[33] Melissa Battler. “Development of an anorthositic lunar regolith simulant: OB1”. PhD thesis. The University of New Brunswick, Sept. 2008, pp. 1–165. URL: https://www.researchgate.net/publication/253477459_Development_of_an_anorthositic_lunar_regolith_simulant_OB1.

[34] Haydar Arslan, Susan Batiste, and Stein Sture. “Engineering Properties of Lunar Soil Simulant JSC-1A”. In: (). DOI: 10.1061/ASCE0893-1321201023:170.

[35] Mandar M Dewoolkar et al. “Shear Strength and Stiffness Characterization of Lunar Simulant GRC-3”. In: (2018). DOI: 10.1061/(ASCE).

[36] L Sibille et al. *Lunar Regolith Simulant Materials: Recommendations for Standardization, Production, and Usage*. Tech. rep. Sept. 2006. URL: http://www.sti.nasa.gov.

[37] *Lunar Sourcebook*. URL: https://www.lpi.usra.edu/publications/books/lunar_sourcebook/.

[38] B K Muirhead et al. “SAMPLE RETREIVAL LANDER CONCEPT FOR A POTENTIAL MARS SAMPLE RETURN CAMPAIGN”. In: *Ninth International Conference on Mars*. Pasadena, California, July 2019.

[39] Catherine M. Weitz et al. “Sand Grain Sizes and Shapes in Eolian Bedforms at Gale Crater, Mars”. In: *Geophysical Research Letters* 45.18 (Sept. 2018), pp. 9471–9479. ISSN: 00948276. DOI: 10.1029/2018GL078972. URL: http://doi.wiley.com/10.1029/2018GL078972.

[40] C. N. Achilles et al. “Mineralogy of an active eolian sediment from the Namib dune, Gale crater, Mars”. In: *Journal of Geophysical Research: Planets* 122.11 (Nov. 2017), pp. 2344–2361. ISSN: 21699097. DOI: 10.1002/2017JE005262. URL: http://doi.wiley.com/10.1002/2017JE005262.

[41] Audouin Dollfus and Marc Deschamps. “Grain-size determination at the surface of Mars”. In: *Icarus* 67.1 (July 1986), pp. 37–50. ISSN: 00191035. DOI: 10.1016/0019-1035(86)90172-7. URL: https://linkinghub.elsevier.com/retrieve/pii/0019103586901727.

[42] Richard W. Shorthill et al. “The ”Soil” of mars (viking 1)”. In: *Science* 194.4260 (Oct. 1976), pp. 91–97. ISSN: 00368075. DOI: 10.1126/science.194.4260.91. URL: http://science.sciencemag.org/.

[43] C. M. Weitz et al. “Soil grain analyses at Meridiani Planum, Mars”. In: *Journal of Geophysical Research: Planets* 111.E12 (Dec. 2006), n/a–n/a. ISSN: 01480227. DOI: 10.1029/2005JE002541. URL: http://doi.wiley.com/10.1029/2005JE002541.

[44] Paul Morgan et al. “A Pre-Landing Assessment of Regolith Properties at the InSight Landing Site”. In: *Space Sci Rev* 214 (2018), p. 104. DOI: 10.1007/s11214-018-0537-y. URL: https://doi.org/10.1007/s11214-018-0537-y.

[45] M. Golombek et al. *Selection of the InSight Landing Site*. Oct. 2017. DOI: 10.1007/s11214-016-0321-9. URL: https://link-springer-com.tudelft.idm.oclc.org/article/10.1007/s11214-016-0321-9.

[46] Xiaojia Zeng et al. “JMSS-1: A new Martian soil simulant Planetary science”. In: *Earth, Planets and Space* 67.1 (Dec. 2015), p. 72. ISSN: 18805981. DOI: 10.1186/s40623-015-0248-5. URL: http://www.earth-planets-space.com/content/67/1/72.

[47] Henry J Moore and Bruce M Jakosky. *Viking Landing Sites, Remote-Sensing Observations, and Physical Properties of Martian Surface Materials*. Tech. rep. 1989, pp. 164–184.

[48] Z22. *File:Martian regolith simulant - pile.JPG - Wikimedia Commons*. Retrieved on 24-09-2020. Apr. 2014. URL: https://commons.wikimedia.org/wiki/File:Martian_regolith_simulant_-_pile.JPG.

[49] Xiangwu Zeng et al. “Geotechnical Properties of JSC-1A Lunar Soil Simulant”. In: *Journal of Aerospace Engineering* 23.2 (Apr. 2010), pp. 111–116. ISSN: 0893-1321. DOI: 10.1061/(ASCE)AS.1943-5525.0000014. URL: http://ascelibrary.org/doi/10.1061/%28ASCE%29AS.1943-5525.0000014.

[50] Gregory H. Peters et al. “Mojave Mars simulant-Characterization of a new geologic Mars analog”. In: *Icarus* 197.2 (Oct. 2008), pp. 470–479. ISSN: 00191035. DOI: 10.1016/j.icarus.2008.05.004. URL: www.elsevier.com/locate/icarus.

[51] Kevin M Cannon et al. “Mars global simulant MGS-1: A Rocknest-based open standard for basaltic martian regolith simulants”. In: (2018). DOI: 10.1016/j.icarus.2018.08.019. URL: https://doi.org/10.1016/j.icarus.2018.08.019.

[52] Nisha K. Ramkissoon et al. “New simulants for martian regolith: Controlling iron variability”. In: *Planetary and Space Science* 179 (Dec. 2019), p. 104722. ISSN: 00320633. DOI: 10.1016/j.pss.2019.104722.

[53] Karsten Seiferlin et al. “Simulating Martian regolith in the laboratory”. In: *Planetary and Space Science* 56.15 (Dec. 2008), pp. 2009–2025. ISSN: 00320633. DOI: 10.1016/j.pss.2008.09.017.

[54] Marsha Presley and Robert Craddock. “Thermal conductivity measurements of particulate materials: 3. Natural samples and mixtures of particle sizes”. In: *Journal of Geophysical Research* 111 (2006). DOI: 10.1029/2006JE002706.

[55] Carlton C. Allen et al. “JSC MARS-1: A Martian Soil Simulant”. In: *Space 98*. Reston, VA: American Society of Civil Engineers, Apr. 1998, pp. 469–476. ISBN: 9780784403396. DOI: 10.1061/40339(206)54. URL: http://ascelibrary.org/doi/10.1061/40339%28206%2954.

[56] Pierre Delage et al. *An Investigation of the Mechanical Properties of Some Martian Regolith Simulants with Respect to the Surface Properties at the InSight Mission Landing Site*. Oct. 2017. DOI: 10.1007/s11214-017-0339-7. URL: https://link-springer-com.tudelft.idm.oclc.org/article/10.1007/s11214-017-0339-7.

[57] John A Happel. “Indigenous Materials for Lunar Construction”. In: *Applied Mechanics Reviews* 46.6 (1993), pp. 313–325. ISSN: 0003-6900. DOI: 10.1115/1.3120360. URL: https://doi.org/10.1115/1.3120360.

[58] E. Hohmann and C. Dalton. *Conceptual design of a lunar colony*. Tech. rep. 1972. URL: https://ntrs.nasa.gov/search.jsp?R=19730002509.

[59] William N. Agosto, John H. Wickman, and Eric James. “Lunar cements/concretes for orbital structures”. In: Publ by ASCE, 1988, pp. 157–168. ISBN: 0872626717.

[60] *Portland Cement Compressive Strength - Pavement Interactive*. URL: https://pavementinteractive.org/reference-desk/testing/cement-tests/portland-cement-compressive-strength/.

[61] Christopher P. Spedding, William J. Nuttall, and Sungwoo Lim. "Energy requirements of a thermally processed ISRU radiation shield for a lunar habitat". In: *Advances in Space Research* 65.11 (June 2020), pp. 2467–2474. ISSN: 18791948. DOI: 10.1016/j.asr.2020.03.015.

[62] Stephen J Indyk and Haym Benaroya. "A structural assessment of unrefined sintered lunar regolith simulant". In: (2017). DOI: 10.1016/j.actaastro.2017.09.018. URL: https://doi.org/10.1016/j.actaastro.2017.09.018.

[63] Eric Faierson et al. "Lunar Habitat Construction Utilizing In-Situ Resources and a Self-Propagating High-Temperature Synthesis Reaction (SHS)". In: *AIAA SPACE 2008 Conference & Exposition*. Reston, Virigina: American Institute of Aeronautics and Astronautics, Sept. 2008. ISBN: 978-1-62410-002-4. DOI: 10.2514/6.2008-7819. URL: http://arc.aiaa.org/doi/10.2514/6.2008-7819.

[64] Eric J. Faierson et al. "Demonstration of concept for fabrication of lunar physical assets utilizing lunar regolith simulant and a geothermite reaction". In: *Acta Astronautica* 67.1-2 (July 2010), pp. 38–45. ISSN: 00945765. DOI: 10.1016/j.actaastro.2009.12.006. URL: https://linkinghub.elsevier.com/retrieve/pii/S0094576509005918.

[65] Gianluca Corrias et al. "Self-propagating high-temperature reactions for the fabrication of Lunar and Martian physical assets". In: *Acta Astronautica* 70 (Jan. 2012), pp. 69–76. ISSN: 00945765. DOI: 10.1016/j.actaastro.2011.07.022. URL: https://linkinghub.elsevier.com/retrieve/pii/S0094576511002335.

[66] Armando Delgado and Evgeny Shafirovich. "Towards better combustion of lunar regolith with magnesium". In: *Combustion and Flame* 160.9 (Sept. 2013), pp. 1876–1882. ISSN: 00102180. DOI: 10.1016/j.combustflame.2013.03.021. URL: https://linkinghub.elsevier.com/retrieve/pii/S0010218013001090.

[67] V Heemskerk, W Van Westrenen, and B H Foing. *Lunar and Martian Regolith Based Concrete as Building Blocks for Future Human Settlements. M*. Tech. rep.

[68] Charles Meyers and Houssam Toutanji. "Analysis of Lunar-Habitat Structure Using Waterless Concrete and Tension Glass Fibers". In: *Journal of Aerospace Engineering* 20.4 (Oct. 2007), pp. 220–226. ISSN: 0893-1321. DOI: 10.1061/(ASCE)0893-1321(2007)20:4(220). URL: http://ascelibrary.org/doi/10.1061/%28ASCE%290893-1321%282007%2920%3A4%28220%29.

[69] Richard N. Grugel and Houssam Toutanji. "Sulfur "concrete" for lunar applications - Sublimation concerns". In: *Advances in Space Research* 41.1 (2008), pp. 103–112. ISSN: 02731177. DOI: 10.1016/j.asr.2007.08.018.

[70] Richard N Grugel and Houssam Toutanji. "Viability of Sulfur "Concrete" on the Moon: Environmental Considerations". In: (). DOI: 10.2514/6.2006-520. URL: http://arc.aiaa.org.

[71] Lin Wan, Roman Wendner, and Gianluca Cusatis. "A novel material for in situ construction on Mars: experiments and numerical simulations". In: *Construction and Building Materials* 120 (Sept. 2016), pp. 222–231. ISSN: 09500618. DOI: 10.1016/j.conbuildmat.2016.05.046.

[72] S. Sen, S. Carranza, and S. Pillay. “Multifunctional Martian habitat composite material synthesized from in situ resources”. In: *Advances in Space Research* 46.5 (Sept. 2010), pp. 582–592. ISSN: 02731177. DOI: 10.1016/j.asr.2010.04.009.

[73] Tzehan Chen et al. “Inorganic–Organic Hybrid of Lunar Soil Simulant and Polyethylene”. In: *Journal of Materials in Civil Engineering* 28.4 (Apr. 2016), p. 06015013. ISSN: 0899-1561. DOI: 10.1061/(ASCE)MT.1943-5533.0001450. URL: http://ascelibrary.org/doi/10.1061/%28ASCE%29MT.1943-5533.0001450.

[74] Tzehan Chen et al. “Formation of polymer micro-agglomerations in ultralow-binder-content composite based on lunar soil simulant”. In: *Advances in Space Research* 61.3 (Feb. 2018), pp. 830–836. ISSN: 18791948. DOI: 10.1016/j.asr.2017.10.050.

[75] H. Roedel, M. D. Lepech, and D. J. Loftus. “Protein-Regolith Composites for Space Construction”. In: *Earth and Space 2014*. Reston, VA: American Society of Civil Engineers, June 2015, pp. 291–300. ISBN: 9780784479179. DOI: 10.1061/9780784479179.033. URL: http://ascelibrary.org/doi/10.1061/9780784479179.033.

[76] Alessio Alexiadis, Federico Alberini, and Marit E. Meyer. “Geopolymers from lunar and Martian soil simulants”. In: *Advances in Space Research* 59.1 (Jan. 2017), pp. 490–495. ISSN: 18791948. DOI: 10.1016/j.asr.2016.10.003. URL: http://dx.doi.org/10.1016/j.asr.2016.10.003.

[77] Allan N. Scott and Christopher Oze. “Constructing Mars: Concrete and Energy Production From Serpentinization Products”. In: *Earth and Space Science* 5.8 (Aug. 2018), pp. 364–370. ISSN: 23335084. DOI: 10.1029/2017EA000353. URL: http://doi.wiley.com/10.1029/2017EA000353.

[78] Jaeho Lee et al. “Feasibility study on lunar concrete landing pad”. In: *Earth and Space 2012 - Proceedings of the 13th ASCE Aerospace Division Conference and the 5th NASA/ASCE Workshop on Granular Materials in Space Exploration*. Reston, VA: American Society of Civil Engineers (ASCE), Apr. 2012, pp. 128–134. ISBN: 9780784412190. DOI: 10.1061/9780784412190.015. URL: http://ascelibrary.org/doi/10.1061/9780784412190.015.

[79] Tai Sik Lee, Jaeho Lee, and Ki Yong Ann. “Manufacture of polymeric concrete on the Moon”. In: *Acta Astronautica* 114 (Apr. 2015), pp. 60–64. ISSN: 00945765. DOI: 10.1016/j.actaastro.2015.04.004.

[80] Jaeho Lee et al. “Bottom-up heating method for producing polyethylene lunar concrete in lunar environment”. In: *Advances in Space Research* 62.1 (July 2018), pp. 164–173. ISSN: 18791948. DOI: 10.1016/j.asr.2018.03.039.

[81] Athanasios Goulas et al. “Mechanical behaviour of additively manufactured lunar regolith simulant components”. In: *Proceedings of the Institution of Mechanical Engineers, Part L: Journal of Materials: Design and Applications* 233.8 (Aug. 2019), pp. 1629–1644. ISSN: 20413076. DOI: 10.1177/1464420718777932.

[82] David Karl et al. “Clay in situ resource utilization with Mars global simulant slurries for additive manufacturing and traditional shaping of unfired green bodies”. In: *Acta Astronautica* 174 (Sept. 2020), pp. 241–253. ISSN: 00945765. DOI: 10.1016/j.actaastro.2020.04.064.

[83] Behrokh Khoshnevis and Jing Zhang. “Extraterrestrial construction using contour crafting”. In: *23rd Annual International Solid Freeform Fabrication Symposium - An Additive Manufacturing Conference, SFF 2012*. University of Texas at Austin (freeform), 2012, pp. 250–259.

[84] Giovanni Cesaretti et al. “Building components for an outpost on the Lunar soil by means of a novel 3D printing technology”. In: *Acta Astronautica* 93 (Jan. 2014), pp. 430–450. ISSN: 00945765. DOI: 10.1016/j.actaastro.2013.07.034. URL: https://linkinghub.elsevier.com/retrieve/pii/S0094576513002889.

[85] Tzehan Chen et al. “High-Pressure Densification of Composite Lunar Cement”. In: *Journal of Materials in Civil Engineering* 29.10 (Oct. 2017), p. 06017013. ISSN: 0899-1561. DOI: 10.1061/(ASCE)MT.1943-5533.0002047. URL: http://ascelibrary.org/doi/10.1061/%28ASCE%29MT.1943-5533.0002047.

[86] Arturo R Ortiz, Vadim Y Rygalov, and Pablo De León. *Radiation Protection Strategy Development for Mars Surface Exploration*. Tech. rep. 2015.

[87] M.-H Y Kim et al. *FABRICATION AND TESTING OF HABITAT COMPONENTS USING IN-SITU MATERIALS FOR MARTIAN EXPLORATION*. Tech. rep. 2004. URL: https://ntrs.nasa.gov/search.jsp?R=20040086076.

[88] Myung-hee Kim et al. “Comparison of Martian Meteorites and Martian Regolith as Shield Materials for Galactic Cosmic Rays”. In: (1998).

[89] John W. Wilson et al. “HZETRN: Description of a Free-Space Ion and Nucleon Transport and Shielding Computer Program”. In: (1995). URL: http://citeseerx.ist.psu.edu/viewdoc/summary?doi=10.1.1.45.7286.

[90] Samiksha Sikarwar et al. “Nanocomposite Material For Packaging of Electronic Goods”. In: *International Journal of Scientific and Innovative Research* 1 (2014), pp. 93–108.

[91] Eral Bele and Vikram S. Deshpande. “The Compressive Response of Idealized Cermetlike Materials”. In: *Journal of Applied Mechanics, Transactions ASME* 82.4 (Apr. 2015). ISSN: 15289036. DOI: 10.1115/1.4029782.

[92] *Handbook of Fillers (4th Edition) - Knovel*. URL: https://app.knovel.com/web/toc.v/cid:kpHFE00031/viewerType:toc//root_slug:handbook-fillers-4th/url_slug:effect-fillers-mechanical?issue_id=kpHFE00031.

[93] J F Shackelford. *Introduction to Materials Science for Engineers*. Always learning. Pearson Education Limited, 2015. ISBN: 9780273793403. URL: https://books.google.nl/books?id=_rufDAEACAAJ.

[94] Eugene Guth. “Theory of Filler Reinforcement ARTICLES YOU MAY BE INTERESTED IN”. In: *Journal of Applied Physics* 16 (1945), p. 20. DOI: 10.1063/1.1707495. URL: https://doi.org/10.1063/1.1707495.

[95] E. Sideridis et al. “The effect of low-filler volume fraction on the elastic modulus and thermal expansion coefficient of particulate composites simulated by a multiphase model”. In: *Journal of Applied Polymer Science* 111.1 (Jan. 2009), pp. 203–216. ISSN: 00218995. DOI: 10.1002/app.28886. URL: http://doi.wiley.com/10.1002/app.28886.

[96] J. L. Willett. “Mechanical properties of LDPE/granular starch composites”. In: *Journal of Applied Polymer Science* 54.11 (Dec. 1994), pp. 1685–1695. ISSN: 00218995. DOI: 10.1002/app.1994.070541112. URL: http://doi.wiley.com/10.1002/app.1994.070541112.

[97] L E Nielsen. *Morphology and the elastic modulus of block polymers and polyblends*. Tech. rep. 1974, pp. 86–92. DOI: 10.1007/BF01526889. URL: https://link-springer-com.tudelft.idm.oclc.org/article/10.1007%2FBF01526889#citeas.

[98] J. C.Halpin Affdl and J. L. Kardos. *The Halpin□Tsai equations: A review*. May 1976. DOI: 10.1002/pen.760160512. URL: https://onlinelibrary.wiley.com/doi/full/10.1002/pen.760160512.

[99] L. Nicolais and M. Narkis. "Stress-strain behavior of styrene-acrylonitrile/glass bead composites in the glassy region". In: *Polymer Engineering and Science* 11.3 (May 1971), pp. 194–199. ISSN: 0032-3888. DOI: 10.1002/pen.760110305. URL: http://doi.wiley.com/10.1002/pen.760110305.

[100] Béla Pukanszky and GyÖrgy VÖRÖS. "Mechanism of interfacial interactions in particulate filled composites". In: *Composite Interfaces* 1.5 (1993), pp. 411–427. ISSN: 15685543. DOI: 10.1080/156855493X00266.

[101] Tsung Han Hsieh et al. "Mechanical properties of glass bead-modified polymer composite". In: *Polymers and Polymer Composites* 26.1 (2018), pp. 35–43. ISSN: 14782391. DOI: 10.1177/096739111802600105.

[102] A. Eucken. "Allgemeine Gesetzmäßigkeiten für das Wärmeleitvermögen verschiedener Stoffarten und Aggregatzustände". In: *Forschung auf dem Gebiete des Ingenieurwesens* 11.1 (Jan. 1940), pp. 6–20. ISSN: 00157899. DOI: 10.1007/BF02584103. URL: https://link-springer-com.tudelft.idm.oclc.org/article/10.1007/BF02584103.

[103] Richard F. Hill and Peter H. Supancic. "Thermal Conductivity of Platelet-Filled Polymer Composites". In: *Journal of the American Ceramic Society* 85.4 (Dec. 2004), pp. 851–857. ISSN: 00027820. DOI: 10.1111/j.1151-2916.2002.tb00183.x. URL: http://doi.wiley.com/10.1111/j.1151-2916.2002.tb00183.x.

[104] Aleksey D. Drozdov and Jesper deClaville Christiansen. "Modeling Thermal Conductivity of Highly Filled Polymer Composites". In: *Polymer Engineering & Science* 59.10 (Oct. 2019), pp. 2174–2179. ISSN: 0032-3888. DOI: 10.1002/pen.25220. URL: https://onlinelibrary.wiley.com/doi/abs/10.1002/pen.25220.

[105] Lawrence E. Nielsen. "Thermal conductivity of particulate-filled polymers". In: *Journal of Applied Polymer Science* 17.12 (Dec. 1973), pp. 3819–3820. ISSN: 00218995. DOI: 10.1002/app.1973.070171224. URL: http://doi.wiley.com/10.1002/app.1973.070171224.

[106] D. A.G. Bruggeman. "Berechnung verschiedener physikalischer Konstanten von heterogenen Substanzen. I. Dielektrizitätskonstanten und Leitfähigkeiten der Mischkörper aus isotropen Substanzen". In: *Annalen der Physik* 416.7 (Jan. 1935), pp. 636–664. ISSN: 15213889. DOI: 10.1002/andp.19354160705. URL: https://onlinelibrary-wiley-com.tudelft.idm.oclc.org/doi/full/10.1002/andp.19354160705%20https://onlinelibrary-wiley-com.tudelft.idm.oclc.org/doi/abs/10.1002/andp.19354160705%20https://onlinelibrary-wiley-com.tudelft.idm.oclc.org/doi/10.1002/andp.19354160705.

[107] William D. Callister and David G. Rethwisch. *Materials Science and Engineering*. Ninth edit. Wiley, 2015. ISBN: 978-1-118-31922-2.

[108] Tran Huu Nam, Guillermo Requena, and Peter Degischer. "Thermal expansion behaviour of aluminum matrix composites with densely packed SiC particles". In: *Composites Part A: Applied Science and Manufacturing* 39.5 (May 2008), pp. 856–865. ISSN: 1359835X. DOI: 10.1016/j.compositesa.2008.01.011. URL: https://linkinghub.elsevier.com/retrieve/pii/S1359835X08000213.

[109] E H Kerner. *The Elastic and Thermo-elastic Properties of Composite Media*. Tech. rep.

[110] C L Hsieh and W H Tuan. “Thermal expansion behavior of a model ceramic-metal composite”. In: *Materials Science and Engineering A* 460 (2007), pp. 453–458. DOI: 10.1016/j.msea.2007.01.109.

[111] Philip S Turner. “Thermal-Expansion Stresses in Reinforced Plastics”. In: *Journal of Research of the National Bureau of Standards* 37 (Oct. 1946), pp. 239–250. URL: https://nvlpubs.nist.gov/nistpubs/jres/37/jresv37n4p239_A1b.pdf.

[112] T. Huber et al. “Thermal expansion studies on aluminium-matrix composites with different reinforcement architecture of SiC particles”. In: *Composites Science and Technology* 66.13 (Oct. 2006), pp. 2206–2217. ISSN: 02663538. DOI: 10.1016/j.compscitech.2005.12.012. URL: https://linkinghub.elsevier.com/retrieve/pii/S0266353805004859.

[113] R A Schapery. *Thermal Expansion Coefficients of Composite Materials Based on Energy Principles*. Tech. rep.

[114] Z. Hashin and S. Shtrikman. “A variational approach to the theory of the elastic behaviour of multiphase materials”. In: *Journal of the Mechanics and Physics of Solids* 11.2 (Mar. 1963), pp. 127–140. ISSN: 00225096. DOI: 10.1016/0022-5096(63)90060-7.

[115] Onur Balkan, Ayhan Ezdeşir, and Halil Demirer. “Microstructural characteristics of glass bead-and wollastonite-filled isotactic-polypropylene composites modified with thermoplastic elastomers”. In: *Polymer Composites* 31.7 (July 2010), pp. 1265–1284. ISSN: 02728397. DOI: 10.1002/pc.20948.

[116] K. Shibata et al. “The role of frictional work in tribological behavior of polyamide 66 composites containing rice bran ceramics particles or glass beads”. In: *Tribologia* 32.1 (2014), pp. 33–40. ISSN: 07802285.

[117] Runzhou Huang et al. “High Density Polyethylene Composites Reinforced with Hybrid Inorganic Fillers: Morphology, Mechanical and Thermal Expansion Performance”. In: *Materials* 6.9 (Sept. 2013), pp. 4122–4138. ISSN: 1996-1944. DOI: 10.3390/ma6094122. URL: https://pubmed-ncbi-nlm-nih-gov.tudelft.idm.oclc.org/28788322/.

[118] N. C. Bleach et al. “Effect of filler content on mechanical and dynamic mechanical properties of particulate biphasic calcium phosphate - Polylactide composites”. In: *Biomaterials* 23.7 (Apr. 2002), pp. 1579–1585. ISSN: 01429612. DOI: 10.1016/S0142-9612(01)00283-6.

[119] Leon Govaert, Brian Brown, and Paul Smith. “Temperature Dependence of the Young’s Modulus of Oriented Polyethylene”. In: *Macromolecules* 25.13 (June 1992), pp. 3480–3483. ISSN: 15205835. DOI: 10.1021/ma00039a027. URL: https://pubs.acs.org/sharingguidelines.

[120] Carlton C. Allen et al. “Sintering of lunar glass and basalt”. In: Publ by ASCE, 1992, pp. 1209–1218. ISBN: 087262868X.

[121] D. R. Saini, A. V. Shenoy, and V. M. Nadkarni. “Dynamic mechanical properties of highly loaded ferrite-filled thermoplastic elastomer”. In: *Journal of Applied Polymer Science* 29.12 (Dec. 1984), pp. 4123–4143. ISSN: 00218995. DOI: 10.1002/app.1984.070291244. URL: http://doi.wiley.com/10.1002/app.1984.070291244.

[122] M. S. Huda et al. “”green” composites from recycled cellulose and poly(lactic acid): Physico-mechanical and morphological properties evaluation”. In: *Journal of Materials Science* 40.16 (Aug. 2005), pp. 4221–4229. ISSN: 00222461. DOI: 10.1007/s10853-005-1998-4. URL: https://link.springer.com/article/10.1007/s10853-005-1998-4.

[123] M. Bakar and M. Kostrzewa. “Effect of glass beads and polyurethane on the fracture properties of epoxy resin”. In: *Journal of Thermoplastic Composite Materials* 23.6 (Nov. 2010), pp. 749–764. ISSN: 08927057. DOI: 10.1177/0892705709347057.

[124] V. Mittal, J. K. Kim, and K. Pal. *Recent Advances in Elastomeric Nanocomposites*. 2011. DOI: 10.1007/978-3-642-15787-5.

[125] Kristina Brandt et al. “Novel ceramic-polymer composites synthesized by compaction of polymer-encapsulated TiO 2-nanoparticles”. In: (2011). DOI: 10.1016/j.compscitech.2011.10.001.

[126] “The mechanical design of nacre”. In: *Proceedings of the Royal Society of London. Series B. Biological Sciences* 234.1277 (Sept. 1988), pp. 415–440. ISSN: 0080-4649. DOI: 10.1098/rspb.1988.0056.

[127] M F H Wolff et al. “Novel, highly-filled ceramic-polymer composites synthesized by a spouted bed spray granulation process”. In: (2013). DOI: 10.1016/j.compscitech.2013.11.006. URL: http://dx.doi.org/10.1016/j.compscitech.2013.11.006.

[128] Zhiyong Tang et al. “Nanostructured artificial nacre”. In: *Nature Materials* 2.6 (May 2003), pp. 413–418. ISSN: 14761122. DOI: 10.1038/nmat906. URL: www.nature.com/naturematerials.

[129] I. A. Ibrahim, F. A. Mohamed, and E. J. Lavernia. *Particulate reinforced metal matrix composites - a review*. Jan. 1991. DOI: 10.1007/BF00544448.

[130] F.J. Lino Alves, A.M. Baptista, and A.T. Marques. “Metal and ceramic matrix composites in aerospace engineering”. In: *Advanced Composite Materials for Aerospace Engineering*. Ed. by Sohel Rana and Raul B T - Advanced Composite Materials for Aerospace Engineering Fangueiro. Elsevier, 2016, pp. 59–99. ISBN: 978-0-08-100939-0. DOI: 10.1016/B978-0-08-100037-3.00003-1. URL: http://www.sciencedirect.com/science/article/pii/B9780081000373000031%20https://linkinghub.elsevier.com/retrieve/pii/B9780081000373000031.

[131] M Y Zhou et al. “Progress in research on hybrid metal matrix composites”. In: (2020). DOI: 10.1016/j.jallcom.2020.155274. URL: https://doi.org/10.1016/j.jallcom.2020.155274.

[132] Sie Chin Tjong. *Recent progress in the development and properties of novel metal matrix nanocomposites reinforced with carbon nanotubes and graphene nanosheets*. Oct. 2013. DOI: 10.1016/j.mser.2013.08.001.

[133] Xiaoyu Huang et al. “Microstructure, mechanical properties and strengthening mechanisms of in-situ prepared (Ti5Si3 + TiC0.67)/TC4 composites”. In: *Journal of Alloys and Compounds* 792 (July 2019), pp. 907–917. ISSN: 09258388. DOI: 10.1016/j.jallcom.2019.04.056.

[134] Essam A.M. Shalaby et al. “Preparation and characterization of hybrid A359/(SiC+Si3N4) composites synthesized by stir/squeeze casting techniques”. In: *Materials Science and Engineering A* 674 (Sept. 2016), pp. 18–24. ISSN: 09215093. DOI: 10.1016/j.msea.2016.07.058.

[135] Jie Hu et al. “Mechanical properties and damping capacity of SiCp/TiNi f/Al composite with different volume fraction of SiC particle”. In: *Composites Part B: Engineering* 66 (Nov. 2014), pp. 400–406. ISSN: 13598368. DOI: 10.1016/j.compositesb.2014.06.013.

[136] Jakob Kübarsepp and Kristjan Juhani. “Cermets with Fe-alloy binder: A review”. In: (2020). DOI: 10.1016/j.ijrmhm.2020.105290. URL: https://doi.org/10.1016/j.ijrmhm.2020.105290.

[137] K. H. Oh and K. S. Han. “Short-fiber/particle hybrid reinforcement: Effects on fracture toughness and fatigue crack growth of metal matrix composites”. In: *Composites Science and Technology* 67.7-8 (June 2007), pp. 1719–1726. ISSN: 02663538. DOI: 10.1016/j.compscitech.2006.06.020.

[138] Ke Chu et al. “Interface and mechanical/thermal properties of graphene/copper composite with Mo2C nanoparticles grown on graphene”. In: *Composites Part A: Applied Science and Manufacturing* 109 (June 2018), pp. 267–279. ISSN: 1359835X. DOI: 10.1016/j.compositesa.2018.03.014.

[139] Baisong Guo et al. “Exploring the size effects of Al4C3 on the mechanical properties and thermal behaviors of Al based composites reinforced by SiC and carbon nanotubes”. In: *Carbon* 135 (Aug. 2018), pp. 224–235. ISSN: 00086223. DOI: 10.1016/j.carbon.2018.04.048.

[140] Subodh Kumar, Hajo Dieringa, and Karl Ulrich Kainer. “Thermal cycling behaviour of the magnesium alloy based hybrid composites in the transverse direction”. In: *Materials Science and Engineering A* 454-455 (Apr. 2007), pp. 367–370. ISSN: 09215093. DOI: 10.1016/j.msea.2006.11.041.

[141] Ali Miserez and Andreas Mortensen. “Fracture of aluminium reinforced with densely packed ceramic particles: Influence of matrix hardening”. In: *Acta Materialia* 52.18 (Oct. 2004), pp. 5331–5345. ISSN: 13596454. DOI: 10.1016/j.actamat.2004.07.038.

[142] Granta Design Limited. *CES EduPack 2019, version 19.2.0*. accessed via TU Delft subscription. 2019.

A

Summary tables

This chapter presents summary tables for a variety of important data. The first section lists the properties of possible matrix materials whereas the second gives a summary of regolith applications and the used material.

A.1. Properties of possible matrix materials

This section gives an overview of the properties of different materials which would be suitable to use as a matrix in regolith composites. All of the data has been obtained from Limited[142]. All values are averages of those presented by the software. Matching values are most likely due to estimates provided for similar properties (e.g. a good first estimation for an unknown flexural modulus is the Young's modulus and vice versa).

Table A.1: *Mechanical and thermal properties of metals found on the Moon and Mars. The cost and production energy required on Earth is also indicated. Data obtained from [142] by taking average listed values and verified, where possible, using information from [107]*

Property	Iron	Aluminium	Titanium	Magnesium
Density [kg/m3]	7870	2700	4515	1740
Young's modulus [GPa]	208	70.5	102.5	44.75
Compressive strength [MPa]	137	30	150	82.5
Flexural modulus [GPa]	208	70.5	102.5	44.75
Fracture toughness [MPa$\sqrt{m}$]	130	32.5	57.5	60
Bulk modulus [GPa]	169	73	123	35
Poisson's ratio	0.3	0.34	0.36	0.2875
T_m [°C]	1535	650	1670	648
k [W/(mK)]	75.5	209	17.15	152.5
CTE [ϵ/K]	1.23E-05	2.28E-05	8.90E-06	2.60E-05
Cost [EUR/kg]	0.646	1.85	11.75	1.935
Primary production energy, embodied energy, primary production [J/kg]	2.44E+07	2.00E+08	5.88E+08	3.26E+08
Recycle	yes	yes	yes	yes

Table A.2: *Mechanical and thermal properties of polymers commonly used on Earth. The cost and production energy required on Earth is also indicated. Data obtained from [142] by taking average listed values and verified, where possible, using information from [107]*

Property	UHMWPE	Epoxy	Polyurethane	Polycarbonate	LaRC-PC1
Density [kg/m3]	940	1255	1050	1200	1380
Young's modulus [GPa]	0.9285 (±0.345)	2.410	4.195	2.380	2.415
σ_c [MPa]	29.4 (±3.7)	137.500	69.800	77.600	200.500
Flexural modulus [GPa]	0.9285 (±0.345)	2.410	4.195	2.305	2.960
Flexural strength [MPa]	60.85 (±5.85)	117.350	131.500	89.600	144.750
Fracture toughness [MPa$\sqrt{m}$]	3.44 (±1.72)	0.600	1.515	2.250	4.280
Bulk modulus [GPa]	1.975 (±0.045)	3.965	5.975	3.930	3.935
Poisson's ratio	0.422	0.399	0.383	0.399	0.399
T_g [°C]	-107.5 (±17.5)	-	-	-	250.000
T_m [°C]	131.5 (±6.5)	117.000	85.000	150.000	388.000
k [W/(mK)]	0.1935 (±0.0035)	0.18850	0.31000	0.20550	0.13615
CTE [ϵ/K]	0.000297	0.0000990	0.0000911	0.0001225	0.0000910
Cost [EUR/kg]	2.3050000	2.2100000	4.0050000	2.8950000	51.1500000
Primary production energy, embodied energy, primary production [J/kg]	9.64E+07	1.29E+08	8.21E+07	1.06E+08	3.31E+08
Recycle	yes	no	no	yes	yes
Downcycle	yes	yes	yes	yes	yes

Table A.3: *Mechanical and thermal properties of ceramics commonly used for ceramic matrix composites. The cost and production energy required on Earth is also indicated. Data obtained from [142] by taking average listed values and verified, where possible, using information from [107]*

Property	Silicon	SiC (fibre)	SiC (matrix)	Al2O3 (fibre)	Al2O3 (matrix)	Mullite	Carbon (matrix)
Density [kg/m3]	2330	2300	3145	3900	3960	2850	24.19
Young's modulus [GPa]	160	176	380	385	400	165	28
Compressive strength [MPa]	3430	2455	1350	5500	2600	935	2935
Flexural modulus [GPa]	160	2455	380	3900	400	165	28
Fracture toughness [MPa$\sqrt{m}$]	0.9	3	3.25	1.75	6	2.2	2.45
Bulk modulus [GPa]	100	84	181	267.5	257,5	86.5	15.55
Poisson's ratio	0.27	0.145	0.15	0.265	0.24	0.25	0.2
T_m [°C]	1440	2835	2400	2050	2050	1845	3605
k [W/(mK)]	160	12.5	1.25E+02	22.8	30	4	3.05
CTE [ϵ/K]	8.90E-06	3.10E-06	4.45E-06	7.10E-06	8.90E-06	4.25E-06	1.60E-06
Cost [EUR/kg]	€ 10.41	€ 3,375.00	€ 15.10	4575	€ 35.30	€ 7.99	
Primary production energy, embodied energy, primary production [J/kg]	1.22E+08	1.67E+08	1.67E+08	3.13E+10	5.21E+07	5.55E+07	2.44E+07
Recycle	no	no	no	no	no	no	no
Downcycle	yes	yes	yes	yes	yes	yes	yes

A.2. Regolith application summary table

Table A.4: *Regolith application summary table.*

Application	Source	Binder	Simulant	FVF	Processing	E	σ_u	Notes
Radiation protection	[87]	Polyimide (LaRC-SI)		101: 40 wt% LaRC-SI 102: 20 wt% LaRC-SI	Compression molding 2.66 MPa	Baseline 101: 5.6-6.2 GPa Baseline 102: 7.5 - 8.7 GPa	Baseline 101: 190 - 198 Mpa compression Baseline 102: 227-233 Mpa”	”Also includes graphs on mass loss Well consolidated and no voids”